Characterization of Novel insect Cytochrome P450-fusion enzymes

INAUGURAL-DISSERTATION

zur Erlangung des akademischen Grades

Dr. rer. nat.

der Naturwissenschaftlichen Fachbereiche

der Justus-Liebig-Universität Gießen

vorgelegt von

Diplom Biochemikerin Lea Talmann

Gießen, im November 2016

1. Gutachter **Professor Dr. Andreas Vilcinskas**
Institut für Insektenbiotechnologie
Fachbereich Agrarwissenschaften,
Ökotrophologie und Umweltmanagement
Justus-Liebig-Universität Gießen

2. Gutachter **Professor Dr.-Ing. Peter Czermak**
Fachbereich LSE-IBPT
THM
Fachbereich Biologie und Chemie
Justus-Liebig-Universität Gießen

"Science never solves a problem without creating ten more"

George Bernard Shaw (1856-1950)

Table of Contents

Summary

Cytochrome P450 monooxygenases (P450s) represent a ubiquitous group of enzymes with a broad substrate spectrum. Their ability to catalyze a variety of reactions, e.g. detoxification of insecticides, makes them interesting enzyme candidates with enormous industrial potential. Unfortunately, they cannot be fully utilized due to their complex characteristic like their necessity of a cytochrome P450 reductase (CPR) for the electron transfer from NADPH. Furthermore, the P450s and CPRs contain membrane anchors leading to insoluble protein. These two factors represent challenges for their artificial production and consequently purification and whole-cell applications.

The aim of this study was to overcome those challenges by construction of P450-fusion enzymes. Those fusion enzymes were designed based on the bacterial CYP102A (BM3) from *Bacillus megaterium*, which is a known natural fusion enzyme and does not possess any membrane anchor. Our fusion enzymes are composed of a changeable insect P450, a variable BM3 linker, BM3 CPR (BMR) and a C-terminal 6xHis-tag. For the first time, three different insect fusion enzymes of the CYP6 family (CYP6A1-BMR, CYP6G1-BMR and CYP6AE14-BMR) and of the CYP4G subfamily (CYP4G1-BMR, CYP4G2-BMR and CYP4GF-BMR) were constructed. Such a fusion made it possible to produce insect CYP6s recombinantly in an *Escherichia coli* system and to purify those without the use of detergents. Suitable LC- and GC-MS methods to characterize the purified enzymes were established in order to verify their ability to oxygenize the substrates imidacloprid and aldrin.

A whole-cell approach was established to exclude the purification process as reason of CYP6-BMR construct inactivity. In this study it was shown that acyl-ACP reductase and aldehyde decarbonylase from the blue algae *Nostoc punctiforme* can be produced recombinantly in *E. coli*. It was demonstrated that they are able to catalyze the transformation of *E. coli* produced long-chain fatty acids to long-chain alkanes. In the next step the aldehyde decarbonylase was replaced by the CYP4G fusion constructs. Thereby the acyl-ACP reductase and the fusion construct generate a whole-cell system for alkane production. For the aldehyde and alkane detection a SPME-GC-MS method was established.

The findings of the present study concerning the construction of novel insect P450-fusion enzymes as well as the established analytical methods serve as a basis for further insect P450 characterization and biocatalyst development.

Zusammenfassung

Cytochrom-P450-Monooxygenasen (CYPs) bilden eine in vielen Organismen vorkommende Enzymgruppe mit einem großen Substratspektrum. Sie besitzen eine große Reaktionsvielfalt, wie zum Beispiel die Entgiftung von Insektiziden, was sie zu besonders interessanten Kandidaten für die industrielle Anwendung macht. Allerdings können CYPs auf Grund ihrer komplexen Eigenschaften, wie die Notwendigkeit einer Cytochrom-P450-Reduktase (CPR) für den Elektronentransfer von NADPH, nicht vollständig genutzt werden. Darüber hinaus sind CYPs und CPRs auf Grund ihrer Membrananker unlöslich. Diese zwei Faktoren stellen Herausforderungen für ihre artifizielle Produktion und anschließende Aufreinigungs- und Ganzzell-Anwendungen dar.

Das Ziel dieser Studie war es, die genannten Schwierigkeiten durch die Konstruktion von CYP-Fusionsenzymen zu überwinden. Die Fusionsenzyme wurden auf Grundlage der bakteriellen CYP102A1 (BM3) aus *Bacillus megaterium*, einem natürlichen Fusionsenzym ohne Membrananker, konstruiert. Die generierten Fusionskonstrukte bestehen aus einer austauschbaren Insekten-CYP, einem variablen BM3-Linker, der BM3-CPR (BMR), und einem C-terminalem 6xHis-tag. Zum ersten Mal wurden drei verschiedene Insekten-Fusionsenzyme der CYP6-Familie (CYP6A1-BMR, CYP6G1-BMR und CYP6AE14-BMR) und der CYP4G-Unterfamilie (CYP4G1-BMR, CYP4G2-BMR und CYP4GF-BMR) konstruiert. Diese Fusion ermöglichte die rekombinante Insekten-CYP6-Produktion in *Escherichia coli* sowie die Aufreinigung ohne den Einsatz von Detergenzien. Mit dem Ziel die Fähigkeit der aufgereinigten Enzyme, die Oxidation der Substrate Imidacloprid und Aldrin, nachzuweisen, wurden passende LC- und GC-MS-Methoden für die Charakterisierung etabliert.

Es wurde ein Ganzzell-Ansatz entwickelt, um den Aufreinigungsprozess als Grund für die CYP6-Inaktivität ausschließen zu können. In dieser Studie wurde gezeigt, dass die aus der Blaualge *Nostoc punctiforme* stammenden Enzyme Acyl-ACP-Reduktase und Aldehyddecarbonylase rekombinant zusammen in *E. coli* produziert werden können und, dass sie die von *E. coli* produzierten langkettigen Fettsäuren in langkettige Alkane umwandeln können. In einem nächsten Schritt wurde die Aldehyddecarbonylase durch ein CYP4G-Fusionskonstrukt ersetzt. Dadurch generieren die Acyl-ACP-Reduktase und das Fusionskonstrukt ein Ganzzell-System zur Alkanproduktion. Zur Detektion der Aldehyde und Alkane wurde eine SPME-GC-MS-Methode etabliert.

Die Ergebnisse dieser Studie, welche die Konstruktion neuer Insekten-CYP-Fusionsenzyme, sowie die etablierten Methoden, dienen als Grundlage für die weitere Charakterisierung und biokatalytische Entwicklung von Insekten-CYPs.

Synopsis

1 Introduction

1.1 Cytochrome P450 monooxygenases

Cytochrome P450 monooxygenases (P450) are a ubiquitous superfamily of mixed function oxidases [1]. The P450 superfamily is one of the largest and oldest gene superfamilies [1]. P450s are heme-thiolated monooxygenases found in all biological kingdoms and fulfill various roles in their hosts. P450s are involved in the metabolism of xenobiotics and drugs [2], steroid biosynthesis [3] and the assimilation of carbon sources for growth [4]. They were first discovered by Garfinkel and Klingenberg and were identified and isolated from mammalian liver microsomes in 1964 by Omura and Sato [5-7]. There are over one thousand P450 families known with around 21000 different P450s and the numbers are still increasing [8]. This indicates their importance for all forms of life. The nomenclature of P450s was introduced in 1987 by Nebert *et al*.. The members of this superfamily, for example CYP6A1, are indicated with a CYP prefix, the following number (6) shows the family, the letter (A) the subfamily and the number (1) the enzyme [9]. Members of one P450 family share >40% amino acid sequence identity, within wide variation across the different families. All P450s form similar secondary and tertiary structures [10-12]. The heme b cofactor forms the catalytic reaction center of the P450. The heme contains an iron atom at its center which is bound to a protoporphyrin ring by four nitrogen ligands, which forms a planar structure. It is coordinated by an evolutionary conserved axial cysteine ligand, *FXXGXXXCXG*, which is located towards the C-terminus of the protein [1]. The iron is often associated with water as a sixth ligand. Heme is responsible for a Soret band absorbance at 420 nm when it is coordinated to water. The absorbance signal shows a typical shift to 450 nm when carbon monoxide is bound at the opposite axial position, as shown in Figure 1-1. This led to the name P450 which stands for Pigment 450 [5].

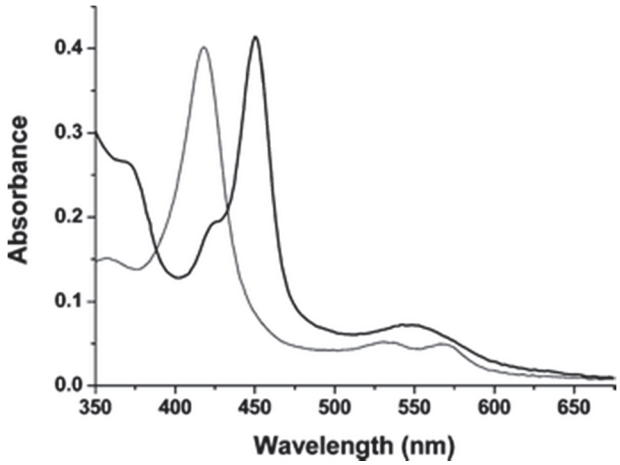

Figure 1-1:Typical absorption spectrum of a P450 enzyme. The light grey line shows the oxidized (ferric state) of the enzyme with A_{max} at 420 nm. The black line shows the dithionite-reduced Fe(II)–CO complex of the enzyme with A_{max} at 450 nm [13]. Reproduced from A. W. Munro, H. M. Girvan, K. J. McLean, Natural Product Reports 2007, 24, 585-609 with permission of The Royal Society of Chemistry.

1.2 P450 reactions

P450s cannot catalyze a reaction on their own as they need to accept electrons from a redox partner, shown in Figure 1-2. The reaction requires two reducing equivalents, derived from a nicotinamide cofactor [14]. Other prosthetic groups, for example FAD and FMN, which are derived from riboflavin, serve as electron transfer centers.

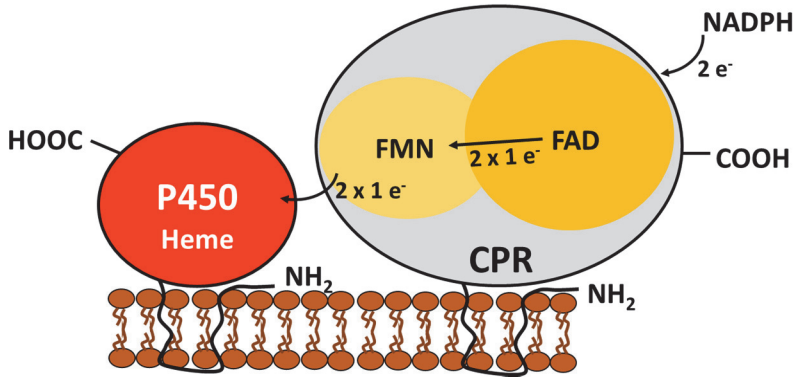

Figure 1-2: Schematic representation of the P450 redox partner (CPR) interaction.

P450s are able to catalyze unique one-step C-H bond oxidations by a subsequent insertion of one oxygen atom into the substrate and the other oxygen atom forming water [15-16]. They can catalyze various reactions (Figure 1-3). The P450 substrates and reactions cannot be determined from their evolutionary proximity to other P450s or their sequence [1]. Most common is the monooxygenation, which leads to a hydroxylation or epoxidation at a carbon center, shown in Figure 1-3 a. Less common

is the oxidation and dealkylation at a heteroatom and complex reactions like single electron reductions, desaturations and ring modifications alongside typical oxidations [17], shown in Figure 1-3 b. All those reactions are difficult to realize by synthetic chemistry where regio- and stereo-selectivity is not easily achieved. This is one reason why the research on P450s is of interest for industrial applications.

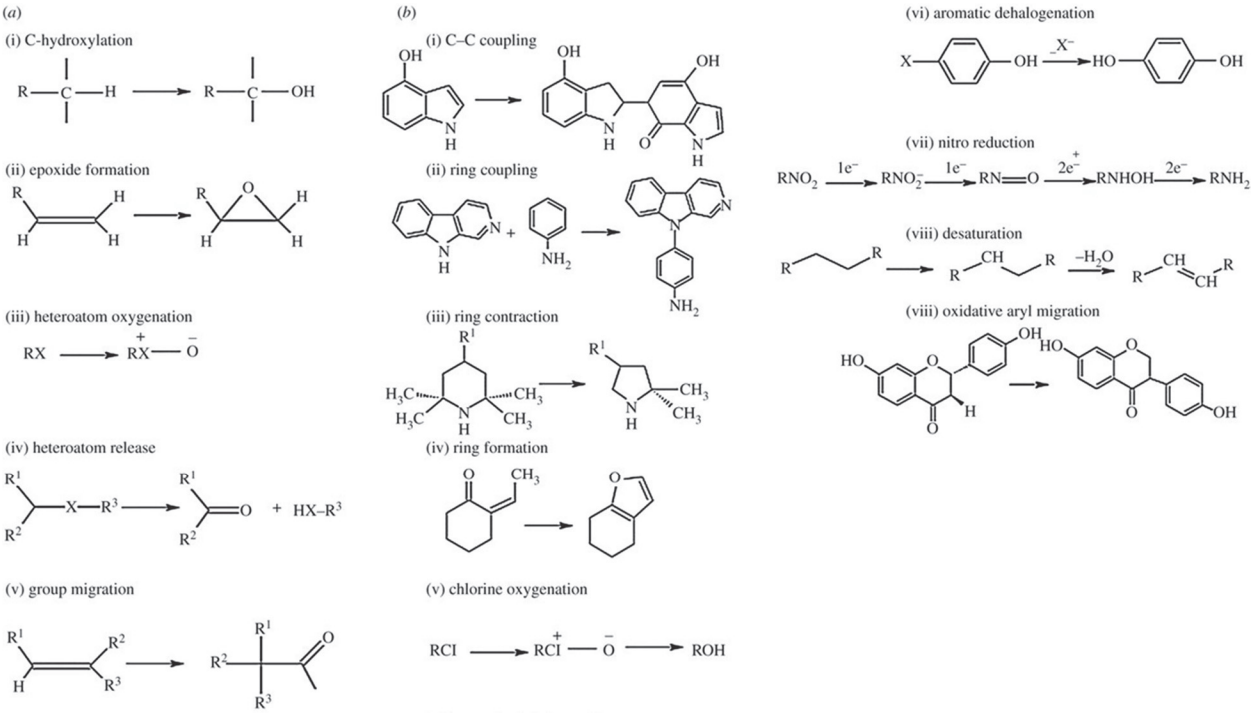

Figure 1-3: Reactions catalyzed by P450 monooxygenases. (a) Common and (b) uncommon reactions [18]. David C. Lamb, Michael R. Waterman, Unusual properties of the cytochrome P450 superfamily, Philosophical Transactions B, The Royal Society, 2013, 368, 1612, by permission of the Royal Society

1.3 Insect P450s

P450s are common in insects, comprise over a hundred different genes [19] and form an extremely important metabolic system. They are involved in the metabolism of endogenous compounds and xenobiotics [20]. P450s show high similarity in reaction mechanism and structure with the well-studied mammalian P450s. Insect P450s can be either microsomal or mitochondrial. Microsomal P450s depend on a P450 reductase or cytochrome b_5 or both as electron donor whereas mitochondrial P450s depend on an adrenodoxin-like ferredoxin coupled to adrenodoxin reductase as electron donor. Six P450 families are known in insects, five of them are insect

specific families (CYP6, 9, 12, 18 and 28). They have a variety of function, caused by a diversity in structure [1]. Insect P450s are involved in growth, development, feeding, pesticide resistance, and tolerance to plant toxins. The expression levels of P450s in insects can vary across different life stages [21] and they are present in several tissues such as Malpighian tubules, fat body and midgut [22]. There is no clear phylogenetic distinction between P450s relevant for detoxification and those involved in the physiological homeostasis, which leads to the assumption that P450s can alter their function over evolutionary time [22]. Research on insect P450s is focused on metabolism, synergism and resistance [22]. Determination of their catalytic competence is difficult, because of their variability and due to the fact that they are membrane-bound and require electron-donating partners [1]. The membrane anchor inhibits the formation of soluble protein and a reconstitution system containing detergents and phospholipids is required for the P450 CPR interaction [23]. The standard procedures to determine the catalytic competence of P450s are heterologous expression and reconstitution experiments [24]. Molecular samples obtained from resistant strains show constitutive overexpression of P450 genes [1]. A common mechanism for insects becoming resistant to insecticides is the P450-mediated metabolism [24]. The first purified insect P450 reductase from *Musca domestica* is similar to mammalian P450 reductases [25]. The first cloned insect P450 was from the CYP6 family. CYP6A1 is a xenobiotic-metabolizing P450 from *Musca domestica.* It was produced in a reconstituted *E. coli* system and aldrin and heptachlor were identified as substrates [26]. CYP6A1 has a spacious heme active site which is compatible with several substrate geometries and orientations [27]. CYP6G1 from *Drosophila melanogaster* can be classified as a multi-pesticide associated enzyme, since it is linked to resistance towards various structurally non related compounds [28]. A very unusual reaction for a P450 enzyme is the decarbonylation of aldehydes which forms alkanes by CO_2 cleavage (Figure 1-4). The formation of hydrocarbons is well known from insects, since they are important for the prevention of desiccation and also function as contact pheromones [29]. The first P450 shown to be able to catalyze this reaction was CYP4G1 from *Drosophila melanogaster* [30].

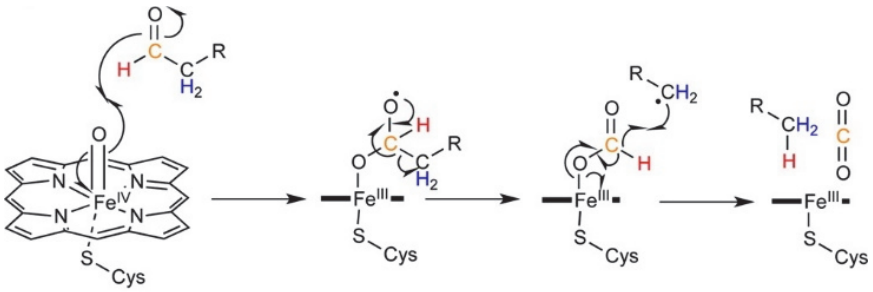

Figure 1-4: Mechanism of reaction catalyzed by CYP4G1 with aldehyde as substrate and alkane and CO_2 as products. The colors indicate the positions of isotopically-labeled substrates used in the study. Reprinted (adapted) with permission from (E. N. G. Marsh, M. W. Waugh, ACS Catalysis 2013, 3, 2515-2521.). Copyright (2013) American Chemical Society. [31].

1.4 P450 Optimization

P450 engineering focused on optimization of the heme domain, to improve or expand its catalytic performance which is limited by the need of an electron-donating partner, dependency on NADPH and the fact that the P450s are membrane-bound [32]. In order to overcome these limitations, different approaches like enzymatic [33] or photochemical [34] cofactor regeneration or chemical [35] and electrochemical [36] cofactor substitution, were developed. Another approach is the construction of artificial P450 fusion enzymes. P450 fusion enzymes are self-sufficient enzymes, where the heme domain is covalently linked to a reductase system [37]. In previous studies this was achieved in three different ways. 1. “LICRED” is a method developed by Bruce and coworkers for generating redox-self-sufficient P450s in a high-throughput manner. A vector containing the reductase domain of CYP116B2 (natural fusion P450) in front of a ligation-independent cloning (LIC) site allows rapid insertion of P450 genes [38] [39]. 2. “PUPPET” is a system developed by Nagamune and colleagues using a platform made of three distinct proliferating cell nuclear agents (PCNAs) which form a heterodimer called “PUPPET”. This is an approach to bring the heme group and its redox partners in close proximity to each other to increase the efficiency of the electron transport [40] [41]. 3. The “Molecular Lego” approach was established by Gilardi creating chimeric P450-reductase fusion using the natural fusion enzyme CYP102A1 [42]. This method is the basis of the work presented here for the construction of insect P450 fusion enzymes.

1.4.1 CYP102A1

CYP102A1 (BM3) is derived from *Bacillus megaterium* where it is involved in the fatty acid metabolism. BM3 is a self-sufficient fatty acid hydroxylase which is able to catalyze reactions without requiring the assistance of additional proteins. BM3 is a natural fusion protein where the catalytic P450 is covalently attached to the N-terminus of the redox domain by a linker on the same peptide chain, which entirely makes it a class II P450 system[43], as shown in Figure 1-5, typical of microsomal eukaryotic P450s [44]. The redox domain (BMR) is 66 kDa in size and binds two flavins, FAD and FMN, as prosthetic groups. The BMR closely resembles the eukaryotic CPR since it also uses FAD and FMN[43]. It has approximately 33% sequence identity to the mammalian hepatic CPR. The P450 domain is 55 kDa in size and has approximately 25% sequence identity to the fatty acid ω-hydroxylases of the CYP family IV[45].

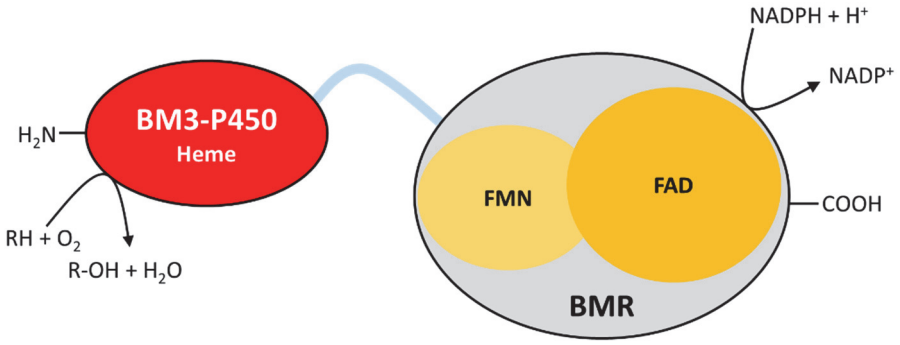

Figure 1-5: Schematic representation of the natural P450-redox partner fusion enzyme BM3.

The electron transfer from the reductase domain to the heme domain influences the enzyme activity. The linker length is of more importance for the enzyme activity than the amino acid composition because it determines the correct position of both domains towards each other [46]. BM3 has the highest known substrate turn-over rate of a P450. It is able to oxidize arachidonic acid at a rate of 5000 min^{-1} [47]. It was shown that the P450 and reductase domain retain their activity when being separated from each other, but the product formation is decreased. They form similar region-isomeric products as the full length enzyme[48]. Due to its self-sufficiency, its high substrate turn-over rate and the fact that it is not membrane bound BM3 serves as an important model for CYP research [43].

1.4.2 Molecular Lego

The “Molecular Lego” method was developed to create soluble new artificial fusion enzymes with a novel catalytic function [49].

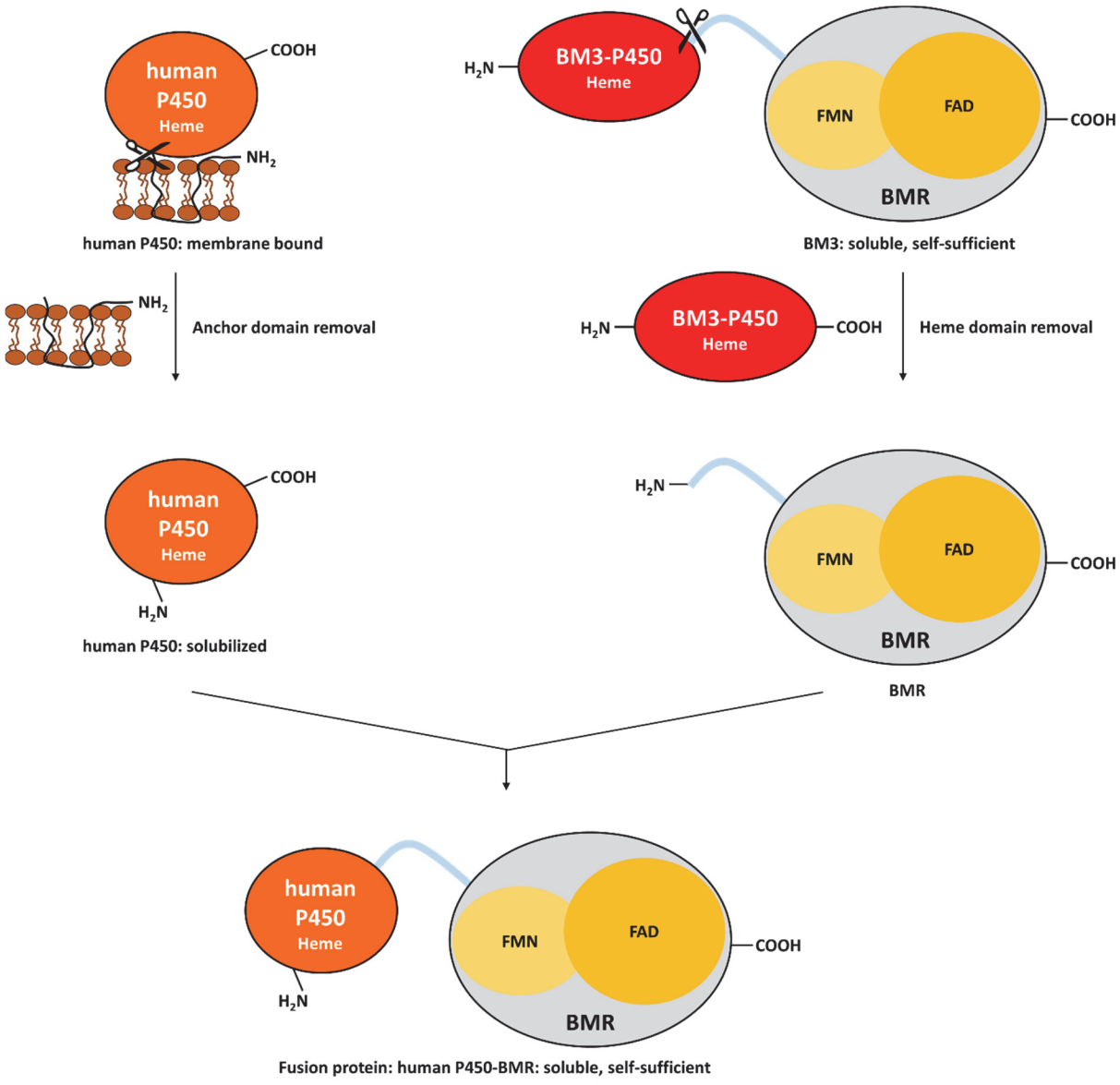

Figure 1-6: Schematic representation of the “Molecular Lego” principle to construct soluble, self-sufficient fusion human P450-BMR enzymes. Figure modified from Sadeghi and Gilardi [32].

This tool was used successfully for the creation of soluble, self-sufficient human P450-BMR fusion enzymes [50]. BM3 was divided into three building blocks, the P450 heme domain, the linker domain and the BMR domain. For the creation of human P450-BMR fusion enzymes the BM3-P450 heme domain was cleaved off and

replaced by a human P450 enzyme. The solubility of the enzyme was achieved by N-terminal modifications (removal of the hydrophobic N-terminal membrane anchor domain) of the former insoluble P450. The process is shown in Figure 1-6. Due to those changes a purification of the constructs without the use of detergents was possible and similar catalytic activities to the wild-type P450s were shown [50]. The BMR domain shows a similar catalytic mechanism to the CPR of *Musca domestica* [1].

2 Aims and Objectives

Insect P450s play important roles in insect growth, development, feeding, tolerance to plant toxins or pesticide resistance [21]. Their direct participation in pesticide resistance as well as their ability to catalyze various reactions attracts researchers from different fields and makes insect P450s interesting research candidates. A key challenge in insect P450s research is their complex characteristic they also share with human P450s. The crucial steps to overcome are (i) the necessity of a cytochrome P450 reductase (CPR) for the electron transfer from NADPH and (ii) P450s and CPR membrane anchors. For human P450s these problems were overcome by the 'Molecular Lego' approach. This approach enabled the creation of soluble, self-sufficient human P450-BMR fusion enzymes [50].

The aim of this project was to apply the same "Molecular Lego" approach for the creation of new insect P450-BMR fusion enzymes. The specific insect P450s were selected based on the P450s insect origin (e.g. CYP4G from *F. auricularia*), sequence availability as well as their potential substrates (e.g. CYP6 is involved in insecticide metabolism). Due to the relatively short production time and high yields *E. coli* expression system was chosen for recombinant production of fusion enzymes. Due to the complexity of P450s, two different production approaches were tested. The goal of the first approach was to produce the CYP6-BMR constructs in *E. coli* with subsequent detergent free purification of soluble enzyme. The second approach focused on the establishment of a whole cell coexpression system, which comprised of the CYP4G-BMR construct and the blue algae acyl-ACP reductase. Specific photometric activity assays as well as GC- and LC-MS methods for detection of relevant P450s substrates and products were established to further characterize the produced enzymes.

3 Methods

3.1 Gene synthesis

All genes were synthesized with a C-terminal His_6-tag (GHHHHHH) and *E. coli* K12 codon optimized (MWG Eurofins). The genes encoding for BM3 and insect P450 genes were flanked by *Bsa*I sites for restriction digestion and ligation into the pASK-IBA33plus vector. During the synthesis of the gene encoding for BM3, *Kpn*I, *Xba*I, and *Sal*I sites were added to enable the removal of the BM3 P450 domain. The *Xba*I site is located 41 base pairs upstream of the start codon, the *Kpn*I site 156 base pairs downstream of the start codon and the *Sal*I site inside the linker, which is 50 amino acids long. The genes encoding for CYP4G1 and CYP4G2 were ordered with a 22 amino acids truncated N-terminus. With this approach six plasmids have been generated: i) pASK-IBA33_BM3, ii) pASK-IBA33_CYP6A1, iii) pASK-IBA33_ CYP6G1, iv) pASK-IBA33_CYP6AE14, v) pASK-IBA33_CYP4G1_d22, vi) pASK-IBA33_CYP4G2_d22. In addition the gene encoding for aldehyde decarbonylase were purchased with an N-terminal His_6-tag, also *E. coli* K12 codon optimized. The gene was flanked by *Bsa*I sites for restriction digestion and ligation into the pASK-IBA33plus vector creating the plasmid pASK-IBA33_aldehyde decarbonylase. Moreover the gene encoding for acyl-ACP reductase was commercially obtained with a C-terminal His_6-tag and *E. coli* K12 codon optimized. The gene was flanked by an *Nco*I site at the N-terminal site of the gene and an *Xho*I site at the C-terminal site of the gene for restriction digestion and ligation into the pCDFDuet-1 vector. By this the second open reading frame and the associated promoter were eliminated creating the plasmid pCDFDuet-1_acyl-ACP reductase.

3.2 PCR

For the N- and C- terminal attachment of restriction enzyme sites to a gene a PCR was performed under the following conditions with either Pfu polymerase or Phusion Flash Master Mix (Table 3-1, Table 3-2, Table 3-3 and Table 3-4).

Table 3-1: Reaction Setup for PCR reactions using Pfu Polymerase.

Reaction Setup (Pfu Polymerase)		
Amount		**Component**
5	µl	Pfu buffer
5	µl	dNTP Mix
1	µl	Pfu polymerase
1	µl	DMSO
0.5	µl	forward primer
0.5	µl	reverse primer
400	ng	template DNA
ad. 50	µl	nuclease free water

Table 3-2: PCR Program for PCR reactions using Pfu Polymerase.

PCR Program (Pfu Polymerase)			
Phase	**Step**	**Temperature [°C]**	**Time**
initial denaturation	denaturation	95	7 min
amplification (35 cycles)	denaturation	95	40 sec
	annealing	60/65/70	40 sec
	extension	72	2 min per 1 kb
final extension	extension	72	14 min
	hold	4	∞

Table 3-3: Reaction Setup for PCR reactions using Phusion Flash Master Mix.

Phusion Flash Polymerase			
Phase	**Step**	**Temperature [°C]**	**Time**
initial denaturation	denaturation	98	10 sec
amplification (30 cycles)	denaturation	98	1 sec
	annealing	72	5 sec
	extension	72	15 sec per 1 kb
final extension	extension	72	1 min
	hold	4	∞

Table 3-4: PCR Program for PCR reactions using Phusion Flash Master Mix.

PCR Program (Phusion Flash Master Mix)			
Phase	**Step**	**Temperature [°C]**	**Time**
initial denaturation	denaturation	98	10 sec
amplification (30 cycles)	denaturation	98	1 sec
	annealing	72	5 sec
	extension	72	15 sec per 1 kb
final extension	extension	72	1 min
	hold	4	∞

3.2.1 Colony PCR

A colony PCR was performed to check if a gene with the correct size was inserted. For this, either the sequencing primers of the corresponding plasmid (Table A.2.4-2) were used or the primer pairs designed for the PCR construction (Table A.2.4-1). The DNA of a picked *E. coli* colony was used as template. The PCR was performed under the following conditions (Table 3-5 and Table 3-6).

Table 3-5: Reaction Setup for PCR reactions using Dream Taq Polymerase.

Reaction Setup (Dream Taq Polymerase)		
Amount		**Component**
1.5	µl	10x Dream Taq buffer green
1.5	µl	dNTP mix
0.075	µl	Dream Taq polymerase
0.75	µl	forward primer
0.75	µl	reverse primer
10.425	µl	nuclease free water

Table 3-6: PCR Program for PCR reactions using Dream Taq Polymerase.

PCR Program (Dream Taq Polymerase)			
Phase	**Step**	**Temperature [°C]**	**Time**
initial denaturation	denaturation	95	3 min
amplification (35 cycles)	denaturation	95	30 sec
	annealing	65	30 sec
	extension	72	1.5 min per 1 kb
final extension	extension	72	5 min
	hold	4	∞

The results of the PCR were checked by agarose gel electrophoresis.

3.3 Agarose Gel Electrophoresis

The separation of gene fragments was achieved by agarose gel electrophoresis. A 1.5% agarose gel was prepared with agarose, TAE buffer and 1 µl SybrSafe for visualization of the DNA fragments. The DNA samples were mixed with six volumes of loading dye and loaded into the wells. 5 µl of a DNA size marker were also loaded as a reference into a separate well. The separation was achieved by running the agarose gel in TAE buffer at 120 mV for 30 to 60 min. The visualization was performed using VersaDoc, Quantity One Software (4.6.9) and the filter setting SYBR Green.

3.4 Restriction Enzyme Analysis

This method was performed to ensure that ligation and transformation were successful. The plasmid was checked using a single cutting enzyme or a double cutting enzyme which cuts inside the new ligated gene fragment and creates distinct fragment sizes. The digestion was performed as recommended by the enzyme supplier (NEB, Thermo Fisher Scientific). The results of the digestion were checked by agarose gel electrophoresis and the fragment sizes were compared to the calculated sizes.

3.5 Double Digestion

Double digestion was carried out for sticky end ligation of elongated PCR products and the plasmids. The digestion was performed as the enzyme supplier recommended with 1 µl enzyme per 1 µg DNA. An agarose gel electrophoresis was performed to separate the double digested DNA. The DNA fragments in the size of interest were excised and purified.

3.6 Purification of PCR Products and double digested DNA Fragments

The excised gel bands containing PCR products or double digested DNA fragments were transferred into 1.5 ml Eppendorf tubes. The purification was performed with

the GeneJet Gel Extraction Kit (Thermo Fisher Scientific) as the supplier recommended. The DNA was eluted into water.

3.7 Sequencing

Sequencing of the plasmid constructs was performed by the company Eurofins MWG with the respective primers (Table A.2.4-2). The results were analyzed using Clone Manager software.

3.8 Computation Tools

Translation of nucleotide sequences to a protein sequence was performed using the ExPASy translate tool (http://web.expasy.org/translate/). Multiple sequence alignments were done using the ExPASy ClustalW tool (http://embnet.vital-it.ch/software/ClustalW.html). Box shading multiple sequence alignments was performed with the ExPASy BoxShade tool (http://embnet.vital-it.ch/software/BOX_form.html) with the following settings: EPS_portrait as output format and other as input sequence format. Determination of physical and chemical parameters of a protein was done with the ExPASy ProtParam tool (http://web.expasy.org/protparam/) with compact as output format.

3.9 Photometric Determination of DNA Concentration

The DNA concentration of plasmids, purified PCR products and double digested DNA fragments was determined photometrically. An absorption of 1 at 260 nm equals a concentration of 50 ng/µl. For the quantification 2 µl reference (H_20 or elution buffer, depending on the eluent of the sample) and 2 µl sample were pipetted on a Take3 plate of the Eon plate reader (BioTek). The absorbance was measured at 260 nm. The purity was determined using the ratio of A_{260nm}/A_{280nm} which should fall between 1.7 and 1.9. A ratio of lower 1.7 and higher 1.9 indicates a contamination with protein or RNA, respectively.

3.10 Ligation

Ligation was performed to create a circular plasmid containing the gene of interest. The ligation solution was 10 µl in total volume and contained 33.3 ng/kb double digested DNA, 33.3 ng/kb double digested plasmid DNA, 1 µl T4 DNA ligase and 1 µl

T4 DNA ligase buffer. The solution was incubated for one to two hours at room temperature and then transformed into *E. coli* cells.

3.11 Preparation of *E. coli* Competent Cells

E. coli competent cells were prepared by inoculating 50 ml LB medium with 500 µl overnight culture of the respective *E. coli* strain. When using *E. coli* containing a plasmid the respective antibiotic was added to the medium. The cells were grown at 37°C with 180 rpm until an OD_{600} of ~4. The cells were harvested by centrifugation at 4°C and 4500 g for 20 min. The cell pellet was resuspended in 2.5 ml TSS medium and 50 µl of this were transferred into precooled 1.5 ml Eppendorf tubes and immediately frozen in liquid nitrogen or on dry ice.

3.12 DNA Transformation

An aliquot of competent *E. coli* cells was gently thawed on ice for 10 min. 10 µl ligation mixture, or 1 µg plasmid DNA or a 1:1 mixture of two different plasmid DNAs (only with commercial competent *E. coli* cells) was given to the cells and incubated on ice for 30 min. The cells were heated at 42°C for 45 sec and placed directly back on ice for 3 min. 200 µl LB medium were added to the cells containing no antibiotics or the suitable antibiotic if competent cells contained a plasmid. The cells were incubated for 60 min at 37°C with 220 rpm. After that they were plated on LB agar plates containing the appropriate antibiotic or antibiotics. The plates were incubated at 37°C overnight.

3.13 Construction of P450 Fusion Enzymes

For the construction of insect P450-BMR fusion enzymes two plasmids types have been generated. i) pASK-IBA33_CYP_BMR_KS (containing a BM3 N-terminus) and ii) pASK-IBA33_CYP_BMR_XS (without BM3 N-terminus).

The construction of the fusion enzymes was started based on the plasmids ordered at MWG Eurofins and selected subsequently as modified by A. Baumann, see section 3.1. A scheme of the construction process is shown in Figure 4-8. *E. coli* TOP10 cells were transformed with the constructed plasmids for amplification and sequencing with the respective primers (Table A.2.4-2). After sequence verification the plasmid

was purified and *E. coli* BL21 (expression cells) cells were transformed with the plasmid.

3.13.1 Construction of P450 Fusion Enzymes with BM3 N-terminus

The pASK-IBA33 vectors containing the insect CYP genes with truncated N-termini were used as template for PCR. The PCR created a *Kpn*I site at the N-terminal end of the gene and a BM3 linker region with a *Sal*I site at the C-terminal end using primers shown in Table A.2.4-1. The PCR fragment and the vector pASK-IBA33_BM3 were double digested with *Kpn*I and *Sal*I creating a ~1500 bp CYP PCR fragment and a 5113 bp vector backbone. Ligating the PCR fragment into the vector backbone pASK-IBA_BMR resulted in the final plasmid pASK-IBA33_CYP-BMR_KS. This created the constructs pASK-IBA33_CYP6A1-BMR_KS, pASK-IBA33_CYP6G1-BMR_KS, pASK-IBA33_CYP6AE14-BMR_KS, pASK-IBA33_CYP4G1-BMR_KS and pASK-IBA33_CYP4G2-BMR_KS.

3.13.2 Construction of P450 Fusion Enzymes without BM3 N-terminus

Construction of P450 fusion enzymes without a BM3 N-terminus, was carried out as described in section 3.13.1 modified by the use of PCR creating an *Xba*I site at the N-terminal site of the CYP gene (Table A.2.4-1). The reverse primers were the same as before (Table A.2.4-1).The *Xba*I-*Sal*I digestion created a ~1530 bp CYP PCR fragment and a 4916 bp vector backbone. Ligating the PCR fragment into the vector backbone pASK-IBA_BMR resulted in the final plasmid pASK-IBA33_CYP-BMR_XS. This created the constructs pASK-IBA33_CYP6A1-BMR_XS, pASK-IBA33_CYP6G1-BMR_XS, pASK-IBA33_CYP6AE14-BMR_XS, pASK-IBA33_CYP4G1-BMR_XS and pASK-IBA33_CYP4G2-BMR_XS.

3.14 Construction of CYP4G fusion enzymes with a short linker

For the construction of fusion proteins with a shortened (20 amino acids) BM3 linker the pASK-IBA33_CYP4G_BMR_XS (without BM3 N-Terminus) constructs were used as templates. A schematic representation of the construction is shown in Figure 4-37. For the PCR amplification the same *Xba*I forward primers and newly designed reverse primers, which were again creating *Sal*I restriction enzyme sites, were used, see Table A.2.4-1. The plasmid pASK-IBA33_BM3 and the PCR products, CYP4G1

and CYP4G2, were double digested with *Xba*I and *Sal*I. The backbone pASK-IBA33_BMR and the PCR fragments were ligated. By this two plasmids have been generated: i) pASK-IBA33_CYP4G1-BMR_shortLinker, ii) pASK-IBA33_CYP4G2-BMR_shortLinker. After that, *E. coli* TOP10 cells were transformed with the constructed plasmid. *E. coli* BL21 (DE3) cells were transformed with the plasmid after the size of the plasmid was verified by colony PCR and the sequence was verified by sequencing with the respective primers (Table A.2.4-2).

3.15 Construction of a CYP4G Fusion Enzyme with a P450 Gene from *Forficula auricularia*

A schematic representation of the construction of CYP4GForficula-BMR fusion is shown in Figure 4-42. For the gene amplification of CYP4G from *Forficula auricularia* ten earwig larvae were frozen in liquid nitrogen and their mRNA was extracted using the mRNA gene isolation kit (Roche). Subsequently, the mRNA was transcribed into cDNA using the primers listed in Table A.2.4-3, to amplify the ORF of CYP4G by PCR on this cDNA pool were designed based on transcriptomic *F. auricularia* data [51] (Table A.2.4-3). The cDNA was used as template for PCR amplification of the CYP4GF gene. The PCR product was ligated into the pCR-TOPO blunt vector. The PCR on plasmid pCR_CYP4GF using a Pfu proofreading polymerase and primers (Table A.2.4-1) that add *Bsa*I restriction sites and a C-terminal His_6-tag to the amplificate was conducted under the conditions mentioned in section 3.2. The PCR product and the vector pASK-IBA33plus were double digested with *Bsa*I, purified and ligated to create the vector pASK-IBA33_CYP4GF. For final construction of pASK-IBA33_CYP4GF_BM3 the vector pASK-IBA33_CYP4GF was used as a PCR template. The PCR was performed with a primer pair that creates an N-terminal *Xba*I or *Kpn*I site and a C-terminal *Sal*I site, which does not include the His_6-tag (Table A.2.4-1). pASK-IBA33_CYP4GF-BMR_XS (without BM3 N-terminus) was generated by ligating the *Xba*I-*Sal*I cut, 1757 bp PCR fragment *CYP4GF_XS* into the 4916 bp vector backbone pASK-IBA33_BMR purified from a *Xba*I-*Sal*I digestion of pASK-IBA33_BM3. pASK-IBA33_CYP4GF-BMR_KS (with BM3 N-terminus), was generated by ligating the *Kpn*I-*Sal*I cut, 1590 bp PCR fragment *CYP4GF_KS* into the 5113 bp vector backbone pASK-IBA33_BMR purified from a *Kpn*I-*Sal*I digestion of pASK-IBA33_BM3. After that *E. coli* TOP10 cells were transformed with the constructed

plasmid and the sequence verified. *E. coli* BL21 cells were transformed with the plasmid for protein production.

3.16 Construction of a Duet-Vector with P450 and hCPR Genes without Linker

For the construction of a pET-Duet-1 vector with an insect P450 gene and the hCPR gene for coexpression without a linker the construct pCDF-Duet-1_hCPR (which was constructed by A. Baumann) and pASK-IBA33_CYP were used. A schematic representation of the construction is shown in Figure 4-46. pCDF-Duet-1_hCPR was double digested with *Nde*I, which cuts at the N-terminal site of the gene, and *Aat*I, which cuts at the C-terminal site of the gene. The same enzymes were used for the double digestion of the pET-Duet-1 vector. The purified fragments were ligated and *E. coli* TOP10 cells were transformed with the constructed plasmid pET-Duet-1_hCPR. After confirming the sequence via colony PCR and sequencing of the plasmid, using the respective primers (Table A.2.4-1) the plasmid was used for further construction. The second plasmid pASK-IBA33_CYP was used as a template for PCR with a primer pair creating a *BamH*I site N-terminal and a *Not*I site C-terminal to the gene (Table A.2.4-1). The PCR product and the pET-Duet-1_hCPR plasmid were double digested with *BamH*I and *Not*I, purified and ligated. *E. coli* TOP10 cells were transformed with the constructed plasmid, pET-Duet-1_CYP_hCPR. *E. coli* BL21 (DE3) cells were transformed with the plasmid whose size was verified by colony PCR.

3.17 Overnight Culture

For overnight cultures 5 ml or 50 ml of LB medium with an appropriate antibiotic were inoculated with either a single colony of an LB agar plate or from a cryo-stock. The cultures were grown at 37°C for 16 hours. 5 ml cultures were shaken at a speed of 220 rpm and 50 ml cultures at a speed of 180 rpm.

3.18 Cryo-Stocks

Cryo-stocks were prepared in order to preserve the plasmid DNA for storage in cloning and expression strains of *E. coli*. For this purpose 500 µl of an overnight culture were transferred into a Roti-Store cryo vial (Roth), mixed and incubated for

two min. After removing the supernatant from the cryo rings the vials were stored at -80°C.

3.19 Plasmid Isolation

Plasmid isolation was performed with the Quick Lyse Miniprep Kit (Qiagen). Cells of 4 ml overnight culture were used according to the vendor's protocol. The plasmid DNA was eluted in either 30 µl water, when used for cloning, or elution buffer when used for DNA transformation.

3.20 Expression

Expression conditions of proteins like medium, temperature, induction time, flask, volume etc. vary depending on the plasmid and the application, see Table 3-7. The media were inoculated with fresh 16 h overnight cultures. The gene expression on plasmid pASK-IBA33plus was induced with 200 µg/l anhydrotetracycline and the gene expression on plasmid pCDFDuet-1 and pETDuet-1 was induced with 1 mM IPTG.

Table 3-7: Overview of Expression Conditions.

Application	Testexpression	Purification		GC measurements GI/Schmallenberg	SPME-GC measurements	
flask volume [ml]	100	1000	1000	100	100	25
flask type	plain	baffled	baffled	plain	plain	GC vial
medium	TB	TB	TB	M9	TB	TB
medium volume [ml]	50	400	800	50	50	5
total volume per construct [ml]	50	2000	2400	50	50	5
additives	no	yes	yes	yes	yes	yes
amount overnight culture for inoculation [ml]	5	40	80	0.5	5	0.5
shaking [rpm]	180	180	180	180	180	180/130
temperature until induction [°C]	37	37	37	37	37	37
induction time	at OD_{600} ~1	after 1.5 h	after 1.5 h	at OD_{600} ~0.1-0.2	after 1.5 h	after 1.5 h
temperature during expression [°C]	37	28	28	37/28	37/28	37
duration [h]	4	4	4	0-48	4	4

3.21 SDS-Polyacrylamide Gel Electrophoresis (SDS-PAGE)

The separation of denatured proteins by their size was enabled by SDS-PAGE with 4-15% Mini- PROTEAN TGX gels (Bio-Rad) with 10 or 15 wells. The protein samples were mixed with 3x Laemmli buffer to a total volume of 15 µl, heated at 95°C for 10 min and loaded into the wells. 5 µl of a protein size marker were also loaded as a reference into one well. Separation was achieved by running the gel in Rotiphorese 10x SDS-PAGE buffer at 300 mV for 17 min. Visualization of the proteins was achieved by immersing the gel in Roti-Blue quick for at least 30 min. The gel was documented using the VersaDoc Quantitiy One Software (4.6.9) with the filter setting for Coomassie Blue.

3.22 Western Blot Immunodetection

Western blot was performed when the protein could not be correctly identified or visualized by SDS-PAGE or when degradation of a protein should be determined. The proteins separated by SDS-PAGE were electrophoretically transferred to a polyvinylidene difluoride (PVDF) membrane by a semi-dry method (Trans-Blot-Turbo, Bio-Rad). The membrane was equilibrated for 10 min in methanol. Afterwards the membrane, the filter papers and the SDS-PAGE gel were incubated for 15 min in SDS-transfer buffer. The protein was transferred for 30 min with 30 mA/cm^2. After blotting, the membrane was washed twice with TBS buffer for 10 min at room temperature. An anti-penta-histidine-antibody (Qiagen) was used, which is directed against the His_6-oligopeptide, since all proteins were expressed with a terminal His_6-tag. The membrane was incubated for one hour in a blocking solution containing 1% casein protein. Then the membrane was washed twice for 10 min with TBS/T buffer and once for 10 min with TBS buffer. After this, the membrane was incubated for one hour with antibody solution (Anti His HRP, 1:1000 in 0.5% blocking solution) and washed again twice with TBS and once with TBS/T for 10 min each. The antibody was labelled with peroxidase and was detected by the oxidation of Luminol following the manufacturer’s protocol. Chemiluminescence was documented using the VersaDoc Quantity One Software (4.6.9) with filter settings Chemie Hi Sensitivity.

3.23 Protein Quantification

3.23.1 BCA-Assay

The determination of the protein amount was performed with the Thermo Scientific Pierce BCA Protein Assay, which is based on the Biuret reaction. In alkaline solution proteins form a complex with bivalent copper ions which reduces them to monovalent copper ions. The cuprous cations together with bicinchoninic acid (BCA) form a purple complex, which can be detected at 562 nm. The microplate assay was carried out as described in the manufacturer's protocol using a bovine serum albumin (BSA) standard curve (BSA concentrations ranging from 5-2000 µg/ml).

3.23.2 Photometric Determination of Protein Concentration

For fast analysis the protein amount was determined using absorption at 280 nm (absorption of aromatic amino acid residues). Absorbance coefficients for the fusion constructs were determined depending on their amino acid sequence, shown in Table 3-8.

Table 3-8: Extinction coefficients at 280 nm of proteins.

Name	Extinction coefficient at 280 nm
CYP6G1-BMR_XS	0.918
CYP6G1-BMR_KS	0.928
CYP6A1-BMR_XS	0.966
CYP6A1-BMR_KS	0.973
BM3	1
hRed	1.279
BMR	1.142
CYP6G1d22	0.826
CYP6A1d22	1.008
Aldehyddecarbonylase	0.834
Acyl-ACP reductase	0.989
CYP4G1-BMR	1.037
CYP4G2-BMR	0.971
CYP6A1-BMR_shortLinker	0.974
CYP6G1-BMR_shortLinker	0.925

Name	Extinction coefficient at 280 nm
CYP4G1-BMR_shortLinker	1.036
CYP4G2-BMR_shortLinker	1.034
CYP4GF-BMR_shortLinker	1.010

The buffer in which the protein was eluted was used as reference. 2 µl reference and 2 µl sample were pipetted on a Take3 plate and the absorbance was measured at 280 nm.

3.24 Cell Lysis

3.24.1 Ultra-Sonic Homogenizer

For cultures with volumes smaller than 100 ml cell lysis was performed using the ultrasonic homogenizer Sonopuls HD2200 with a MS 72 sonotrode (Bandelin). The cell lysis was performed on an ice water bath in a rosett cell. The size of the rosett cell was chosen depending on the culture volume. Sonication was performed four times for one minute at 32% power and 3 times 10% cycles with two min breaks in between to prevent overheating of the sample.

3.24.2 Homogenizer

Cultures with volumes bigger than 100 ml were lysed using the homogenizer M-110P (Microfluidics). The interaction chambers of the device were cooled by an ice water bath. The sample was passed through the machine twice with 1500 bar and collected on ice.

3.25 Protein Purification

3.25.1 Fusion Protein Purification (at RT)

3.25.1.1 IMAC via His_6-tag (Ni-NTA)

The cells were resuspended in 200 ml lysis buffer (RT) (pH 7.5, 30 mM Tris-HCl, 100 mM NaCl, 20% glycerol, proteinase inhibitors, 1% CHAPS was added after cell lysis) (Table A.2.7-2) and lysed twice by microfluidization. The lysed cells were centrifuged at 75600 g for 30 min at 10°C. The supernatant was filtered through a Rotilabo-syringe filter with a pore size of 0.22 µm and loaded on a freshly packed

and conditioned 12 ml Ni-NTA column, connected to the SE04 system (ECOM) at room temperature with a flow-rate of 1 ml/min. The column was washed with buffer A (RT) (pH 7.5, 30 mM Tris-HCl, 100 mM NaCl, 20 % glycerol (v/v), 0.1% CHAPS) (Table A.2.7-2) at 3 ml/min until the baseline was reached. The enzyme was eluted with 200 mM imidazole at 3 ml/min flow-rate. The purification was monitored using two channels with 280 nm and 410 nm. The collection of the fractions of interest was started when A_{280} and A_{410} started to increase and stopped when the baseline was reached.

3.25.1.2 Anion-Exchange Purification (at RT)

For the anion exchange purification the pooled IMAC fractions were used. After dilution (10 fold) in anion exchange buffer A (RT) (pH 7.4, 10 mM NaOH, 20% glycerin, 0.1% CHAPS) (Table A.2.7-2) the sample was loaded on a 20 ml DEAE-Sepharose column at 1 ml/min flow-rate and washed with anion exchange buffer A until the baseline was reached. The enzyme was eluted in two steps, first with 500 mM NaCl at 1 ml/min flow-rate, which eluted the protein of interest and then the column was rinsed with 1 M NaCl. Collection of the fractions of interest was started when the A_{280} and A_{410} started to increase and stopped when the baseline was reached.

3.25.2 Fusion Protein Purification

3.25.2.1 IMAC via His_6-tag (Ni-NTA) (at 4°C)

All steps were performed on ice. The cells were resuspended in 40-60 ml lysis buffer 1 (pH 7.5, 30 mM Tris-HCl, 100 mM NaCl, 20% glycerol) (Table A.2.7-3), depending on their growth and lysed. The lysed cells were centrifuged at 75600 g for 1 hour at 10°C. The supernatant was loaded on a freshly packed and conditioned 3 ml Ni-NTA column, connected to the ÄktaPrime (at 4°C) with 1 ml/min. The column was washed with buffer A (pH 7.5, 30 mM Tris-HCl, 100 mM NaCl, 20% glycerol (v/v), 30 mM imidazole) (Table A.2.7-3) at 3 ml/min flow-rate until the baseline was reached. The enzyme was eluted with 250 mM imidazole at 3 ml/min flow-rate.

3.25.2.2 Anion-Exchange Purification at (4°C)

All steps were performed on ice. For the anion exchange purification 3 ml of pooled IMAC fractions were used. They were diluted 10 fold in anion exchange buffer A (pH 7.4, 20 mM Tris-HCl, 20 % glycerin) (Table A.2.7-3) to a final volume of 30 ml. The sample was loaded on a 1 ml DEAE-Sepharose column, connected to the ÄktaPrime (at 4°C) at 0.5 ml/min flow-rate and washed with anion exchange buffer A (Table A.2.7-3) until the baseline was reached. The enzyme was eluted with 500 mM NaCl at 1 ml/min flow-rate. The collection of the fractions of interest was started when the A_{280} started to increase and stopped when the baseline was reached.

3.25.3 hCPR Purification

3.25.3.1 IMAC via His_6-tag (Ni-NTA)

The cells of 2.4 l culture were resuspended in 200 ml lysis buffer (Table A.2.7-4) and lysed twice by microfluidization. The lysed cells were centrifuged at 75600 g for 60 min at 10°C. When Table A.1.1-1 shows only one centrifugation step the supernatant was filtered through a Rotilabo-syringe filter with a pore size of 0.22 µm and loaded on a freshly packed and conditioned 10 ml Talon or Ni-NTA column (Table A.1.1-1), connected to the SE04 system (ECOM) at room temperature with a flow-rate of 5 ml/min. If Table A.1.1-1 indicates two centrifugation steps the supernatant was discarded and the cells were resuspended in lysis buffer (Table A.2.7-4) and lysed by ultrasonication. After centrifugation at 75600 g for 30 min at 10°C the supernatant was filtered through a Rotilabo-syringe filter with a pore size of 0.22 µm and loaded on 10 ml Ni-NTA column, as described above. The column was washed with buffer A (Table A.2.7-4) at 5 ml/min flow-rate until the baseline was reached. The enzyme was eluted with 100 mM imidazole at 5 ml/min flow-rate. The purification was monitored using three channels with 280 nm. The collection of the fractions of interest was started when the A_{280} started to increase and stopped when the baseline was reached.

3.25.3.2 Anion-Exchange Purification

For the anion exchange purification the pooled IMAC fractions were used. Those were diluted in 10 volumes of IMAC buffer A (Table A.2.7-4). The sample was loaded on a 3 ml Source Q 15 column at 1 ml/min flow-rate and washed with anion exchange

buffer A until the baseline was reached. The enzyme was eluted with an increasing NaCl gradient from 0 mM to 500 mM over 20 column volumes, which eluted the protein of interest and then the column was rinsed with 1 M NaCl. The collection of the fractions of interest was started when A_{280} started to increase and stopped when the baseline was reached.

3.25.4 BM3 Purification

3.25.4.1 IMAC via His_6-tag (Ni-NTA)

The cells of 2.4 l culture were resuspended in 200 ml lysis buffer and lysed twice by microfluidization. The lysed cells were centrifuged at 75600 g for 30 min at 10°C. The supernatant was filtered through a Rotilabo-syringe filter with a pore size of 0.22 µm and loaded on a freshly packed and conditioned 15 ml Ni-NTA column, connected to the SE04 system (ECOM) at room temperature with a flow-rate of 5 ml/min. The column was washed with buffer A (pH 7.5, 30 mM Tris-HCl, 100 mM NaCl, 20 % glycerol (v/v)) (Table A.2.7-5) at 5 ml/min flow-rate until the baseline was reached. The enzyme was eluted with 100 mM imidazole at 5 ml/min flow-rate. The purification was monitored using two channels with 280 nm and 410 nm. The collection of the fractions of interest was started when the A_{280} and A_{410} started to increase and stopped when the baseline was reached.

3.25.4.2 Anion-Exchange Purification

For the anion exchange purification the pooled IMAC fractions were used. Those were diluted in 10 volumes of anion exchange buffer A (pH 7.4, 10 mM NaOH, 20% glycerol) (Table A.2.7-5). The sample was loaded on a 5 ml Q Sepharose column at 5 ml/min flow-rate and washed with anion exchange buffer A (Table A.2.7-5) until the baseline was reached. The enzyme was eluted with an increasing NaCl gradient from 0 mM to 500 mM over 10 min, which eluted the protein of interest and then the column was rinsed with 1 M NaCl. The collection of the fractions of interest, was started when the A_{280} and A_{410} started to increase and stopped when the baseline was reached.

3.26 Photometric Heme Detection

A photometric measurement of purified fusion enzyme fractions was performed to determine if the heme is still present after purification. The test was performed using the photometer (analytic Jena) and 1 ml cuvettes scanning from 300 to 500 nm. 500 µl of appropriate buffer was used as blank and 500 µl of undiluted elution samples were tested afterwards.

3.27 Enzyme Activity Test

3.27.1 Photometric NADPH Detection

$NADP^+$ absorbs in UV at 259 nm due to the adenine base, whereas NADPH absorbs at 259 nm and 340 nm. This difference allows the detection of a conversion of one to the other when monitoring the absorption at 340 nm.

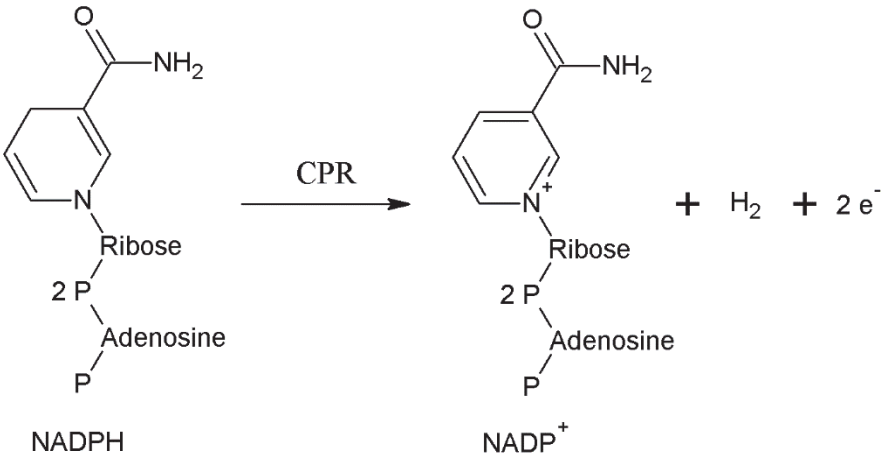

Figure 3-1: Reaction of NADPH to NADP+ catalyzed by P450 reductase.

This method was used to determine the activity of the reductase domain by monitoring the conversion of NADPH to $NADP^+$. The reaction is shown in Figure 3-1. It can be used to measure the fusion enzyme activity indirectly by measuring the turnover of NADPH by the reductase domain. The electron flow is shown in Figure 3-2.

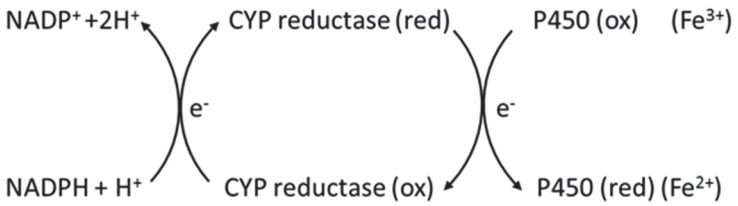

Figure 3-2: Electron flow from NADPH to reduced P450.

Equal amounts of NADPH and substrate were used. The 200 µl reaction mixtures contained 10 µl/100 µl purified fusion enzyme, 0.1 mM NADPH, 0.1 mM substrate and 25 mM Tris-HCl, with 20% glycerin (v/v), pH 7.5. All measurements were run with three controls in comparison, without NADPH, without substrate and with denatured enzyme using the Eon plate reader (Biotek). The oxidation of NADPH was monitored at 340 nm over time with one read per minute.

3.27.2 Photometric Cytochrome c Assay

The photometric cytochrome c assay was used for the hCPR activity determination. Thereby cytochrome c is used as a surrogate substrate for hCPR, which changes its color from its oxidized to reduced form. The color change is detectable at 550 nm. The assay was performed based on the Nature protocol by Guengerich and coworkers [52]. The reaction mixtures contained 40 µM cytochrome c, a determined volume of purified hCPR and 300 mM potassium phosphate buffer pH 7.7 added to a final volume of 990 µl. The baseline was determined at 550 nm for 3 min. After this the reaction was started by adding 100 µM NADPH and measuring for 3 min at 550 nm.

3.27.3 Photometric *p*NCA-Assay

The enzyme activity of BM3 can be tested directly by the photometric *p*NCA-assay. *p*-nitrophenoxycarboxylic acids (pNCA) can be used as surrogate substrates for BM3. The enzyme catalyzes *p*NCA to yellow *p*-nitrophenolate, which is detectable at 410 nm, and the corresponding *ω*-oxycarboxylic acid [53], see Figure 3-3.

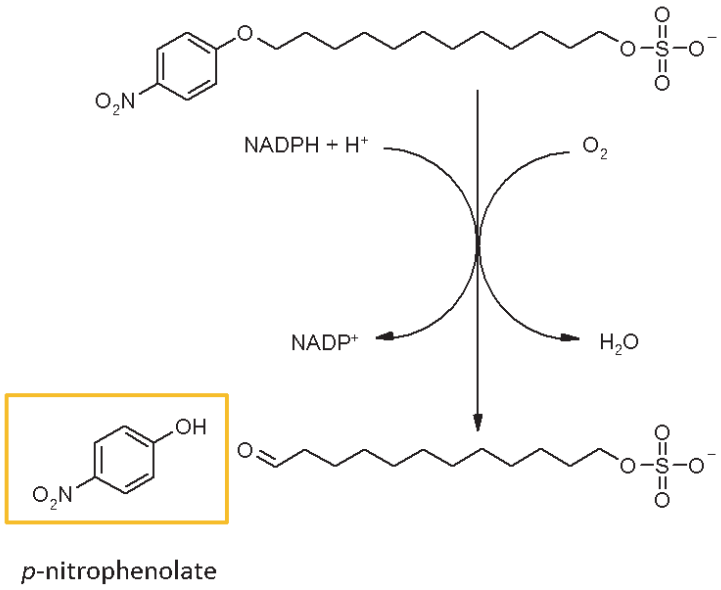

Figure 3-3: Enzyme catalysis of *p*NCA to yellow *p*-nitrophenolate and the corresponding *ω*- oxycarboxylic acid.

3.28 Lyophilization

Lyophilization was performed to exchange solvent for GC- or LC-MS analysis. The samples containing substrate dissolved in dichlormethane (imidacloprid) or methanol (aldrin) were lyophilized in 2 ml Eppendorf tubes in an CHRIST RVC 2-33IR for about 1.5 hours until all solvent was dissolved.

3.29 Liquid Chromatography Mass Spectrometry (LC-MS)

3.29.1 In-House Measurements

Prior to the sample measurements the LC-MS protocol was developed for the analyte imidacloprid. For this, the standards were measured using different LC settings and analyte concentrations, starting with 1 µg/ml and decreasing. The photometrically measured samples were either desalted or mixed 1:2 with acetonitrile for LC-MS measurements. For desalting SEP-PAK PlusLight C_{18} cartridges (Waters) were used. They were conditioned with 2 ml methanol followed by 2 ml water. The sample was loaded on the cartridge, washed with 3 ml water and eluted in 1 ml methanol. The substrates were concentrated by lyophilization and the solvent was exchanged to acetonitrile. The substrate and products were determined by LC-MS measurements using an Ultimate 3000 (Dionex) equipped with a reversed-phase column (Kinetex

2.6 u C18, 100 Å, 150 x 2.1 mm, Phenomenex) connected to an Ion Trap amaZon ETD mass spectrometer (Bruker). The HPLC method used water with 0.1% formic acid as solvent A and acetonitrile with 0.1% formic acid as solvent B. The method lasted 20 min at a flow-rate of 250 µl/min with 20% solvent B at the beginning for two min. The solvent B concentration was increased to 90% over 8 min. The concentration was kept for 8 min. The MS program used electrospray ionization with alternated polarity with a scan from 80-550 m/z. The ESI nebulizer ran with 1 bar, dry gas with 8 l/min and the dry temperature was set to 220°C.

3.29.2 Ultraperformance Liquid Chromatography (UPLC)-MS

UPLC-MS measurements were performed at the company Chromicent in Berlin following the method of Kamel [54]. A LC-MS/MS instrument consisted of a Waters UPLC equipped with an AQUITY HSS T3 column (100 x 2.1 mm internal diameter, 1.8 µm particle size) (Waters) coupled to a Waters Xevo TQ-S micro MS detector. The HPLC method used water with 0.1% formic acid as solvent A and acetonitrile as solvent B. The method lasted 17 min with a flow-rate of 0.5 ml/min with 95% solvent A at the beginning for three min. The solvent B concentration was linearly increased to 60% in 12 min. The concentration was held for two min. The injection volume was 5 µl. The MS operated in the positive electrospray ionization mode. The source temperature was set at 120°C with nitrogen flow-rates of 20 l/h for the cone gas and 1000 l/h for the desolvation gas. The desolvation temperature was 600°C. Prior to the measurements standard curves of imidacloprid and imidacloprid-olefin (3.125 µg/ml, 6.25 µg/ml, 12.5 µg/ml, 25 µg/ml, 50 µg/ml, 100 µg/ml, 200 µg/ml) were measured in triplicates whereby the 200 µg/ml concentrations were excluded since they were too high. Imidacloprid and imidacloprid-olefin were quantified by the corresponding standard curve. The stocks of the standards were set up in a 10 fold concentration in methanol and mixed as shown in Table 3-9. The samples were prepared as shown in Table 3-10.

Table 3-9: Setup of Imidacloprid and Imidacloprid-Olefin Standards for UPLC-MS measurements.

Setup Standards			
		total volume [µl]	200
substrate	starting concentration	final concentration	vol [µl]
tris buffer (pH 7.5)	100 mM	25 mM	50
imidacloprid	10x standard	1x standard	20
NADPH	10 mM	0.5 mM	10
CYP6G1-BMR			100
water			20

Table 3-10: Setup of enzyme reaction with imidacloprid as substrate for UPLC-MS measurements.

Reaction Setup			
		total volume [µl]	500
substrate	starting concentration	final concentration	vol [µl]
tris buffer (pH 7.5)	100 mM	25 mM	125
imidacloprid	1 mg/ml	100 µg/ml	50
NADPH	10 mM	0.5 mM	25
CYP6G1-BMR			160
water			140

After incubation at room temperature for 25 h the samples were mixed 1:1 with acetonitrile and send on ice to the company.

3.30 Gas Chromatography Mass Spectrometry (GC-MS)

3.30.1 Aldrin and Dieldrin Detection by GC-MS (in-house)

Substrate and product were determined by GC-MS measurements using an Agilent 5977 Series GC/MSD System equipped with a HP-5ms Ultra Inert (30 m x 250 µm x 0.25 µm) column. From the photometrically measured samples (400 µl) aldrin and dieldrin were mixed with 10 µl chlorden (1 mg/ml) as internal standard and extracted twice with two times 400 µl methylene chloride. The dichloromethane extracts were dried with sodium sulfate and concentrated by lyophilization (3.28). The solvent was exchanged to a final volume of 200 µl hexane. 1 µl of the sample was injected with a splitless injection mode for 1 min. The GC

program started with 50°C column oven temperature hold for 2 min, then heated up to 300°C with 10°C/min and a final hold for 8 min. The carrier gas was helium with a flow-rate of 1 ml/min. The MSD transfer line temperature was 250°C and the MS was operated with EI energy of 70 eV and full scan mode with a mass range of m/z 50 to 400.

3.30.2 Alkane Detection by GC-MS (in house)

The measurements were performed on a GC-MS CT 1128 (Constellation Technology Corporation) equipped with a VF-5MS column (30 m x 0.25 mm internal diameter, 0.25 µm film thickness, Agilent Technologies). The injector and transfer line temperatures were 230°C and 260°C, respectively. The GC method was established by analyzing an alkane standard (C8-C20) (4 µg/µl) which was added to an *E. coli* culture. 25 mg pellets of expression cultures were mixed with ethyl acetate and sonicated for 5 min at 33% power (3.24.1). After this the mixture was centrifuged at 14000 g for 20 min at 4°C. The supernatant was transferred into a glass vial and analyzed by GC-MS. The method was 26 min long and started at 70°C oven temperature. The temperature increased linear to 300°C at a rate of 10°C per minute.

3.30.3 Alkane Detection by GC-MS (Schmallenberg)

For sample preparation expression cultures from 400 ml and 800 ml TB medium or 50 ml and 400 ml M9 medium were harvested. For the analysis 140 mg pellet of the M9 cultures or 220 mg pellet of TB cultures were mixed with 1 ml ethyl acetate. The mixtures were sonicated on ice for 3 min at 20% power with a MS 72 sonotrode in a glass centrifuge tube (3.24.1). Subsequently, the samples were centrifuged for 1 min at 4500 rpm and 4°C. The supernatants were transferred with a glass pipette into a glass vial. 5 ml of the supernatant of the expression cultures were mixed with 2.5 ml ethyl acetate. The samples were sonicated in the ultrasonic water bath for 3 min. After this the samples were centrifuged for 1 min at 4500 rpm and 4°C. The supernatants were transferred with a glass pipette into a glass vial.

For the GC-MS detection an Agilent Technologies 5973 equipped with a Rxi-5HT column (30 m x 0.25 mm internal diameter, 0.25 µm film thickness) (Restek) was used. The program started at 50°C which was held for 4 min. The temperature increased linearly to 300°C at a rate of 20°C/min. The temperature was held for

25 min. After this the temperature increased to a final temperature of 350°C at a rate of 15°C/min. The temperature was held for 3 min. The helium carrier gas ran at a flow-rate of 1.2 ml/min. The MS source temperature was 250°C and the MS quad temperature 180°C.

3.30.4 Solid-Phase Microextraction (SPME)-GC-MS

The detection of aldehydes and alkanes in coexpression cultures was performed with SPME-GC-MS. Analytes were enriched at 37°C for 30 min on a SPME fiber (Supelco polydimethylsiloxane, 100 µm thickness) exposed to the headspace of a 5 ml sample of a 4 h expression culture in a 20 ml glass vial. The analysis was performed using an Agilent 5977 Series GC/MSD System equipped with a HP-5ms Ultra Inert (30 m x 250 µm x 0.25 µm) column. The SPME desorption was performed for 1 min in the GC injector in a splitless injection mode. The GC injector temperature was 250°C and the SPME fiber was conditioned under helium in an independent injector port for 5 min at 250°C. The GC-MS method is the same as for aldrin detection using GC-MS (in-house) (3.30.1)

3.30.5 SPME Measurements with added Aldehyde (no Coexpression)

The detection of produced alkanes in single-expression cultures was performed with SPME-GC-MS. The substrate octadecanal (1 µg/µl) or a C8-C20 aldehyde (4 ng/µl) mixture were added (10 µl or 100 µl respectively) to the expression system at t_0 of the protein production. The enrichment and measurements were performed as described in 3.30.4.

3.31 Photometric Heme Substrate Binding Test

The binding of a substrate at the heme binding domain of a P450 enzyme leads to a peak absorption shift from its former maximum towards higher wavelength, depending on the P450. The test was performed at a photometer (analytic Jena) using 1 ml cuvettes. The baseline was determined using 400 µl of the appropriate buffer plus 40 µl DMSO (solvent of the substrate). The first measurement from 300 to 500 nm was performed with 400 µl of an undiluted elution sample of CYP6G1-BMR, or denatured CYP6G-BMR and 40 µl DMSO. After this measurement 400 µl of the same samples were mixed with 40 µl 1 mg/ml imidacloprid in DMSO and

measured from 300 nm to 500 nm. The different measurements were compared to see if the peak shifts from 425 nm to another wavelength.

4 Results and Discussion

4.1 Purification Approach

To establish the "Molecular Lego" system for insect P450s the following approach was performed. First the insects P450s had to be selected. The selection was based on the P450s origin, the sequence availability and their potential substrates should be known to enable activity measurements (Table 4-1).

Table 4-1: Overview of selected insect P450s for this study.

P450	Origin	Substrates	GenBank
CYP6A1	*Musca domestica*	heptachlor, aldrin [55]	M25367.1
CYP6G1	*Drosophila melanogaster*	imidacloprid, DDT, methoxychlor [56]	AAF58557.1
CYP6AE14	*Helicoverpa armigera*	(gene expression is induced by) gossypol [57]	DQ986461.1
CYP4G1	*Drosophila melanogaster*	C24 C26 and C28 aldehydes [30]	Q9V3S0.1
CYP4G2	*Drosophila melanogaster*	octadecanal [30]	EF615002.1

The aim was to design and construct a variable insect P450-BMR fusion where the insect P450 can be swapped and produced in *E. coli* and purified without the addition of detergents. *E. coli* was chosen as expression host since it is well described and often used for the expression of soluble proteins. To be sure that the building blocks can be produced active in *E. coli* pretests were performed to determine the best conditions (A.1).

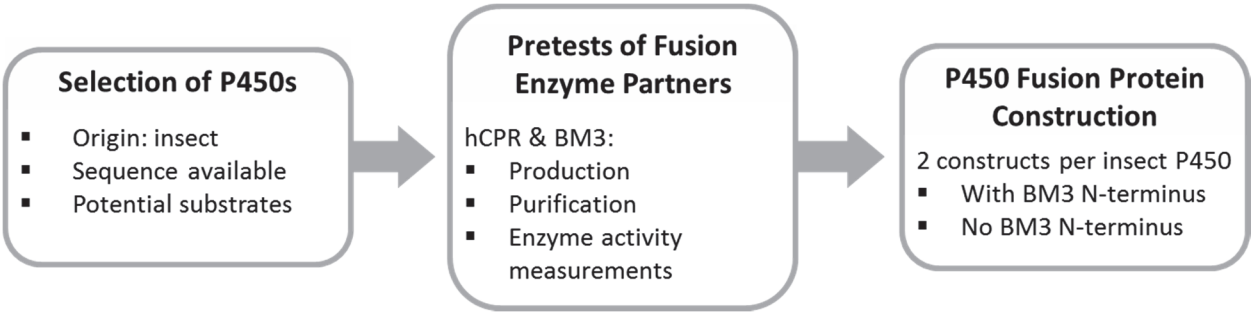

4.2 Construction of Insect P450 Fusion Enzymes

4.2.1 Genetic Analysis of CYP6A1, CYP6G1, CYP6AE14, CYP4G1, CYP4G2

The multiple sequence alignments of all used insect P450s are shown in Figure 4-1 and Figure 4-2. Within the CYP6 family the CYP6AE14 does have more differences towards CYP6A1 and CYP6G1 than CYP6A1 to CYP6G1. The sequence difference is reflected by their catalytic reactions. CYP6A1 and CYP6G1 both oxidize insecticides, aldrin and imidacloprid, respectively [55-56]. CYP6AE14, on the other hand, is predicted to have gossypol as substrate [57]. The size, shape and amino acid composition of the enzyme binding pocket determines the substrate specificity[58]. The substrates molecule size is an important factor for the substrate specificity. This can be seen here for the selected enzymes and their substrates. Gossypol has a molar mass of 518.563 g/mol, which is bigger than aldrin with a molar mass of 364.91 g/mol and imidacloprid with a molar mass of 255.66 g/mol.

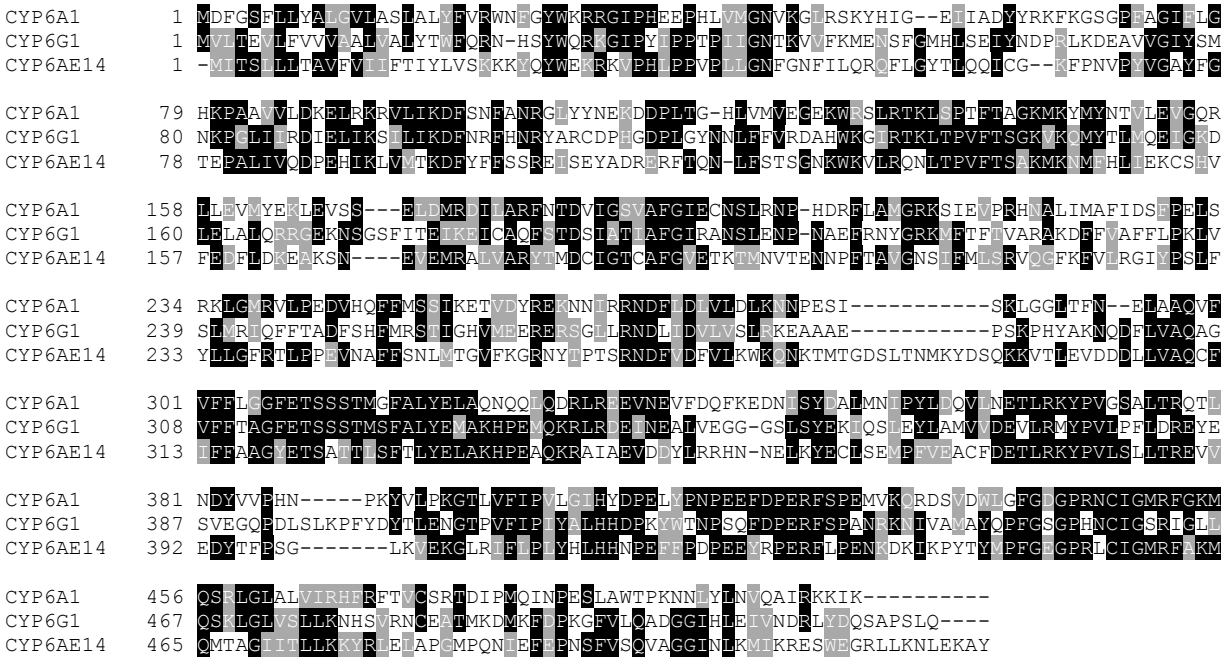

Figure 4-1: Multiple sequence alignment of the family CYP6 P450s (CYP6A1, CYP6G1 and CYP6AE14) used in this study. Black and gray shading represent amino acid identity and similarity, respectively.

The members of subfamily CYP4G show very high sequence similarities (Figure 4-2). Similar catalytic activities have also been demonstrated for CYP4G1 and CYP4G2, they both use long-chain aldehydes as substrates and catalyze them to long-chain alkanes.

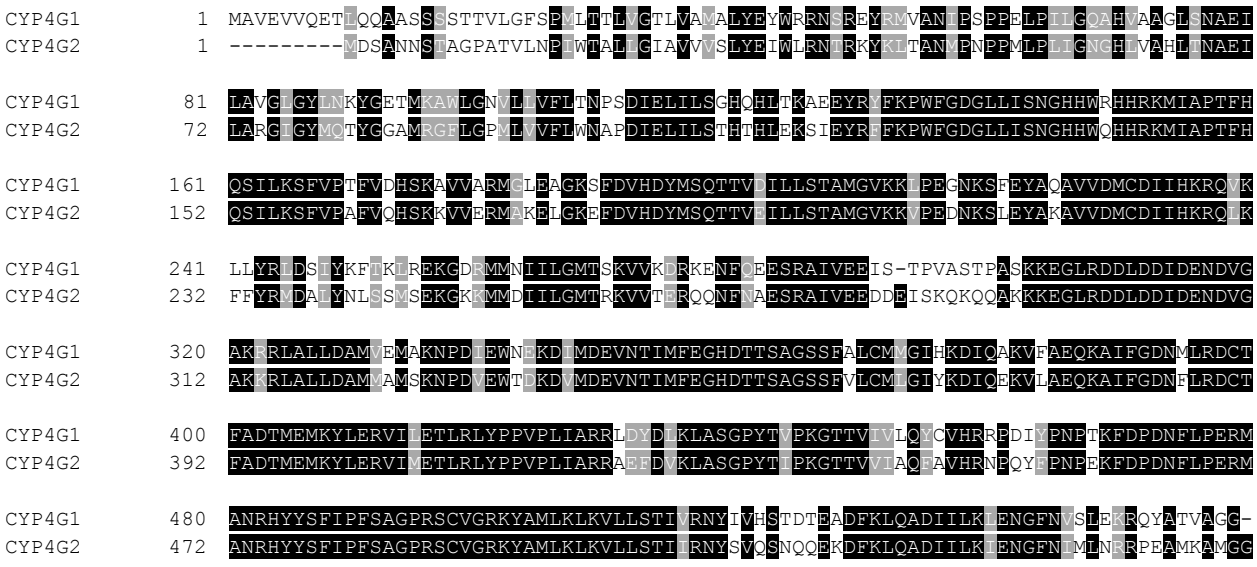

Figure 4-2: Sequence alignment of the subfamily 4G P450s (CYP4G1 and CYP4G2) used in this study. Black and gray shading represent amino acid identity and similarity, respectively.

As representatives of the two families CYP6G1 and CYP4G1 from the same organism, *Drosophila melanogaster*, were aligned to identify similarities (Figure 4-3). The amino acid sequence *EXXR* (yellow) and *CXG* (blue) are conserved in P450s. Otherwise both sequences do not show many similarities, which is typical for the different P450 families with their broad range of substrates [59].

```
CYP6G1     1 ------------------------MVLTEVLFVVVAALVALYTWFQRNHSYWQRKGIPYIEPTPIIGNTKVVFKMENSFG
CYP4G1     1 MAVEVVQETLQQAASSSSTTVLGFSPVLTTLVGTLVAVALYEYWRRNSREYRMVANIPSPELPILGQAIVAAGLSNAEI

CYP6G1    57 MHLSEIYNDPRLKDEAVVGIYSMNKPGLIIRDIELIKSILIKDFNRFHNRYARCDPHGDPLGYNNLFFVRDAHWKGIRTK
CYP4G1    81 LAVGLGYLNKYGETMKAWLGNVLLVFLTNPSDIELILSG------HQHLTKAEEYRYFKPWFGDGLLISNGHHWRHHRKM

CYP6G1   137 ITPVFTSGKVKQMYTLMQEIGKDLELALQRRGEKNSGSFITEIKEICAQFSTDSIATIAFGIRANSLENPNAEFRNYGRK
CYP4G1   155 IAPTFHQSILKSFVPTFVDH---SKAVWARMGLEAGKSFD--VHDYMSQTIVDILLSTAMGVKLPEGNKSFEYAQAVVD

CYP6G1   217 MFTFTVARAKDFFVAFFLPKLVSLMR-----------------IQFFTADFSHFMRSTIGHVME----------ERERSG
CYP4G1   230 MCDIIHKRQVKLLYRLDSIYKFTKLREKGDRMMNIILGMTSKVVKDRKENPQEESRAIVEELSTPVASTPASKKEGLRDD

CYP6G1   270 LLRNDLIDVLVS----LRKEAAAEPSKPHYAKNQDFLVAQAGVFFTAGFETSSSTMSFALYEMAKHPEMQKRLRDEINEA
CYP4G1   310 LDDIDENDVGAKRRLALLDAMVEMAKNPDIEWNEKDINDEVNTIMFEGHDTTSAGSSFALCMMGIHKDIQAKVFAEQKAI

CYP6G1   346 LVEGGG-SLSYEKIQSLEYLAMVVDEVLRMYPVLPFLDREYESVEGQPDLSLKPFYDYTLENGTPVFIPIYALHHDPKYW
CYP4G1   390 FGENMLRDCTFADTMEMKYLERVTLETLRLYPPVPLLARRLDYDLKLASG------PYTVPKGTTVIVLQYCVHRPDIY

CYP6G1   425 TNPSQFDPERFSPANRKNIVAMAYQPFGSGPHNCIGSRIGLLQSKLGLVSLLKNHSVRNCEATMKDMKFDPKGFVLQADG
CYP4G1   464 PNPTKFDPDNFLPERMANRHYYSFIPFSAGPRSCVGRKYAMLKLKVLLSTIVRNYIVHSTETEADFKLQADIILKLENGF

CYP6G1   505 GIHLEIVNDRLYDQSAPSLQ
CYP4G1   544 NVSLEKRQYATVAGG-----
```

Figure 4-3: Sequence alignment of the representatives (CYP6A1 and CYP4G1) of each P450 family (CYP6 and CYP4). Black and gray shading represent amino acid identity and similarity, respectively. The conserved amino acid patterns *EXXR* (yellow) and *CXG* (blue) are characteristic for P450s.

4.2.2 Construction of Insect P450 Fusion Enzymes based on the Natural Fusion Enzyme BM3

Eukaryotic P450s and their P450 reductases are dependent on each other and membrane bound. This makes them difficult to produce recombinantly, but there are bacterial P450 enzymes, which do not have a membrane anchor and thus are easier to produce recombinant. A remarkable bacterial enzyme is the enzyme CYP102A1 (BM3) from *Bacillus megaterium.* The enzyme is not membrane bound and furthermore a natural fusion enzyme. It contains three domains, the N-terminal P450 (BM3-P450), a linker and the C-terminal reductase (BMR) (Figure 4-4) which makes it a self-sufficient fusion enzyme, which is independent of further enzymes.

Figure 4-4: Schematic representation of the three domain structure of BM3.

The construction of P450 fusion enzymes based on BM3 shall overcome the disadvantages of eukaryotic P450s described above. This approach will enable the soluble recombinant production, purification and activity measurements of insect P450s.

Our approach is following the “Molecular Lego” principle constructed by Gilardi for membrane bound human P450s [23]. Following this principle the P450 domain of the BM3 will be replaced by an insect P450, which leads to a construct of a C-terminal insect P450 attached to the BM3 linker and N-terminal BMR domain (Figure 4-5).

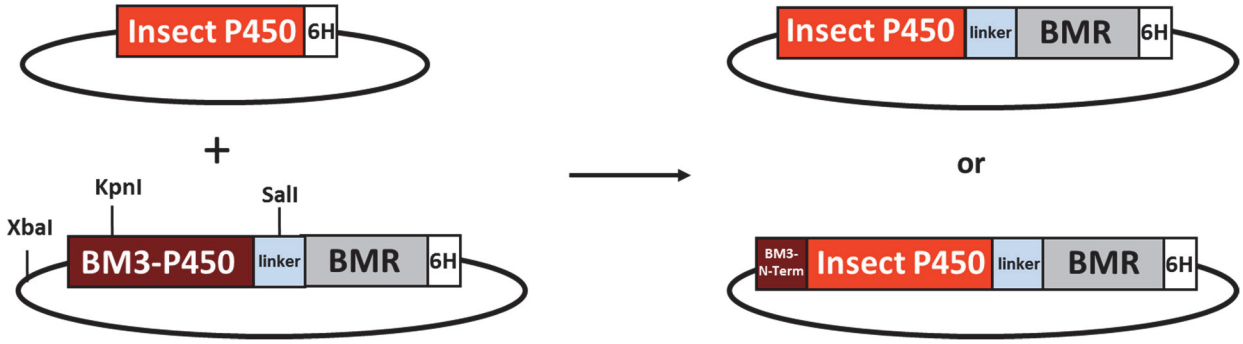

Figure 4-5: Schematic representation of starting genes and final fusion constructs. Starting genes: insect P450 and BM3, including the utilized restriction enzyme sites *Xba*I, *Kpn*I and *Sal*I. Final fusion constructs: insectP450-BMR without BM3 N-Terminus and insectP450-BMR with BM3 N-Terminus.

To enable better solubility of our fusion construct the N-terminus of the insect P450, which contains the membrane anchor domain, was truncated by approximately 20 amino acids. In the process it is important not to truncate too much, otherwise the P450 activity is decreased, the study showed that the amino acid residues 21-82 of the human CYP2E1 are crucial for heme incorporation and correct heme pocket folding [60]. The N-terminus should not include hydrophobic amino acids and the exact amount was determined based on human P450 studies used for fusion enzyme construction [23]. Figure 4-6 and Figure 4-7 show the N-terminus of the constructs with the selected positions, highlighted in green, where the N-terminus is truncated.

Figure 4-6: Sequence alignment of the N-termini of CYP6A1, CYP6G1 and CYP6AE14. / indicates the determined start of the N-terminally truncated P450. . -//- indicates that the sequence is not shown in complete length.

Figure 4-7: Sequence alignment of the N-termini of CYP4G1 and CYP4G2. / indicates the determined start of the N-terminally truncated P450. -//- indicates that the sequence is not shown in complete length.

To further optimize the solubility of the designed fusion enzymes a construction setup was established, which contains 52 amino acids of the BM3 N-terminus in front of the insect CYP N-terminus (Figure 4-8 A) which will be called *KS*. To compare if this yields to a higher solubility an additional construction setup without a BM3 N-terminus was created (Figure 4-8 B). The construction of those two different fusion enzymes was achieved by using either the *Kpn*I or the *Xba*I cloning site. The *Kpn*I site is located 156 base pairs downstream the N-terminus of the BM3 P450 domain. Using this site will create a construct with a BM3 N-terminus. Using the *Xba*I cloning site, which is located on the vector backbone 42 base pairs upstream of the BM3 N-terminus, will create the construct without the BM3 N-terminus. The construction of both fusion enzymes is based on the same starting plasmids and shown in Figure 4-8.

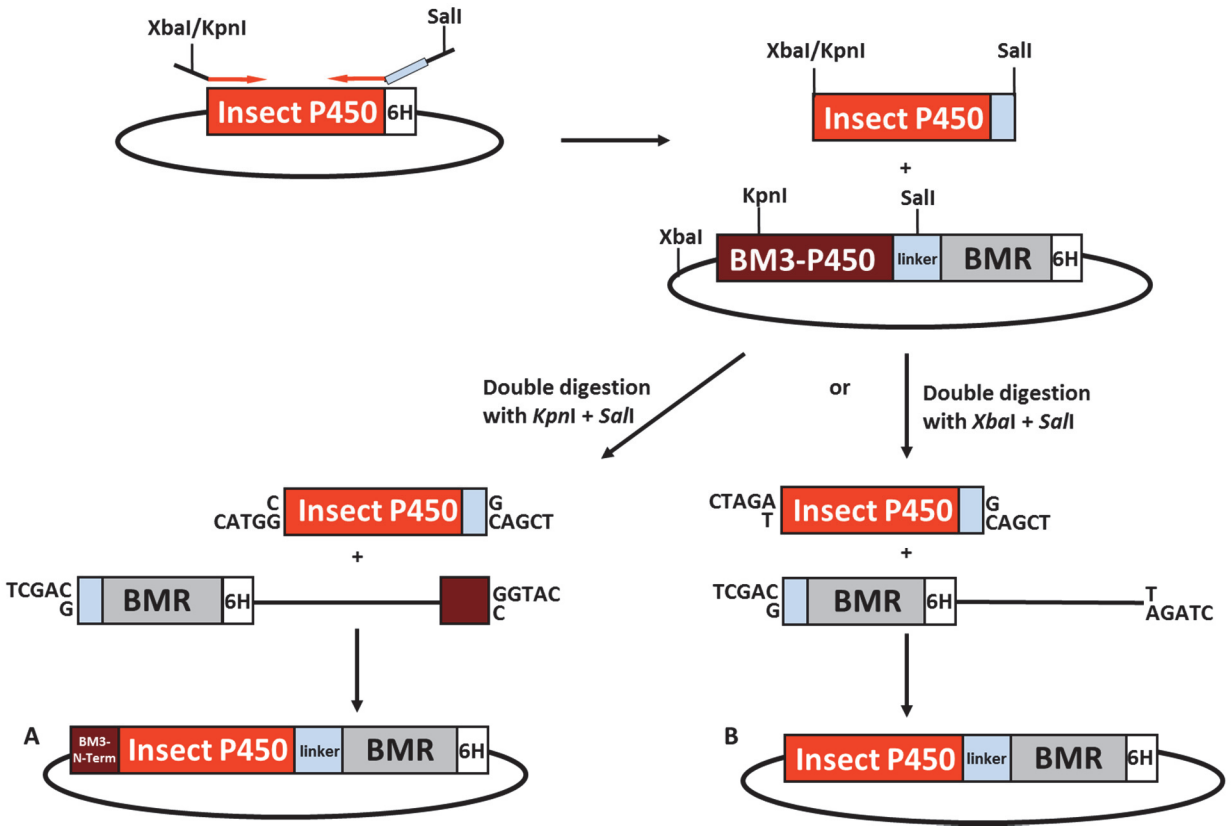

Figure 4-8: Schematic representation of insect P450-BMR fusion enzyme construction. **A**: Construct CYP-BMR_KS, **B**: Construct CYP-BMR_XS

The linker length is very important for the fusion enzyme activity since it determines the interaction of the BMR domain and the P450 domain, thus allowing electron flow from BMR to the catalytic center of the P450 domain [61-63]. A BM3 linker reduced by six amino acids inactivates the fusion enzyme by inhibiting the domain interaction [46]. Therefore, we chose a linker length of 29 amino acids. An overview of all constructs generated by this method is listed below in Table 4-2.

Table 4-2: Overview of constructed fusion proteins.

P450	Origin	Cloning Sites	Name Fusion Protein	Abbreviation
CYP6A1	*Musca domestica*	*Kpn*I, *Sal*I	pASK-IBA33_ CYP6A1_BM3_*KS*	CYP6A1-BMR_KS
		*Xba*I, *Sal*I	pASK-IBA33_ CYP6A1_BM3_*XS*	CYP6A1-BMR_XS
CYP6G1	*Drosophila melanogaster*	*Kpn*I, *Sal*I	pASK-IBA33_ CYP6G1_BM3_*KS*	CYP6G1-BMR_KS
		*Xba*I, *Sal*I	pASK-IBA33_ CYP6G1_BM3_*XS*	CYP6G1-BMR_XS
CYP6AE14	*Helicoverpa armigera*	*Kpn*I, *Sal*I	pASK-IBA33_ CYP6AE14_BM3_*KS*	CYP6AE14-BMR_KS
		*Xba*I, *Sal*I	pASK-IBA33_ CYP6AE14_BM3_*XS*	CYP6AE14-BMR_XS
CYP4G1	*Drosophila melanogaster*	*Kpn*I, *Sal*I	pASK-IBA33_ CYP4G1_BM3_KS	CYP4G1-BMR_KS
		*Xba*I, *Sal*I	pASK-IBA33_ CYP4G1_BM3_XS	CYP4G1-BMR_XS
CYP4G2	*Drosophila melanogaster*	*Kpn*I, *Sal*I	pASK-IBA33_ CYP4G1_BM3_KS	CYP4G2-BMR_KS
		*Xba*I, *Sal*I	pASK-IBA33_ CYP4G1_BM3_XS	CYP4G2-BMR_XS

4.2.3 Discussion of the Construction of Insect P450 Fusion Enzymes

P450s are present in various forms in all insect species investigated in this regard. The knowledge about them is limited since it is difficult to produce them as heterologous proteins [1]. Gilardi and coworkers were able to show by the “Molecular Lego” approach the possibility of soluble expression of membrane bound human P450s [49, 64]. They showed that the construct, P450 2E1-BMR with 21 amino acid reduced N-terminus, was active and that this method can be transferred to other human P450s [23]. The goal of this study was to the transfer the approach to insect P450s. For the soluble expression of insect P450s in *E. coli*, insect P450s were combined with the BMR domain of BM3, which was not yet shown. The selection of the insect P450s was based on the availability of their sequences and the knowledge of their potential substrates (Table 4-1). CYP6A1, CYP6G1 and CYP6AE14 are

members of the xenobiotic metabolism and able to hydroxylate their substrates [57, 65- 66]. CYP4G1 and CYP4G2 are able to decarbonylate aldehydes and thus part of the insect defense, reproduction and communication [30]. *E. coli* was selected as expression organism because it was described best for the production of human P450 fusion enzymes constructed by the "Molecular Lego" method [23, 60]. Furthermore, it was characterized best for soluble protein production [67], which is necessary for the direct activity detection. Usually the vector pCW ori+ is used for the expression of P450s in bacteria. For this work the vector pASK-IBA33plus was selected since it showed good soluble expression of other insect enzymes in *E. coli* [68-69].To enable higher solubility the N-terminal domain of the P450s was truncated. By this the hydrophobic amino acids were discarded which usually bind to the membrane. Further solubility should be achieved by creating constructs which have a BM3 N-Terminus domain in front of the optimized P450 [60]. This created the constructs called KS. As comparison fusion enzymes without a BM3 N-terminus, called XS, were created. The construction was achieved by restriction enzyme cloning. The following chapters of this thesis shall verify if the constructs are expressed soluble and can be purified without detergents and if their activity can be determined.

4.3 Production and Purification of Human Reductase and BM3

To determine the best expression conditions for vector pASK-IBA33plus in *E. coli* BL21 we performed several tests. Each test consisted of separate expressions of the human P450 reductase (hCPR) with a truncated N-terminus and the BM3 enzyme under different conditions (Table A.1.1-1). The results of the tests are shown in appendix (A.1) and were important for the determination of protein production and purification conditions of the fusion enzyme constructs. The enzyme activity measurements (A.1.3 and A.1.4) show that the basic building blocks of the fusion enzymes are produced active.

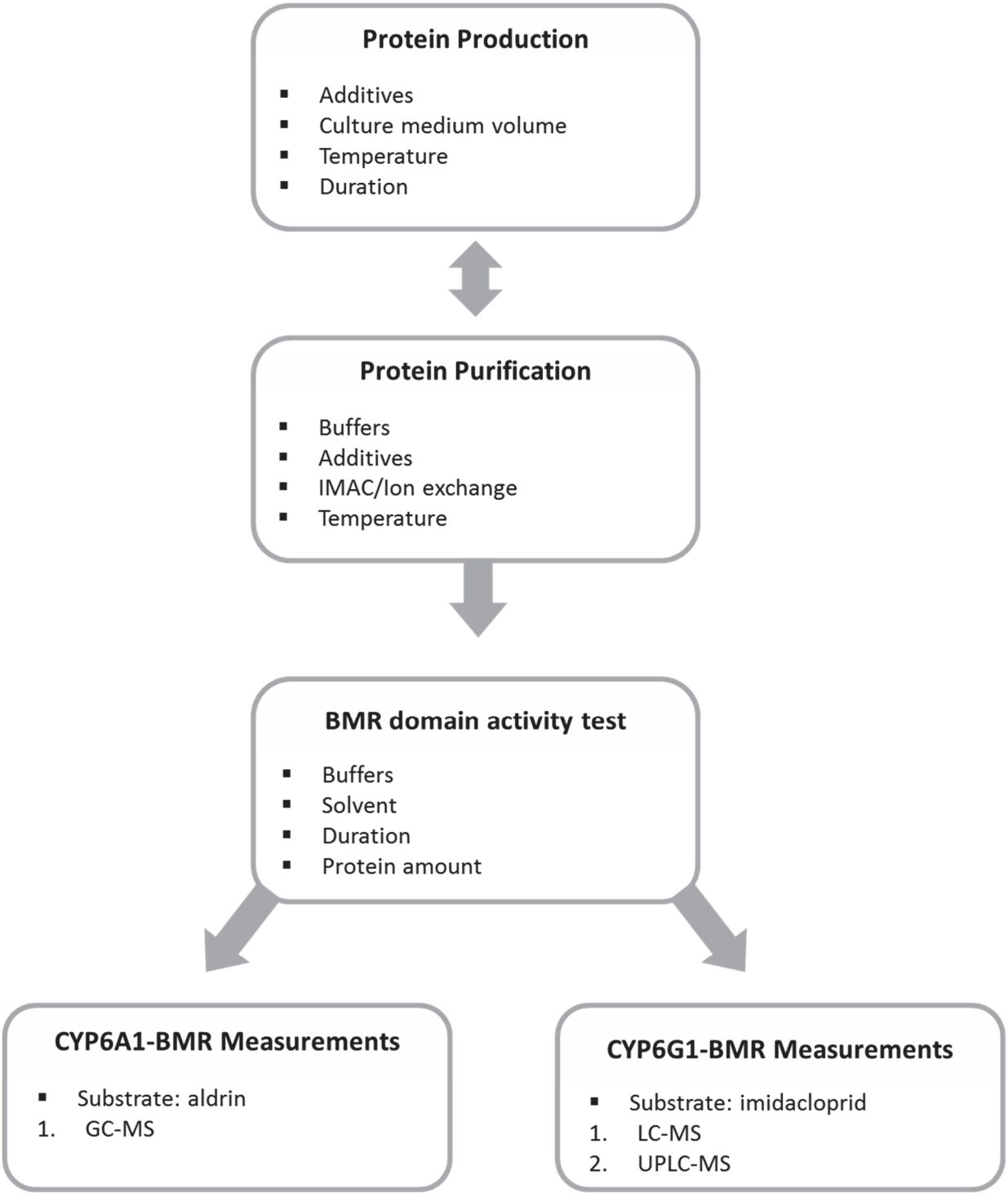
Protein Production
Additives
Culture medium volume
Temperature
Duration
Protein Purification
Buffers
Additives
IMAC/Ion exchange
Temperature
BMR domain activity test
Buffers
Solvent
Duration
Protein amount
CYP6A1-BMR Measurements
Substrate: aldrin
1. GC-MS
CYP6G1-BMR Measurements
Substrate: imidacloprid
1. LC-MS
2. UPLC-MS

4.4 Protein Production and Purification of Insect P450 Fusion Enzymes

4.4.1 Overexpression of Insect P450 Fusion Enzymes in *E. coli*

The overexpression of the insect P450 fusion enzymes for subsequent IMAC purifications was performed based on the knowledge obtained at the preliminary expression tests of hCPR and BM3 (A.1). The expression was performed in TB medium with 1 mM 5-aminolevulinic acid, 1 mM thiamin, 2µM riboflavin, 0,5 mg/l $FeCl_3$ and 80/160 mM D(+)-glucose. The δ-aminolevulinic acid and thiamine are important for the build-up of the heme ring in the P450 domain and glucose shall support the stability of the reductase domain. Protein production was triggered by anhydrotetracycline once *E. coli* cells reached an OD_{600} of 0.5. Cells were grown at 37°C for 4.5 h and harvested by centrifugation prior lyses.

The constructs based on CYP6AE14 did not show good overexpression yields compared to the CYP6A1 and CYP6G1 constructs. Furthermore, the first purification trials did not show any good results. Therefore, we performed all further expression and purification modifications only with the constructs based on CYP6A1 and CYP6G1.

4.4.2 Purification of Insect P450 Fusion Enzymes

4.4.2.1 Purification without Detergents at Room Temperature

The cells were treated as described previously (A.1.2). The supernatant was loaded on a fresh, equilibrated 15 ml Ni-NTA column. The target protein CYP6A1-BMR was eluted with 200 mM imidazole.

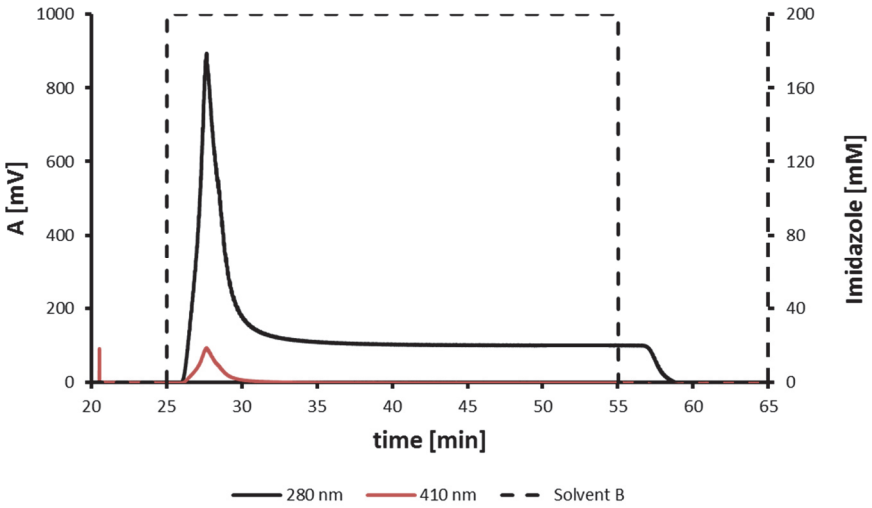

Figure 4-9: Purification of CYP6A1-BMR. Elution profile of the IMAC purification of CYP6A1-BMR.

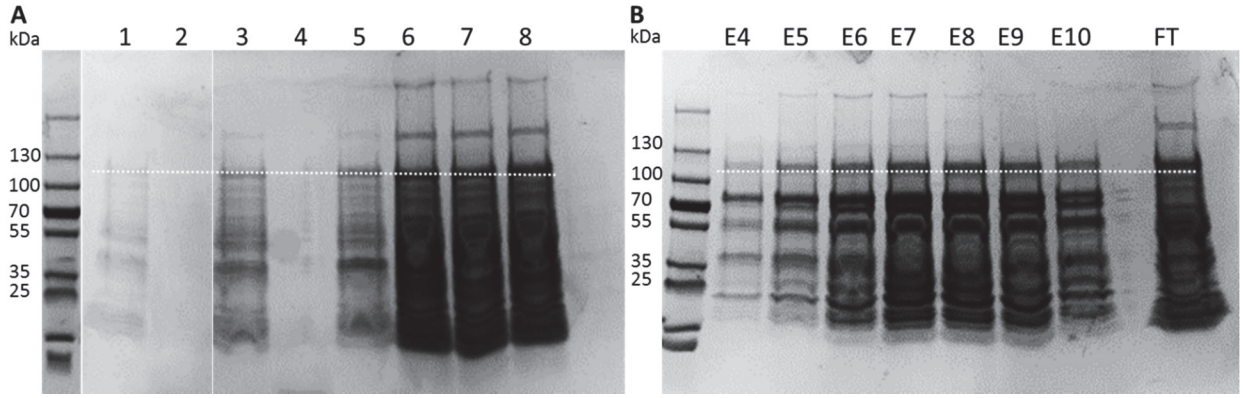

Figure 4-10: SDS-PAGE analysis of sample preparation for IMAC purification and IMAC purified CYP6A1-BMR fractions. **A**: 1-2: t_0 pellet and supernatant, 3-4: $t_{4.5h}$ pellet and supernatant, 6-7: pellet and supernatant after microfluidization, 7: supernatant after centrifugation, 8: after filtration **B**: E4-E10: elution fractions, FT: flow through.

The theoretical molecular weight of the construct CYP6A1-BMR is 121.36 kDa. We did not observe any overexpression in expected size, see Figure 4-10 A well 3 and 4 (indicated by scattered line), and purification did not show satisfactory results, see Figure 4-10 B. This is why we had to modify the approach. The first try was to purify the IMAC samples further by anion exchange purification. The fractions E5-E10 of the IMAC purification were pooled and diluted in ten volumes of anion exchange buffer A (Table A.2.7-2) to enable binding of the protein on a freshly-conditioned 10 ml DEAE-Sepharose anion exchange column.

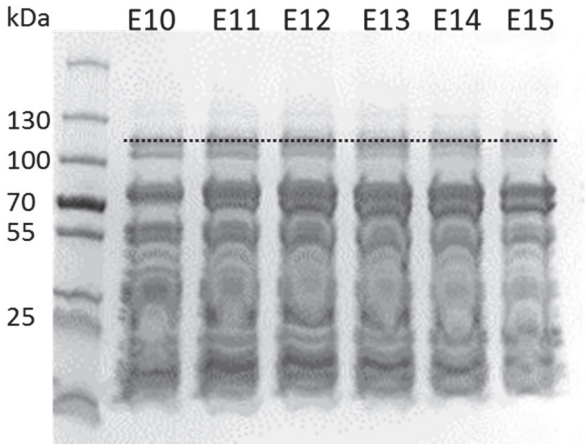

Figure 4-11: SDS-PAGE analysis of the elution fractions E10-E15 of the anion exchange purification of CYP6A1-BMR. M: marker. The scattered line indicates the height of the expected protein size.

This approach was performed with the constructs CYP6G1-BMR as well. CYP6G1-BMR yielded similar results based on SDS-PAGE to the ones shown above from CYP6A1-BMR. The two different constructs, which are based on a single CYP6, KS and XS, show similar results (not shown). For this reason the following experiments were still performed with both constructs.

4.4.2.2 Purification with Detergents at Room Temperature

The anion exchange purification did not lead to any further purification of the target protein. This is why we established new purification approach using CHAPS in the buffers (Table A.2.7-2). Apart from that the cells were treated as before (A.1.2) and the supernatant was loaded on a freshly-equilibrated 12 ml Ni-NTA column. The target protein was eluted with 200 mM imidazole.

To remove the imidazole an anion exchange purification was performed. The fractions E3-E8 of the IMAC purification were pooled and diluted in ten volumes of anion exchange buffer A (0.1% CHAPS) (Table A.2.7-2) to enable binding of the protein on a fresh, conditioned 10 ml DEAE-Sepharose anion exchange column. The chromatogram of the purification using CHAPS as detergent show a single elution peak of the protein of interest, indicated by the 410 nm absorption peak, Figure 4-12.

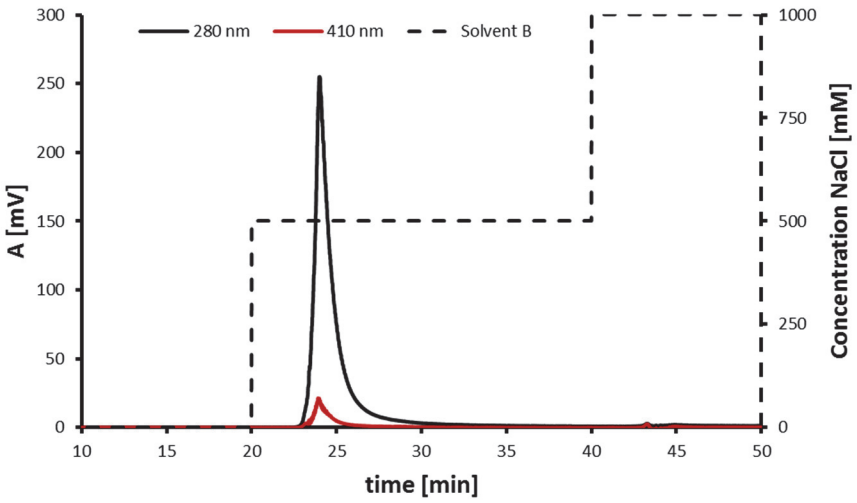

Figure 4-12: Purification of CYP6A1-BMR with CHAPS. Elution profile of the anion exchange purification of CYP6A1-BMR on a DEAE-Sepharose column with buffers containing 0.1% CHAPS.

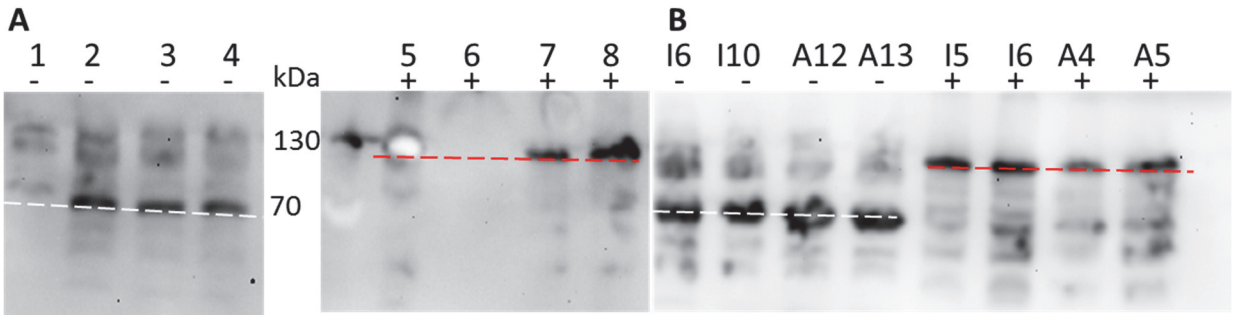

Figure 4-13: Western blot analysis of IMAC and anion exchange purifications of CYP6A1-BMR with or without CHAPS. -: without CHAPS, +: with CHAPS, white scattered line: fragment size of BMR, red scattered line: size of complete CYP6A1-BMR **A**: 1: $t_{4.5h}$ pellet, 2: supernatant after sonication, 3: supernatant after centrifugation, 4: supernatant after filtration, 5: $t_{4.5h}$ pellet, 6: supernatant after sonication, 7: supernatant after centrifugation, 8: supernatant **B**: I5, I6, I10: IMAC fractions 5, 6, 10, A4, A5, A12, A13: anion exchange fractions 4, 5, 12, 13.

The Western blot gels show a comparison of the CYP6A1-BMR samples from before (Figure 4-10 and Figure 4-11) and samples from the new approach using CHAPS. The samples which do not contain CHAPS (Figure 4-13 A+B, white scattered line) show more protein in the size of the BMR domain than the targeted CYP6A1-BMR fusion enzyme. The BMR domain is detectable by Western blot since it contains the His_6-tag at the N-terminus. The samples of the purification preparation containing CHAPS (Figure 4-13 A, red scattered line) show almost only the full fusion protein, but the purified fractions (Figure 4-13 B, red scattered line) show the fusion protein and its degraded products.

4.4.2.3 Final Purification Method without Detergents at 4°C

To enable purification of the complete fusion protein without the use of detergents a new expression and purification approach was tested. For this the expression temperature was changed to 28°C to enable better production of soluble protein. Furthermore, buffers without detergents (Table A.2.7-3) were used and the whole procedure was performed on ice or at cooled devices. The purification was performed as described in section 3.25.2.1. The elution profile (Figure 4-14 A) of the CYP6A1-BMR_XS construct shows a single elution peak when eluting with 250 mM imidazole.

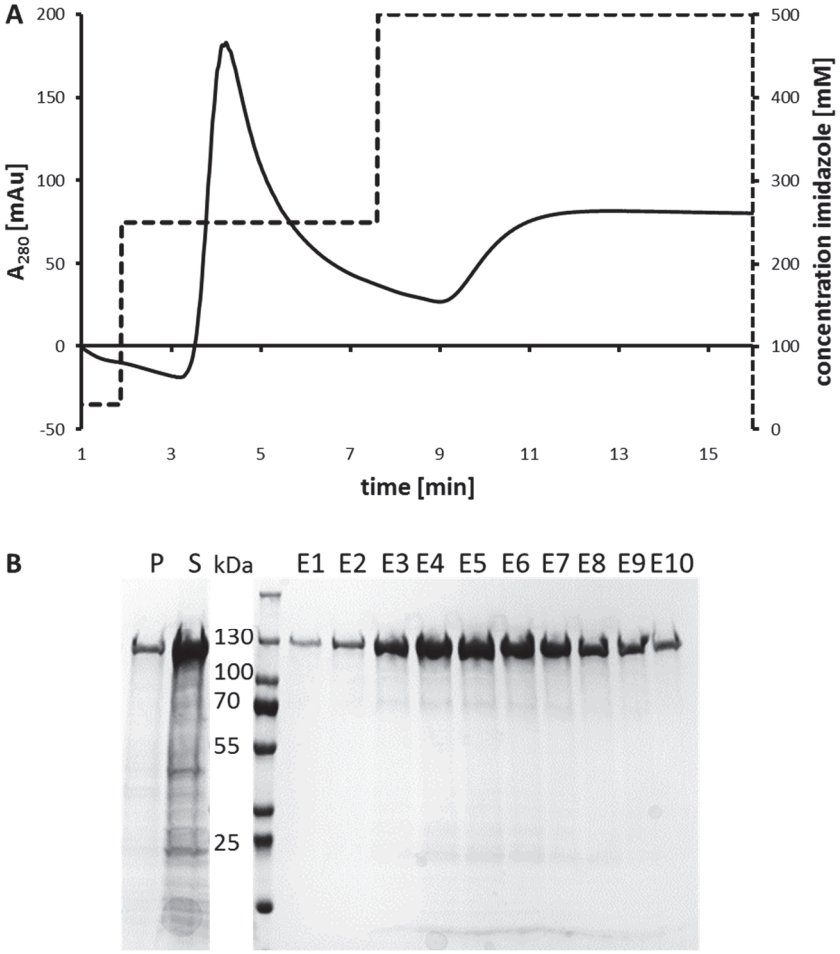

Figure 4-14: Purification of CYP6G1-BMR and CYP6A1-BMR without detergent at 4°C with 250 mM imidazole as eluent. **A**: Elution profile of the IMAC purification of CYP6G1-BMR and CYP6A1-BMR. **B**: SDS-PAGE analysis of the IMAC purified CYP6G1-BMR. P: pellet after sonication and ultracentrifugation, S: supernatant after sonication and ultracentrifugation, 1-10: elution fractions. A single dominant band corresponding to the 120 kDa CYP6G1-BMR is seen in lanes 1-10.

The SDS-PAGE (Figure 4-14 B) shows that the fusion protein is purified and unimpaired which was not the case in the former purifications (Figure 4-13). The IMAC purification yielded a protein concentration of 400 µg/ml. To remove the imidazole an anion exchange purification was performed. The pooled fractions were diluted in 10 volumes of anion exchange buffer (Table A.2.7-3) to enable binding on the DEAE-Sepharose column. A fresh, conditioned 1 ml DEAE-Sepharose anion exchange column was used for anion exchange purification. The diluted protein was loaded on the column with a flow-rate of 0.5 ml/min to enable protein binding. The protein was eluted with sodium chloride. The anion exchange elution profile of CYP6A1-BMR_XS (Figure 4-15 A) shows a major elution peak at approximately 9 min and a smaller elution peak at approximately 11 min. Only the fractions of the major peak were analyzed further.

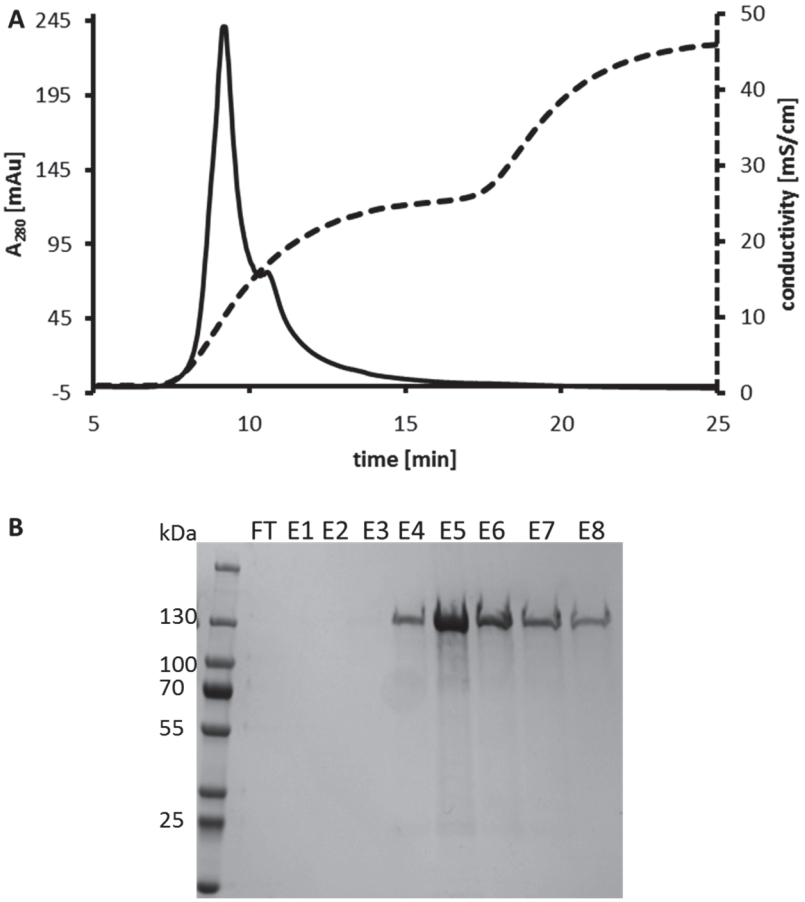

Figure 4-15: Purification of CYP6A1-BMR without detergents at 4°C. **A**: Elution profile of the anion exchange purification of CYP6A1-BMR. **B**: SDS-PAGE analysis of the anion exchanged purified CYP6G1-BMR. M: marker, FT: flow-through, 1-8: elution fractions. A single dominant band corresponding to the 120 kDa CYP6G1-BMR is seen in lanes 4-8.

The SDS-PAGE of the anion exchange purification (Figure 4-15 B) shows as well the fusion protein at its estimated weight. A high purity was reached but only lower concentrations of 300 µg/ml were reached. The purification of CYP6G1-BMR_XS show similar results (not shown), but the constructs with the BM3 N-terminus, CYP6A1-BMR_KS and CYP6G1-BMR_KS, show lower amounts of purified protein. Since the activity of the constructs shall be detected with several methods, a higher protein yield is a big advantage. For this reason the following activity measurements were performed with the constructs without a BM3 N-terminus.

4.4.3 CYP6-BMR BMR Domain Activity

It was not shown before if the cooperative function between the fused domains is possible. To assess whether the BMR domain is correctly folded and fully functional the catalytic activity of the BMR was tested by detection of NADPH consumption. The activity was measured in the presence of aldrin (substrate for CYP6A1 [70]), and imidacloprid (substrate for CYP6G1 [56]), respectively. The assays were performed for 12 h with measurements every minute. Denatured proteins were used as negative control. Figure 4-16 shows the results of IMAC purified CYP6A1-BMR_XS. The relative activity of 100%, determined by NADPH consumption, was reached by CYP6A1-BMR as well as the setup without substrate. The negative control with denatured CYP6A1-BMR shows on the contrary only a residual relative activity of less than 20%.

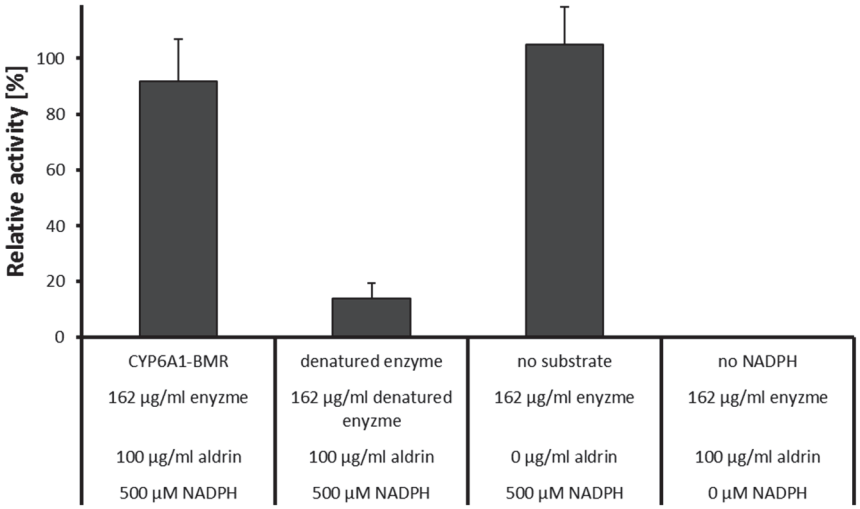

Figure 4-16: BMR activity assay. NADPH turnover of IMAC purified CYP6A1-BMR with aldrin as substrate and of the controls denatured CYP6A1-BMR, no substrate and no NADPH.

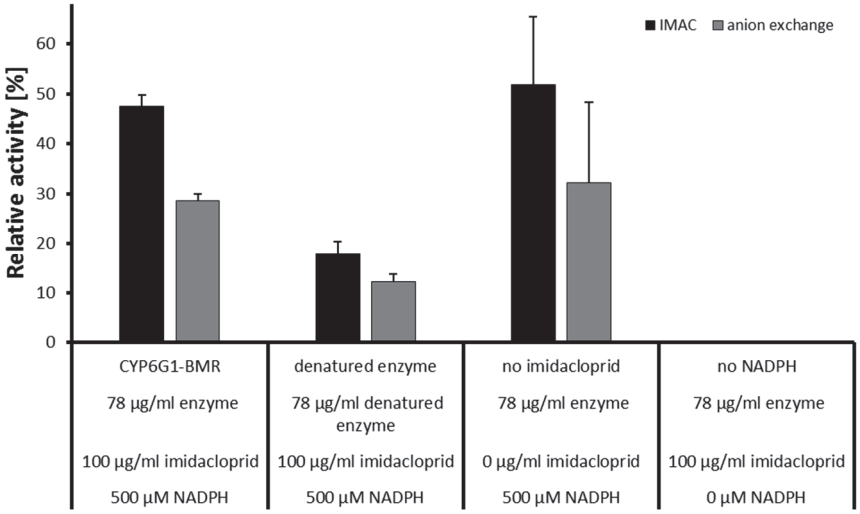

Figure 4-17: BMR activity assay. NADPH turnover of IMAC and anion exchange purified CYP6G1-BMR with imidacloprid as substrate and of the controls denatured CYP6G1-BMR, no substrate and no NADPH.

The measurements with purified CYP6G1-BMR_XS show similar results (Figure 4-17) as the ones with CYP6A1-BMR_XS (Figure 4-16), the lower activity is based on the lower enzyme concentrations used. Additionally, the measurements were performed with anion exchanged purified CYP6G1-BMR_XS. Clear differences between the IMAC and anion exchange samples can be seen (Figure 4-17). The turnover rate of the anion exchange purified sample is only half of the turnover rate of the IMAC purified, except for the negative control with denatured enzyme.

4.4.4 Discussion of Protein Production and Purification of Fusion Enzymes

The verification of the soluble expression and purification without detergents of the insect P450-BMR constructs is described in this chapter. *E. coli* BL21 cells were used as expression system in 400 ml TB cultures with added supplements. The parameter evaluation of the expression and purification process lead to stable, purified insect P450 fusion enzymes. The best results were achieved when expressing at 28°C for 4 h and purification was performed at 4°C without the use of detergents. The expression at 28°C caused a lower protein production rate with the effect of more soluble produced protein [67]. This is an important factor for the purification. Furthermore, the reduction of the temperature during the purification from room temperature to 4°C allowed the stable purification of the fusion proteins without detergents. CYP6A1 was the first purified insect P450. The protein was expressed in *E. coli* and 50% of it were associated with the membrane fraction [26]. The soluble, purified protein was used for direct electrochemistry, which avoids the construction of a fusion protein [71-72]. *E. coli* produced and purified CYP6G1 was shown for the first time in 2013 by Cheesman *et al.*. A two-step purification for the removal of formerly used detergents was necessary [28]. The protein expression and purification of CYP6AE14 was not shown before. Former studies only focused on the detection of its upregulation due to xenobiotic and gossypol treatment [57], this lead to the use of RNAi mediated crop protection against the cotton bollworm [73-75]. The stable produced proteins CYP6A1-BMR and CYP6G1-BMR allowed further experiments. BMR activity could be determined fast photometrically and was performed after each purification to verify if further activity measurements by GC- or LC-MS were useful. The assay was developed and used to ensure that the redox domain was functional and not inhibited by any of the used reagents. The high activity in the no substrate control can be explained with the independent activity of the BMR domain. Govindaraj and Poulos showed that the BMR domain can be produced recombinant active without the P450 domain [48]. This is why the presence of the P450 substrate is not necessary for the BMR activity determination, but it was still added to exclude inhibiting factors for the BMR activity. The KS constructs showed lower protein yields after expression and purification, especially for the CYP6G1 construct. Furthermore the KS constructs showed lower NADPH turnover

than the XS constructs. Those were the reasons to only proceed further with the XS constructs.

As initial conclusion it can be said that the soluble expression in *E. coli* and purification of insect P450-BMR fusion enzymes is possible and that the solubility was increased in comparison to the unmodified insect P450s (Figure 4-18).

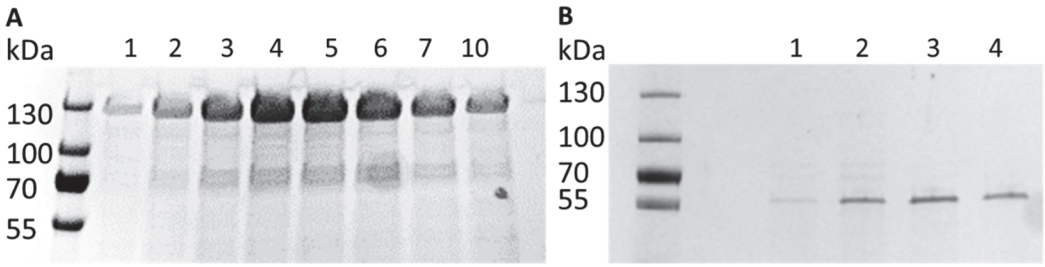

Figure 4-18: SDS-PAGE of IMAC purified protein. **A**: CYP6G1-BMR **B**: CYP6G1.

All following experiments were performed with the XS constructs, since they showed the better protein yields and the subsequent activity tests were performed immediately after purification to avoid impairment of the protein.

4.5 GC-MS Measurements of Aldrin Conversion to determine CYP6A1-BMR activity

4.5.1 Establishment of GC-MS method

The activity of the P450 domain and a good cooperative function between the fused domains of the fusion construct CYP6A1-BMR can be determined by the turnover rate of the CYP6A1 substrate aldrin to dieldrin, Figure 4-19 [26].

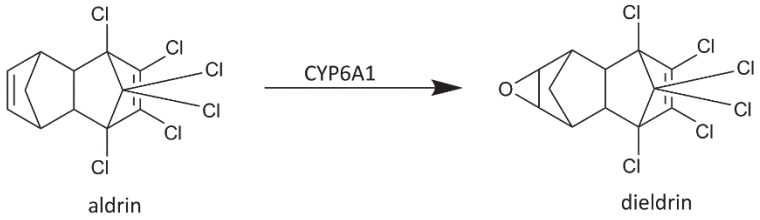

Figure 4-19: Reaction from aldrin to dieldrin catalyzed by CYP6A1.

Activity tests of the fusion construct CYP6A1-BMR were performed in two different setups. The first approach included activity assays of purified enzyme in buffer. For the setup a method for aldrin and dieldrin extraction and a GC-MS method had to be established. Prior to the activity measurements extraction tests without enzyme were performed. The sample volume (100 µl, 200 µl or 500 µl) had to be determined. It

should contain enough enzyme for the conversion of a detectable amount of substrate but also allow the setup of all controls from a single enzyme purification. Furthermore, the volume had to be big enough for phase removal with standard pipet tips. The extraction parameters had to be evaluated since the published protocol was developed for big scale extraction from water samples (http://www.atsdr.cdc.gov/toxprofiles/index.asp, PB2003-100134). The final extraction parameters were that 500 µl dichloromethane containing 10 µl chlorden internal standard (IS) (1 mg/ml) were added to 500 µl incubated sample, because the lower volumes interfered with the phase extraction. Chlorden was selected as IS based on chromatographic behavior and extraction efficiency, which should be similar to the substrates. To test different extraction procedures the upper (aqueous) or lower (dichloromethane) phase was removed and the aqueous phase was re-extracted with an additional 500 µl dichloromethane. The organic phases were pooled and lyophilized until all solvent was evaporated. The sample was dissolved in 250 µl hexane.

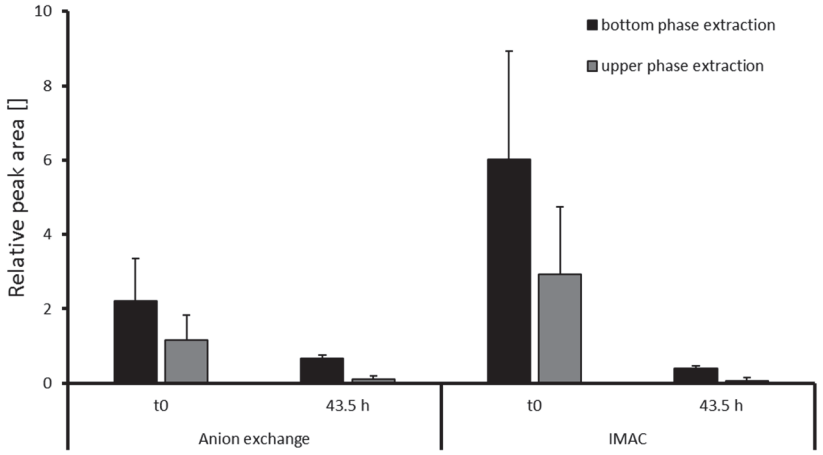

Figure 4-20: Test extraction of aldrin at t_0 and after 43.5 h using dichloromethane. The relative peak area is based on the IS peak area. n=3.

The results (Figure 4-20) show that there is no difference whether to transfer the supernatant or lower phase of the dichloromethane-sample-mixture. The measured amount of aldrin at t_0 in ion exchange buffer is smaller than the amount in IMAC buffer. Whether the ion exchange or IMAC buffer were used the amount of recovered aldrin shrank by incubation time. A significant difference was detected for the different points of time. No significant differences were detected for the upper and bottom phase extraction. The significance was determined using ANOVA single factor test.

4.5.2 Final GC-MS Method and Results

For the activity measurements of purified CYP6A1-BMR 500 µl samples (30 µg/ml or 100 µg/ml CYP6A1-BMR, 100 µg/ml aldrin, 0.5 mM NADPH) were incubated at room temperature for 0 min, 30 min, 1 h, 4 h, 24 h and 43.5 h. After the incubation the substrates were extracted using the method described in (3.30.1).

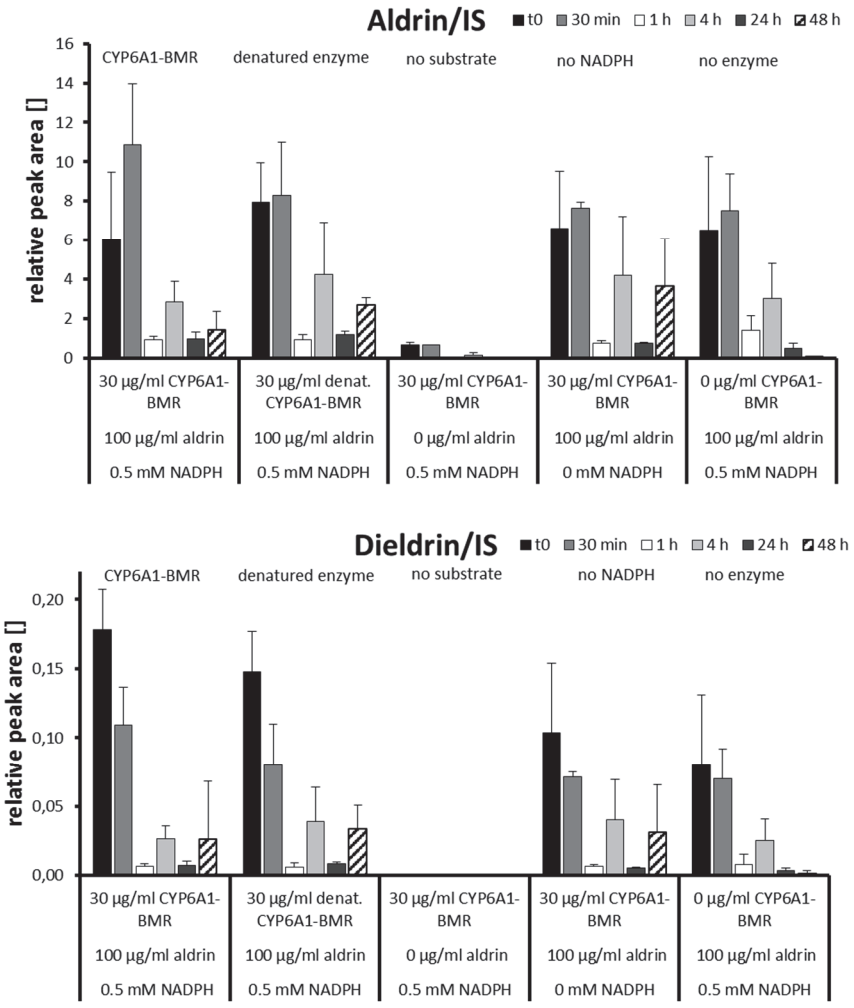

Figure 4-21: GC-MS measurement of IMAC purified CY6A1-BMR incubated with aldrin as substrate at room temperature followed by extraction. The relative peak area is based on the IS peak area. n=3

The same measurement was performed with anion purified CYP6A1-BMR to eliminate imidazole as an inhibiting factor.

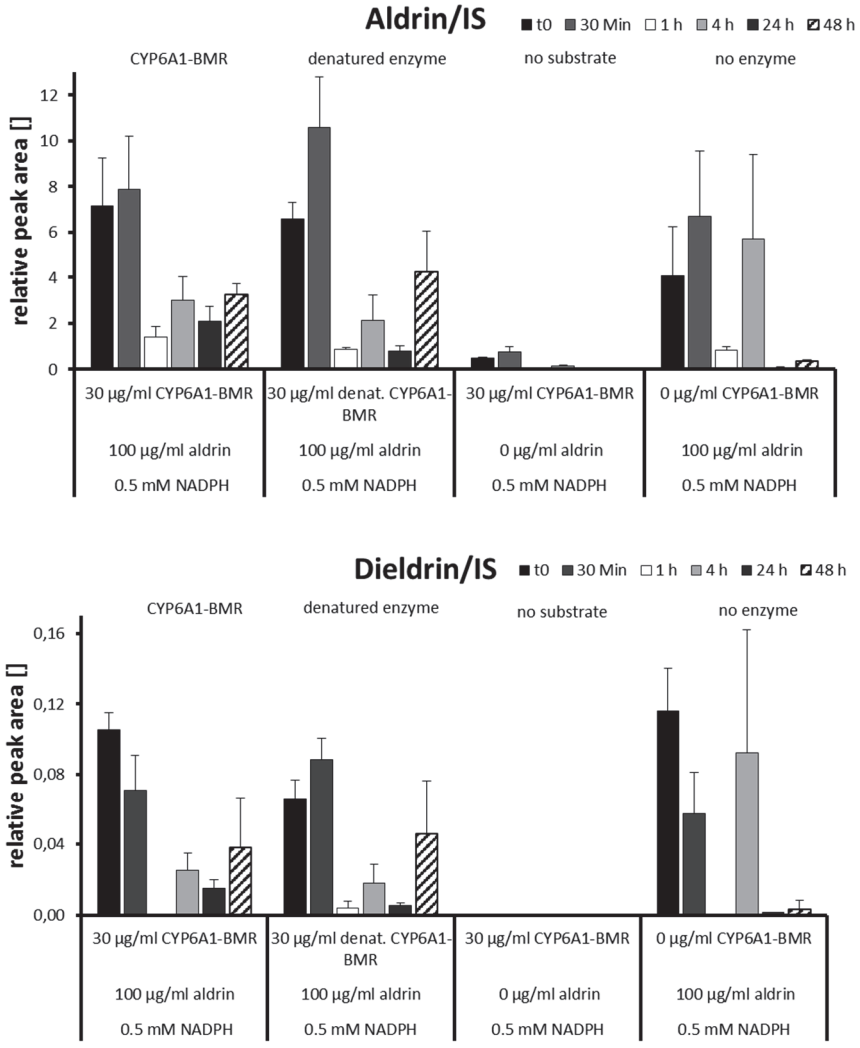

Figure 4-22: GC-MS measurement of ion exchanged CY6A1-BMR incubated with aldrin as substrate at room temperature followed by extraction. The relative peak area is based on the IS peak area. n=3

The results for aldrin/IS show similar patterns in IMAC and anion exchange purified enzyme incubation, with a drastic decrease of aldrin after 1 h (Figure 4-21 and Figure 4-22). If the amount of aldrin that is lost after 1 h is turned into dieldrin the amount of dieldrin should increase after 1 h. However, the dieldrin/IS results show a similar pattern as the aldrin/IS results, but with lower values. The observed pattern do not show enzyme activity, but rather a non-enzymatic degradation over time of incubation. The variation of the dieldrin amount, which is found in the aldrin standard itself, can be based on measurement inaccuracy due to the low concentrations of dieldrin.

To find the reason for the missing CYP6A1-BMR activity the following parameters of the experimental setup were changed. To enable better substrate-enzyme-interaction the enzyme concentration was increased and aldrin was dissolved in DMSO instead of methanol. DMSO is a bipolar solvent which should increase the solubility in the buffer system and support the aldrin-enzyme contact.

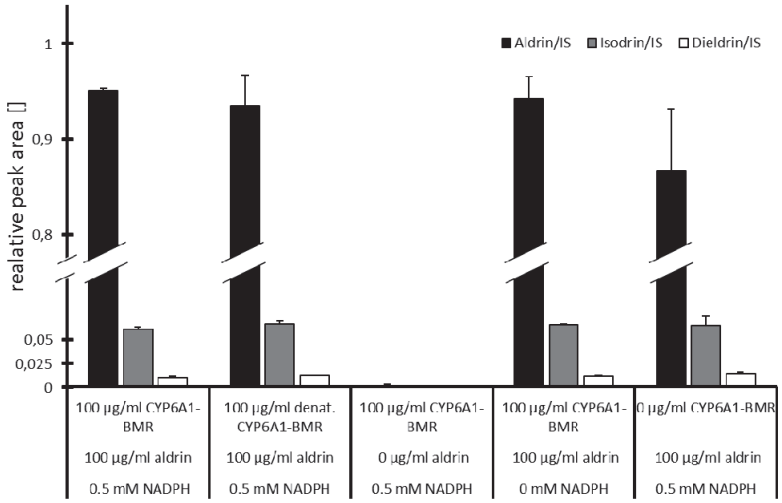

Figure 4-23: GC-MS measurements of IMAC purified CY6A1-BMR incubated with aldrin as substrate at room temperature for 1 h followed by extraction. The relative peak area is based on the IS peak area. n=3

Figure 4-23 shows similar results for all measured experimental variations. Aldrin is the most abundant analyte with a relative peak area of approximately 0.95 in all cases except the control without aldrin. Dieldrin has only a relative peak area of 0.05 in all cases except the non-aldrin control. This shows that the exchange of substrate solvent from methanol to DMSO and the increasing of enzyme concentration from 30 µg/ml to 100 µg/ml does not yield in higher dieldrin concentrations.

4.5.3 Discussion of GC-MS Measurements of Aldrin Conversion to determine CYP6A1-BMR Activity

This chapter shows the establishment of a GC-MS detection method including an extraction protocol for aldrin and the product dieldrin from enzyme incubation samples. The extraction protocol was established based on the test extraction of aldrin without enzyme. This lead to the conclusion that it is not important, which of the phases was transferred first, and that the total assay volume had to be at least 500 µl to assure good phase separation. Furthermore, the pretest showed that aldrin

is not stable in buffer at room temperature for 48 h. For this reason the activity of the CYP6A1-BMR construct was measured at different points of time. The measurements showed a similar concentration pattern for aldrin and dieldrin but with lower concentrations of dieldrin. This shows that no CYP6A1-BMR activity is measured only aldrin reduction over time, which was already shown in the performed pretests. A possible reason for the inactivity could be the solvent of the substrate. For this reason methanol was exchanged to DMSO which should enhance the solubility of aldrin in the assay mixture and support the substrate enzyme interaction [76-77]. An incubation time of 1 h was selected to exclude the aldrin degradation as far as possible, but give the enzyme time to react. It was shown by Andersen and coworkers that 0.015-0.065 nmol of CYP6A1 can catalyze aldrin with turnover rates of turnover rates of 12 min^{-1} at 30 °C [26]. The measurements with DMSO showed the same results as before, no CYP6A1-BMR activity. Another reason for the missing activity could be the P450 itself, that it was not produced correctly folded. This can be further evaluated by replacing the CYP6A1 with CYP6G1 which has imidacloprid as substrate, which shows different substrate properties than aldrin.

4.6 LC-MS Measurements of Imidacloprid Conversion to determine CYP6G1-BMR Activity

4.6.1 Establishment of LC-MS/MS Method

The activity of the P450 domain and a good cooperative function between the fused domains of the fusion construct CYP6G1-BMR can be determined by the turnover rate of the CYP6G1 substrate imidacloprid to 4-hydroxy-, 5-hydroxy-imidacloprid or 4,5-dihydroxy-imidacloprid [66] shown in Figure 4-24.

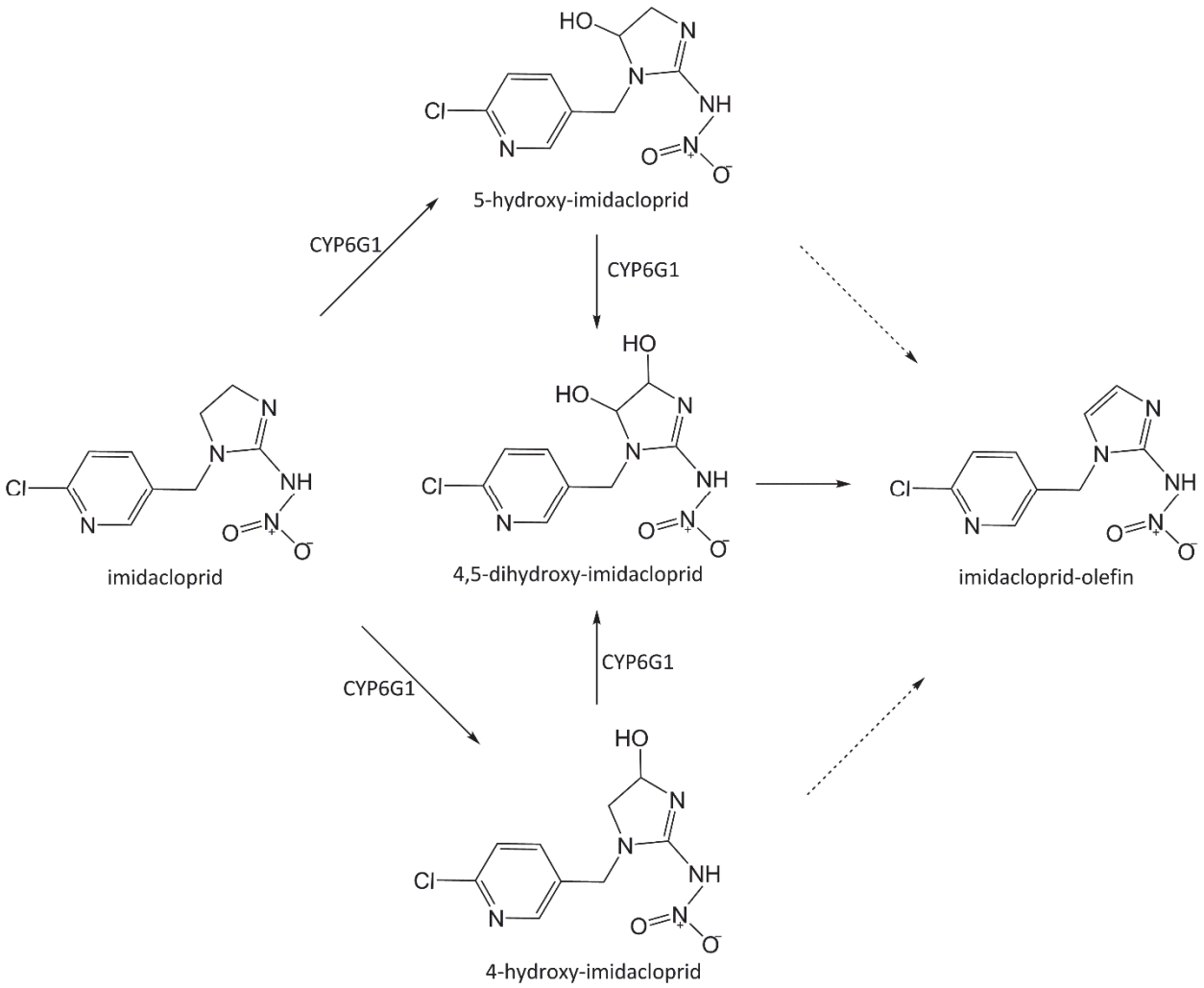

Figure 4-24: Schematic reaction of CYP6G1 catalyzed imidacloprid to its various products. Figure modified from Joußen *et al*. [66].

Activity tests of the fusion construct CYP6G1-BMR were performed in two different setups. Both approaches included simultaneous NADPH activity assays of purified enzyme in buffer. The first tested setup included desalting of the buffer-enzyme-system before LC-MS measurements whereas the second setup needed no desalting before LC-MS measurement. Methods are described in 3.29.1.

Prior the activity measurements a LC-MS method had to be established and the process parameters had to be evaluated to maximize sensitivity for detection of imidacloprid and its derivatives. A major drawback for the method establishment was that the products 4- and 5-hydroxy-imidacloprid were not commercially available as standards. To establish a method for imidacloprid detection imidacloprid was injected in different concentrations directly into the MS. This showed us that we would need

a minimum concentration 250 ng/ml per sample to receive a good signal. Other settings that had to be determined were the column, the corresponding HPLC method and the sample preparation. To receive the best sensitivity the sample preparation was tested in two different setups. The first sample preparation included a desalting step. Buffer samples were loaded on a C18 cartridge, washed and eluted with methanol. A disadvantage of this method is that it was not possible to determine if the reaction product got lost during this procedure since 4- and 5-hydroxy-imidacloprid were not available as standards. For the second sample preparation method the samples were mixed 1:1 (v:v) with acetonitrile. This mixture was loaded on the HPLC column and the flow through of salt components was discarded before the components of interest were transferred to the MS. This was the most promising method since the loss of analytes was prevented by loading of the complete sample on the HPLC column. The final LC-MS settings are shown in (3.29.1). The preliminary measurements with samples of purified CYP6G1-BMR did not show detectable hydroxylated products. It is possible that the sensitivity of the LC-MS was not high enough to detect the small traces of the products 4- and 5-hydroxy-imidacloprid. Therefore, measurements were performed at Chromicent on a UPLC-MS/MS based on the published protocol from Kamil [54].

4.6.2 Results of UPLC-MS/MS Measurements

Prior to the UPLC-MS/MS measurement the purified enzymes were detected photometrically at 340 nm to determine their ability of NADPH oxidation. The measurements were performed as described in (3.27.1).

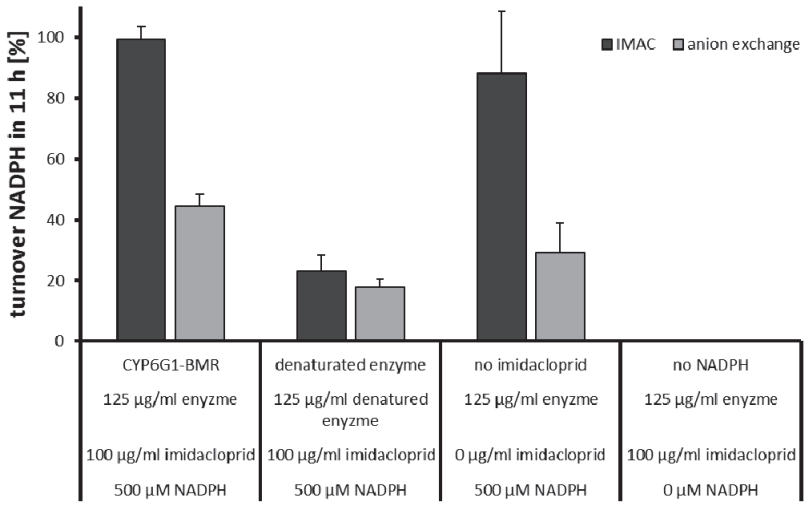

Figure 4-25: Photometric detection of NADPH consumption over time.

The results in Figure 4-25 show that 100% of NADPH were consumed after 11 h by the IMAC purified enzyme at the presence and absence of imidacloprid. The negative control with denatured enzyme shows in both cases a turnover of about 20%. The anion exchanged purified samples show a weaker activity, the turnover was, with or without imidacloprid present, only about 45%. Based on these results one would expect the best enzyme activity in the IMAC purified samples. After determination of the reductase domain activity the activity of the complete fusion construct was determined using UPLC-MS/MS. This method was selected to analyze the samples, since it is more sensitive than the LC-MS used before.

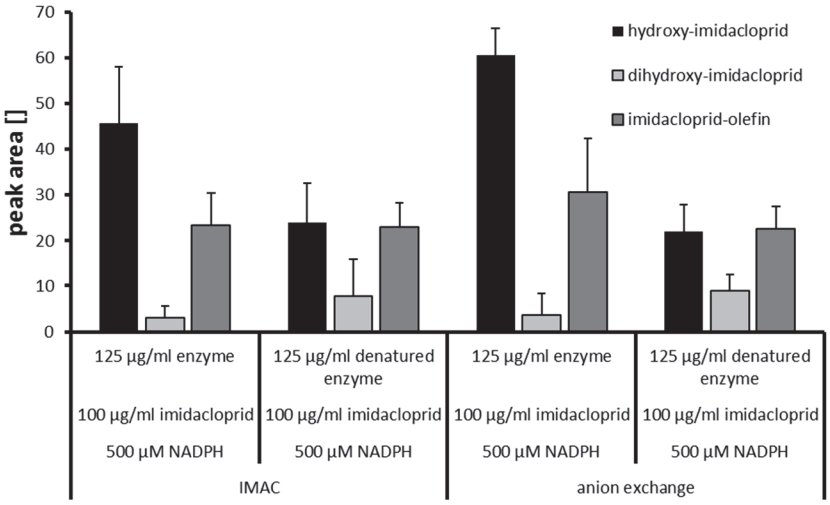

Figure 4-26: Results of UPLC-MS/MS measurements detecting products hydroxy-imidacloprid, dihydroxy-imidacloprid and imidacloprid-olefin. n=3

The results of the UPLC-MS/MS measurements, shown in Figure 4-26, show very small peak areas, which are below the detection limit. The results are similar to the results of the CYP6A1-BMR construct. The detected imidacloprid-olefin is most likely a contamination of the substrate imidacloprid, since it is present in all samples at the same level. The amounts of dihydroxy-imidacloprid are at the detection limit. Hydroxy-imidacloprid, is the most prominent product in the incubated samples. Nevertheless, the total amounts of hydroxy-imidacloprid cannot account for the amount of imidacloprid that was reduced in the incubation, see Figure 4-27, which were about 1 million counts.

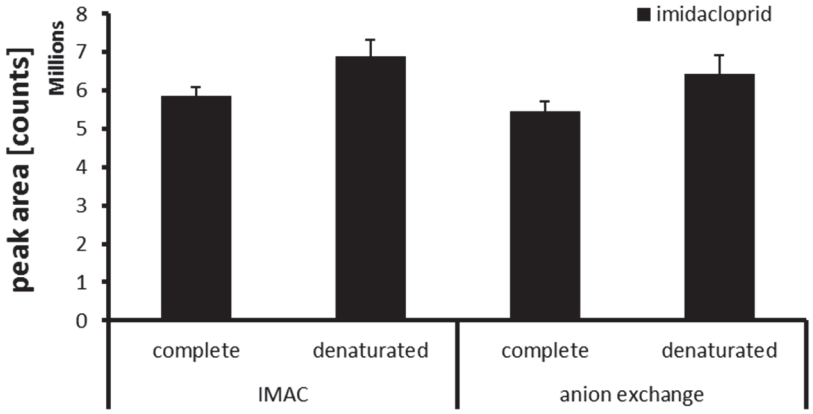

Figure 4-27: Results of UPLC-MS/MS measurements detecting substrate imidacloprid. n=3

Further investigation of the missing CYP6A1-BMR and CYP6G1-BMR activity lead to repetition of the IMAC purification for validation of heme presence. The ÄktaPrime

used for the former purifications at 4°C was replaced by the SE04 system (ECOM), which is able to detect four different wavelength at the same time. It is capable to detect the presence of the heme group with detection at 410 nm at the same time as detecting the protein at 280 nm. This way we could make sure that the heme is present at the time of purification.

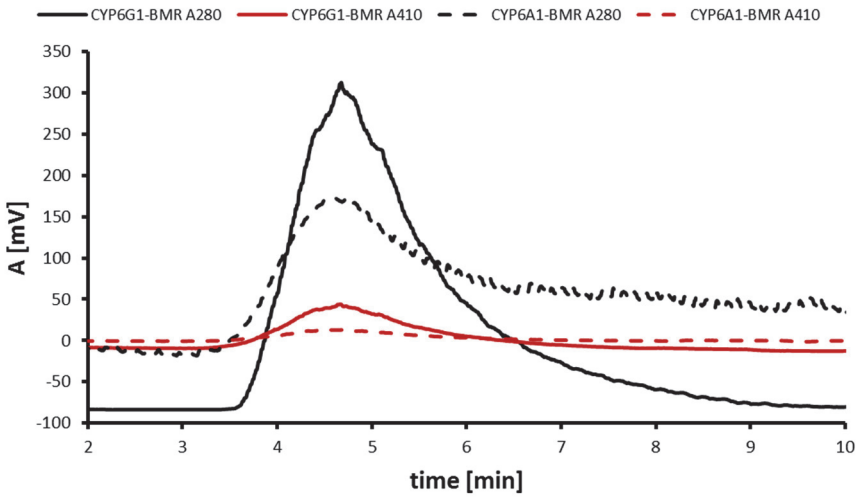

Figure 4-28: Purification of CYP6A1-BMR and CYP6G1-BMR without detergent at 4°C with 250 mM imidazole as eluent using SE04 system. Elution profile of the IMAC purification of CYP6A1-BMR and CYP6G1-BMR.

The ratio of the peaks (410 nm: 280 nm) in this purification (Figure 4-28) of 1:10 corresponds to the former purification (Figure 4-12). To verify the heme presence in the fractions they were checked for their heme absorbance peak at 420 nm afterwards (Figure 4-29). The measurements from 300 nm to 500 nm were performed in a 1 ml cuvette in photometer with the appropriate buffer mix as blank.

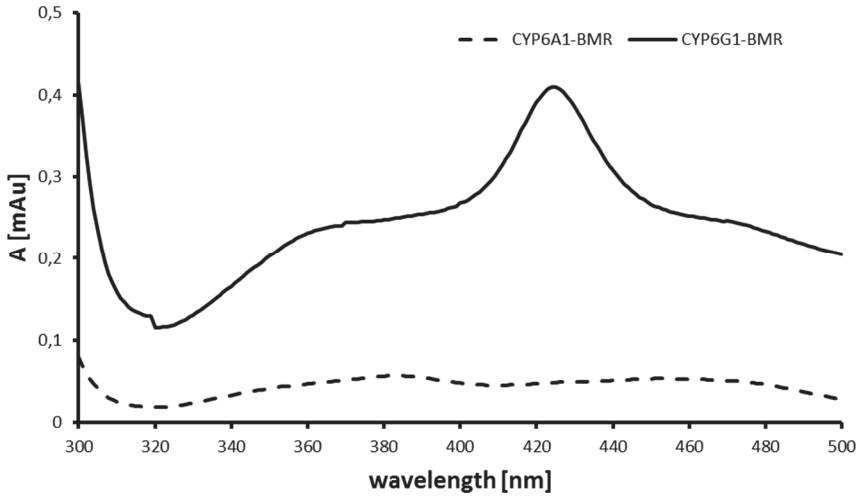

Figure 4-29: Absorbance spectrum of purified BM3-CYP6A1 and BM3-CYP6G1 from 380 nm to 600 nm. The peak at 420 nm indicates the presence of the heme group in the P450 domain.

The heme peak at 420 nm is well detectable for the CYP6G1-BMR construct, but not for the CYP6A1-BMR construct.

4.6.3 Photometric Heme Substrate Binding Test

To determine if the substrate is able to bind to the catalytic heme domain of the purified fusion enzyme construct a photometric heme substrate binding test was performed as described in section 3.31. The test could only be performed with purified CYP6G1-BMR since only for this the heme is detectable photometrically as seen in Figure 4-29.

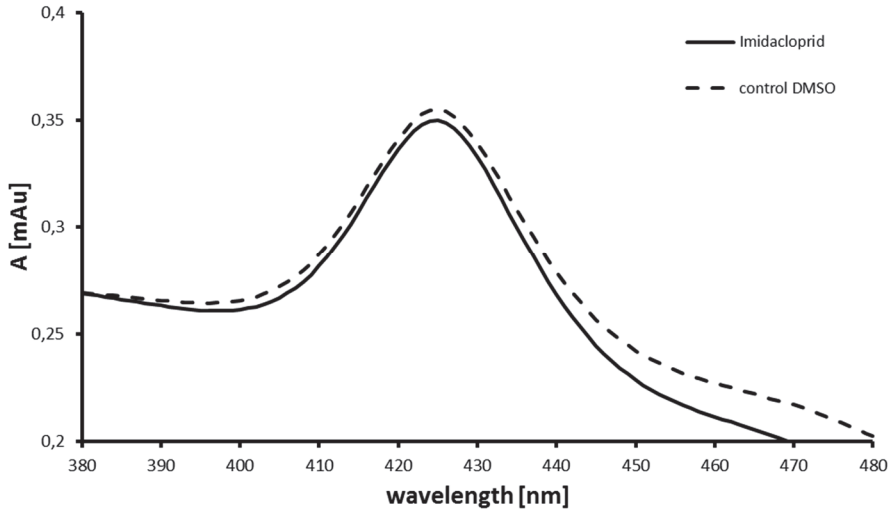

Figure 4-30: Photometric heme substrate binding test with IMAC purified CYP6G1-BMR and imidacloprid as substrate.

The test did not show any heme peak shift when adding the substrate imidacloprid compared to the negative control with DMSO, Figure 4-30.

4.6.4 Discussion of LC-MS Measurements of Imidacloprid Conversion to determine CYP6G1-BMR Activity

Imidacloprid can be catalyzed into three different products, 4-hydroxy-imidacloprid, 5-hydroxy-imidacloprid, and 4,5-dihydroxy-imidacloprid by CYP6G1, Figure 4-24. Furthermore 4- and 5-hydroxy-imidacloprid can be converted to imidacloprid-olefin [66]. Based on this knowledge the enzyme activity determination of the CY6G1-BMR construct was performed. Using imidacloprid as substrate the BMR activity of the fusion construct CYP6-BMR was shown with the photometric NADPH reduction activity assay. The primary aim of the work in this chapter was the activity determination of CYP6G1-BMR by detection of the products using LC-MS methods. To enable the substrate detection by LC-MS a suitable method and sample preparation had to be established. For the in-house LC-MS measurements the following two preparation methods were evaluated. First a desalting method using C18 cartridges was tested. This method showed the following drawbacks. At first the product could be lost due to the necessary working steps. Furthermore, the method could not be evaluated with the expected hydroxy-imidacloprid products, since they were not commercially available. Due to those reasons the first method was excluded and the direct injection approach was selected. This approach involves the addition

of the same volume of solvent to the sample and direct measurement. Using the in-house LC-MS detection no traces of the possible products were detected suggesting, that the turnover rate of the CYP6G1-BMR might be very low. Thus the small amounts of products could not be detected by our in-house LC-MS method with a detection limit of 250 ng/ml. This lead to the decision to measure the samples using the published protocol from Kamel on an UPLC-MS/MS at Chromicent GmbH which has a lower detection limit [54]. Due to the costs of external measurements only selected samples were measured. The results showed a reduction of imidacloprid but the low formation of products does not correlate to this. The imidacloprid concentration was reduced about 1 million counts compared to the control with denatured protein. On the other hand only 50 to 60 counts of 4- and 5-hydroxy-imidacloprid were measured. A former study showed that 83% of 400 µg imidacloprid were converted in 48 h by CYP6G1 expressed in tobacco cells, 6 l culture, into 58% 4-hydroxy-imidacloprid, 19% 5-hydroxy-imidacloprid and 6% imidacloprid-olefin [66]. Transferred to our samples this would mean that approximately 14.3 µg imidacloprid would have been converted and 8.29 µg 4-hydroxy-imidacloprid, 2.72 µg 5-hydroxy-imidacloprid and 0.86 µg imidacloprid-olefin should have been produced. Those values should be detectable using the UPLC-MS/MS approach. Since CYP6G1-BMR activity was not detected the remaining controls were not measured.

In order to determine a possible reason for the missing CYP6G1-BMR and CYP6A1-BMR activity the constructs were produced recombinant once more for the verification of the presence of the heme group in the constructs. During purification heme was present in both constructs. After the purification heme presence could only be detected in the CYP6G1-BMR construct. This explains the absence of CYP6A1-BMR activity since it does not contain a catalytic center after purification. The heme might have not been bound properly to the enzyme and got detached due to protein instability after purification due to the temperature change from 4°C to room temperature during the photometric measurement [78]. The construct CYP6G1-BMR does have a catalytic center after purification, but its activity is missing as well. To determine the reason for the lack of activity, the heme substrate interaction was investigated. Heme shows a specific absorbance spectrum with an absorbance maximum at 420 nm, when no substrate is bound. This was detected during the purification and the subsequent photometric measurement. The absorbance maximum changes to higher wave length when the heme binds the substrate [13]. This

effect was the basis for the heme substrate photometric assay. The construct CYP6G1-BMR did not show any change in the absorbance peak after addition of imidacloprid. The missing heme substrate interaction could be explained by a poor accessibility of the substrate binding site which prevents the formation of a catalytically productive binding mode [79]. This effect might be caused by one of the purification steps, which was investigated in the whole-cell section of the thesis.

4.7 Whole-cell Approach

As shown in the purification approach part of the results and discussion section the production and purification of the constructed insect P450-BMR fusions is working very well, but the activity of those constructs cannot be shown. To eliminate the purification process as a possible reason for the missing activity a whole cell approach was established. The selection of P450s was based on their ability to produce long-chain alkanes from long-chain aldehydes, which is not a typical P450 reaction [31]. To achieve a complete whole cell setup the long-chain aldehydes should not be added but produced in *E. coli* by the recombinant acyl-ACP reductase which is catalyzing the production of long-chain aldehydes from *E. coli*'s naturally produced long-chain fatty acids. The whole reaction is shown in Figure 4-31. The plasmid constructs in the *E. coli* coexpression setup is shown in Figure 4-32.

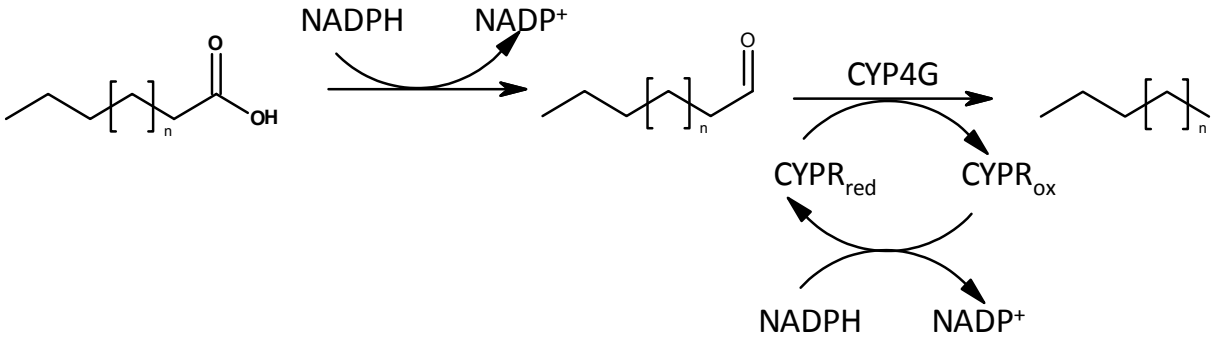

Figure 4-31: Reaction from long-chain fatty acids to long-chain alkanes. Reaction of long-chain fatty acids to long-chain aldehydes catalyzed by reductase. Follow up reaction of long-chain aldehydes catalyzed to long-chain alkanes by P450 of the group CYP4G.

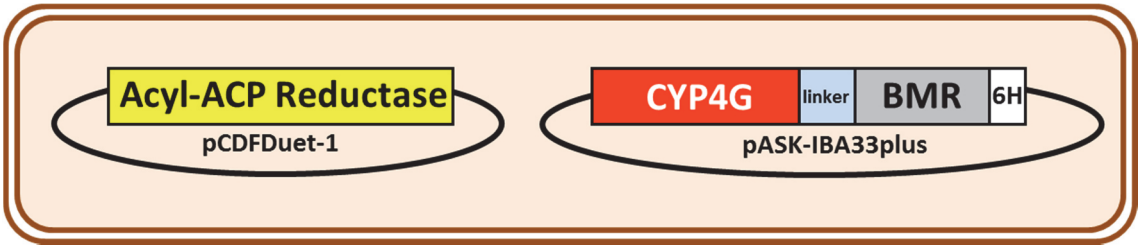

Figure 4-32: Schematic representation of the coexpression for alkane production in *E. coli*. Acyl-ACP reductase on a pCDFDuet-1 plasmid and the CYP4G-BMR fusion construct on a pASK-IBA33plus plasmid in *E. coli*.

4.8 Construction of Alkane producing *E. coli* as Positive Control with Aldehyde Decarbonylase and Acyl-ACP Reductase from *Nostoc punctiforme*

The genes with an added His_6-tag were synthesized, *E. coli* K12 codon optimized and cloned into their appropriate vector by MWG Eurofins. The vectors, pASK-IBA33plus and pCDFDuet-1, were selected based on their compatibility for coexpression, they are using tac and T7 promoters, respectively, and include ampicillin and streptomycin resistance, respectively. The construction is described in 3.1 and resulted in the plasmids pCDFDuet-1_AcylACPRed and pCDF-Duet-1_AcylACPRed. To achieve co-transformed *E. coli* BL21 (DE3) cells, *E. coli* had to be transformed with pCDF-Duet-1_AcylACPRed first, then made chemically competent and then be co-transformed with pASK-IBA33_Alddec. This is described in section 3.11 and 3.12. This lead to *E. coli* BL21 (DE3) cells containing both plasmids as shown in Figure 4-37.

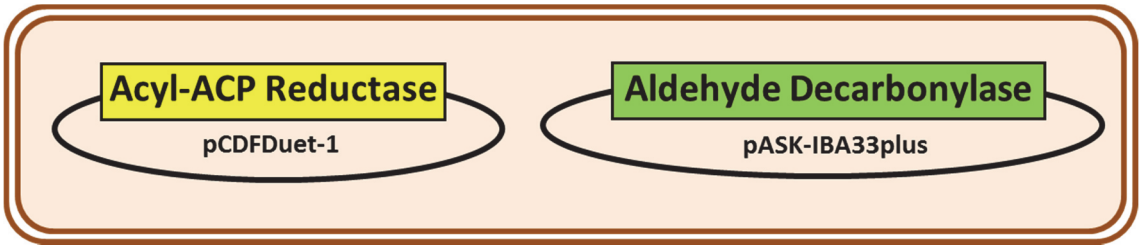

Figure 4-33: Schematic representation of the coexpression positive control. Acyl-ACP reductase on a pCDFDuet-1 plasmid and the aldehyde decarbonylase on a pASK-IBA33plus plasmid in *E. coli*.

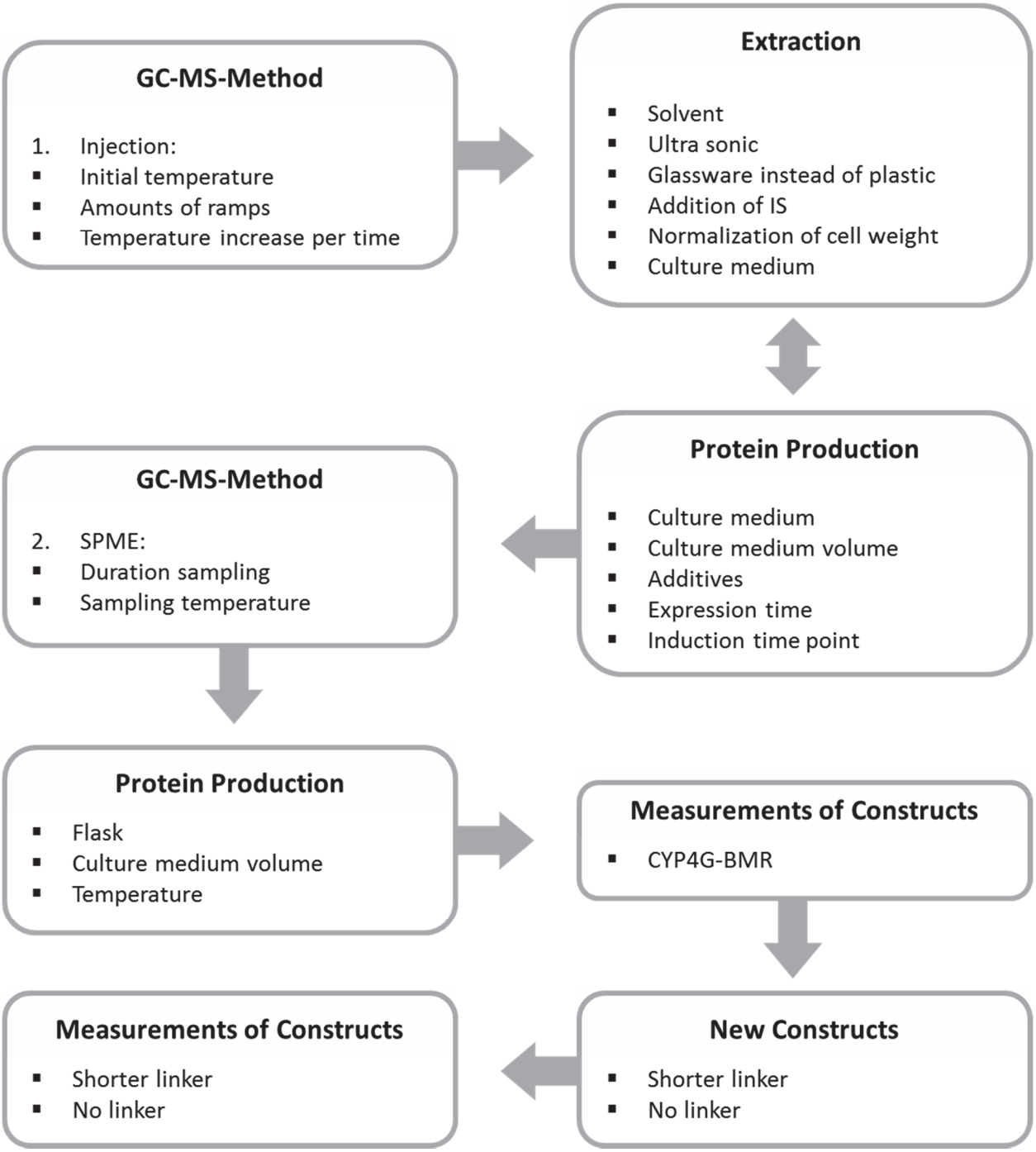
GC-MS-Method
1. Injection:
Initial temperature
Amounts of ramps
Temperature increase per time
Extraction
Solvent
Ultra sonic
Glassware instead of plastic
Addition of IS
Normalization of cell weight
Culture medium
Protein Production
Culture medium
Culture medium volume
Additives
Expression time
Induction time point
GC-MS-Method
2. SPME:
Duration sampling
Sampling temperature
Protein Production
Flask
Culture medium volume
Temperature
Measurements of Constructs
CYP4G-BMR
New Constructs
Shorter linker
No linker
Measurements of Constructs
Shorter linker
No linker

4.9 Parameter evaluation for GC-MS Alkane Detection

The GC-MS method parameter evaluation was performed with the alkane standard C8-C20 and afterwards with the positive control *E. coli* BL21 (DE3) with coproduced acyl-ACP reductase and aldehyde decarbonylase. The evaluation of parameters for protein production was as well performed with the positive control. Following this the CYP4G-BMR constructs were measured and evaluated.

4.9.1 GC-MS-Method parameter evaluation

The first measurements were performed on a GC-MS CT1128 (Constellation Technology Corporation) equipped with a VF-5MS column (30 m x 0.25 mm internal diameter, 0.25 µm film thickness (Agilent Technologies)). Three initial column oven temperatures (50°C, 70°C, 100°C) were tested. From the initial temperature the temperature increased at a rate of 20°C/min over two ramps up to 300°C, see 3.30.2. The best results were achieved by using an initial temperature of 70°C. This method was then used for the evaluation of sample preparation and for further evaluations of protein production. The second, more detailed analysis of the samples was performed at Fraunhofer IME for applied ecology, Schmallenberg, on a GC-MS 5973 from Agilent Technologies equipped with a Rxi-5HT column (30 m x 0.25 µm internal diameter, 0.25 µm film thickness). The method for this GC-MS was based on the final method but had to be adjusted for this instrument. The method started with an initial temperature of 50°C increased at 20°C/min up to 300°C with a 25 min hold and a second ramp at 15°C/min to final temperature of 350°C, see 3.30.3.

4.9.2 Extraction and Protein Production

To evaluate the extraction and the protein production for best possible GC-MS data several parameters were tested, see Table 4-3 for extraction parameters and Table 4-4 for protein production parameters.

Table 4-3: Overview of changed parameters for evaluation of extraction for GC-MS measurement of alkanes.

Variable	1	2	3	4	5	6	final
solvent	Metha-nol	Ethyl acetate	Hexane	Ethyl acetate		Hexane/ Dichloro-methane	**Ethyl acetate**
ultra-sonication	30 min	10 min		5 min	no	3 min	**3 min**
centrifugation	3 min, 13000 g	30 min, 14000 g		20 min, 14000 g	10 min, 4500 g		**10 min, 4500 g**
lab ware	plastic				glass		**glass**
cell weight normalization	no				220 mg/ml		**220 mg/ml**
internal standard	no				Octadecane		**Octadecane**

For the final extraction parameters ethyl acetate was selected as solvent, since it dissolved alkanes best with this extraction method out of *E. coli* positive control cells. The time of ultra-sonication was reduced to 3 min to avoid evaporation of substances. The centrifugation speed had to be reduced to 4500 g based on the glass vials that were used. Glass ware was used to reduce the amount of contamination peaks that appeared, because plastic components were dissolved by the solvent and detected by GC-MS. The cell weight normalization was performed to enable better comparison between the different samples. The internal standard octadecane was selected since it was no expected alkane produced by one of the constructs and to enable better comparison [30]. The evaluation of the protein production was performed simultaneously to the extraction evaluation, since some parameters influence each other, for example the usage of M9 minimal medium. M9 medium reduced the background of the GC-MS measurements drastically, but it had the disadvantage of lower growth speed and protein production. To see at which point in time of protein production the alkane yield is highest several measurements were taken after specific time periods as seen in Table 4-4.

Table 4-4: Overview of changed parameters for evaluation of protein production for GC-MS measurement of alkanes.

Variable	1	2	3	4	5	6	final
medium	TB	M9				M9/TB	**M9**
volume	50 ml			400 ml	800 ml	400 ml	**50 ml**
inoculation volume of overnight culture	5 ml	500 µl		4 ml	4.5 ml	4 ml	**500 µl**
duration protein production	4 h	48 h	8 h, 42 h, 7 d	42 h	48 h	4 h, 6 h, 24 h, 48 h	**t_0, 2 h, 4 h, 16 h, 24 h, 42 h**

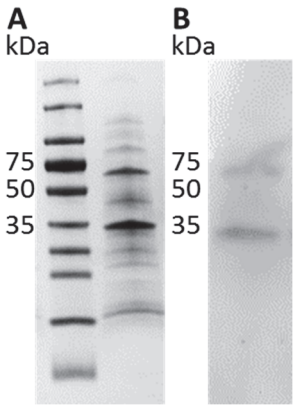

Figure 4-34: Coexpression of acyl-ACP reductase and aldehyde decarbonylase. SDS-PAGE (**A**) and Western blot analysis (**B**) of the in *E. coli* BL21 (DE3) coexpressed acyl-ACP reductase and aldehyde decarbonylase. The acyl-ACP reductase shows a band at the expected size of 35 kDa and the aldehyde decarbonylase with its expected size at 70 kDa.

Figure 4-34 shows the coexpression of acyl-ACP reductase and aldehyde decarbonylase. For the final protein production settings M9 minimal medium was selected since it immensely reduced the background peaks. The selection of minimal medium defined the inoculation volume, since as little LB medium should be transferred to the main culture as necessary. The culture volume allowed a higher sample size which determined the amount of time point samples.

4.9.3 GC-MS-Method (SPME)

To reduce the matrix effect from the sample medium and to eliminate the requirement of sample extraction a SPME-GC-MS-method was established. By this the full spectrum of volatile products can be detected. Another advantage of this method is that cells can be grown in TB medium with their regular growth and expression rate, since the salt content of TB is beneficial for the analysis because of a reduced solubility. The establishment of this method was performed using the alkane standard (C8-C20) in culture medium to find the correct sampling time. In Figure 4-35 an overlay of total ion chromatogram (TIC), extracted ion chromatogram (EIC) 57 and EIC 71 of the alkane standard in TB medium and glucose is shown. The masses 57 and 71 were selected for the EIC based on the typical fragmentation pattern of alkanes.

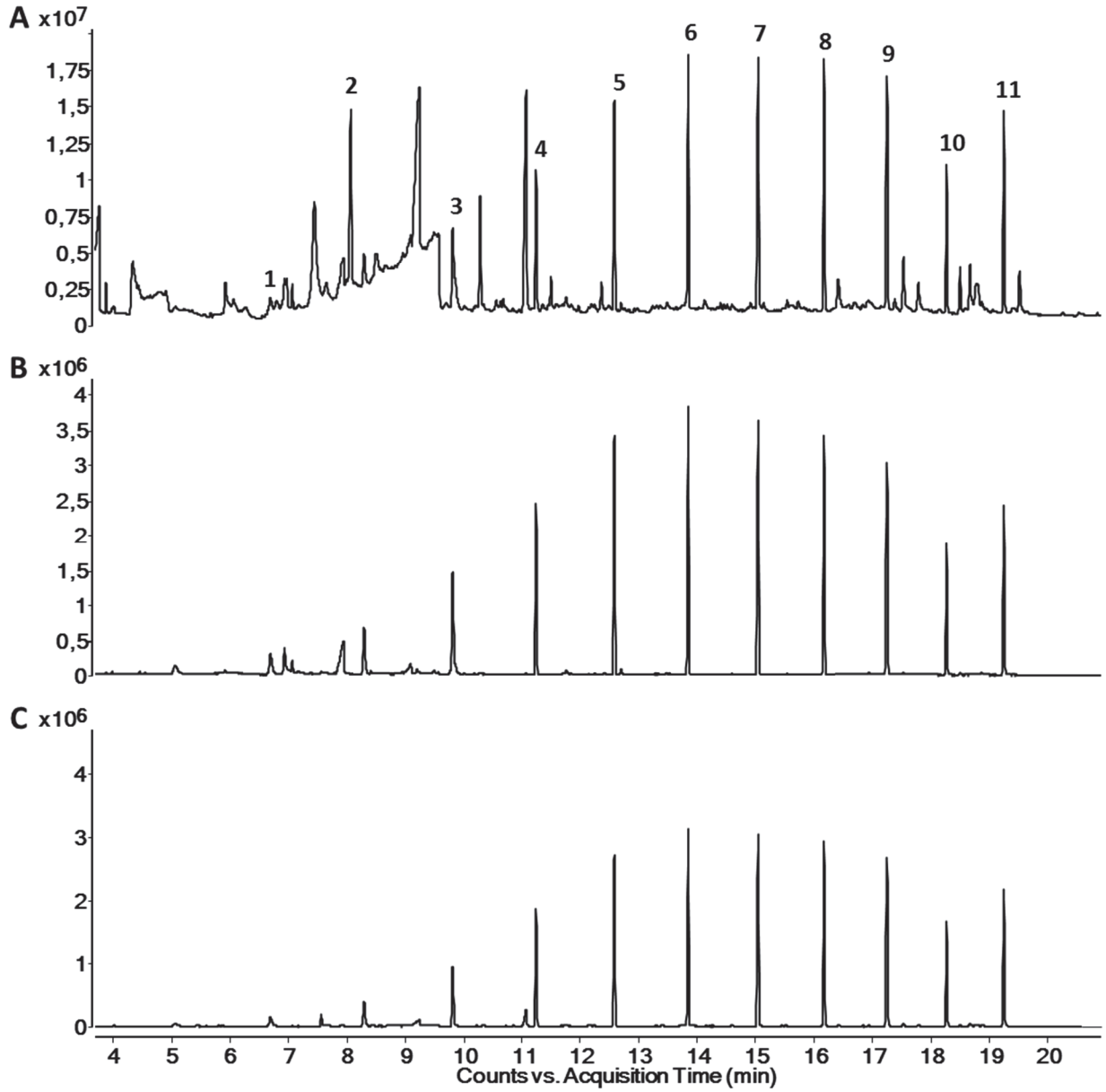

Figure 4-35: SPME-GC-MS measurement of alkane standard in TB + glucose medium and 30 min sampling time at 37°C. **A**: TIC, **B**: EIC m/z 57, **C**: EIC m/z 71. 1: decane, 2: undecane, 3: dodecane, 4: tridecane, 5: tetradecane, 6: pentadecane, 7: hexadecane, 8: heptadecane, 9: octadecane, 10: nonadecane, 11: eicosane.

To see if this method is also suitable for *E. coli* produced alkanes in TB-medium the positive control *E. coli* BL21 (DE3) with coproduced acyl-ACP reductase and aldehyde decarbonylase were measured after 4 h protein production at 37°C. The results in Figure 4-36 show the production of five different alkanes: undecane ($C_{11}H_{24}$), dodecane ($C_{12}H_{26}$), tridecane ($C_{13}H_{28}$), pentadecane ($C_{15}H_{32}$), heptadecane ($C_{17}H_{36}$) and one alkene: heptadecene ($C_{17}H_{34}$).

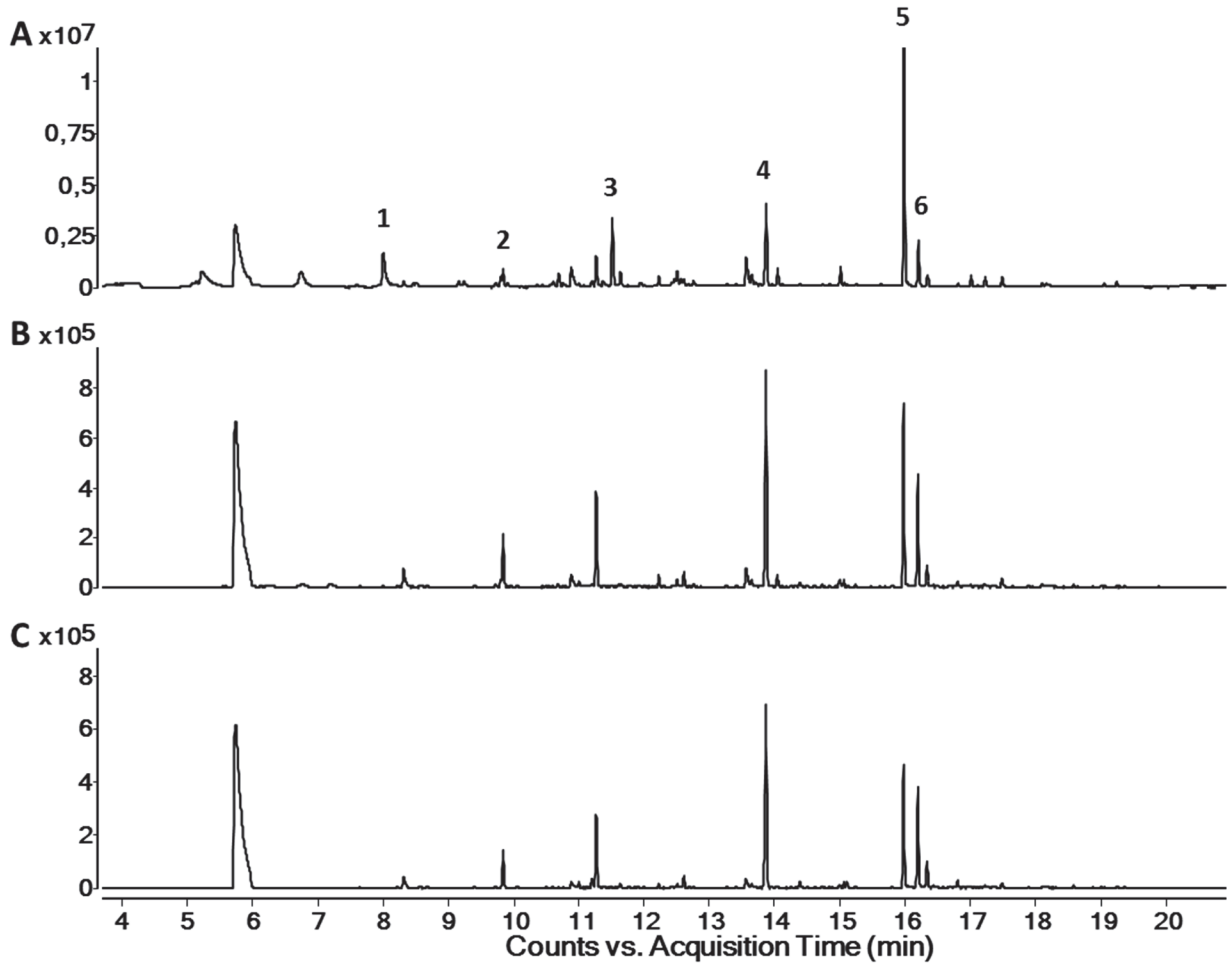

Figure 4-36: SPME-GC-MS measurement of positive control *E. coli* BL21 (DE3) with coproduced acyl-ACP reductase and aldehyde decarbonylase with a sampling time of 30 min at 37°C. **A**: TIC, **B**: EIC m/z 57, **C**: EIC m/z 71. 1: undecane, 2: dodecane, 3: tridecane, 4: pentadecane, 5: heptadecene, 6: heptadecane.

The alkanes show well detectable peaks with good separation in the TIC, which suggests that this method is the right one to analyze the fusion enzyme constructs, where we expect lower amounts of alkanes and side products.

Next to the produced alkanes the production of their precursor, even long-chain aldehydes, produced by acyl-ACP reductase can be shown as seen in Figure 4-37. The produced aldehydes are tetradecanal, hexadecanal and octadecanal, which corresponds to the produced alkanes by the positive control.

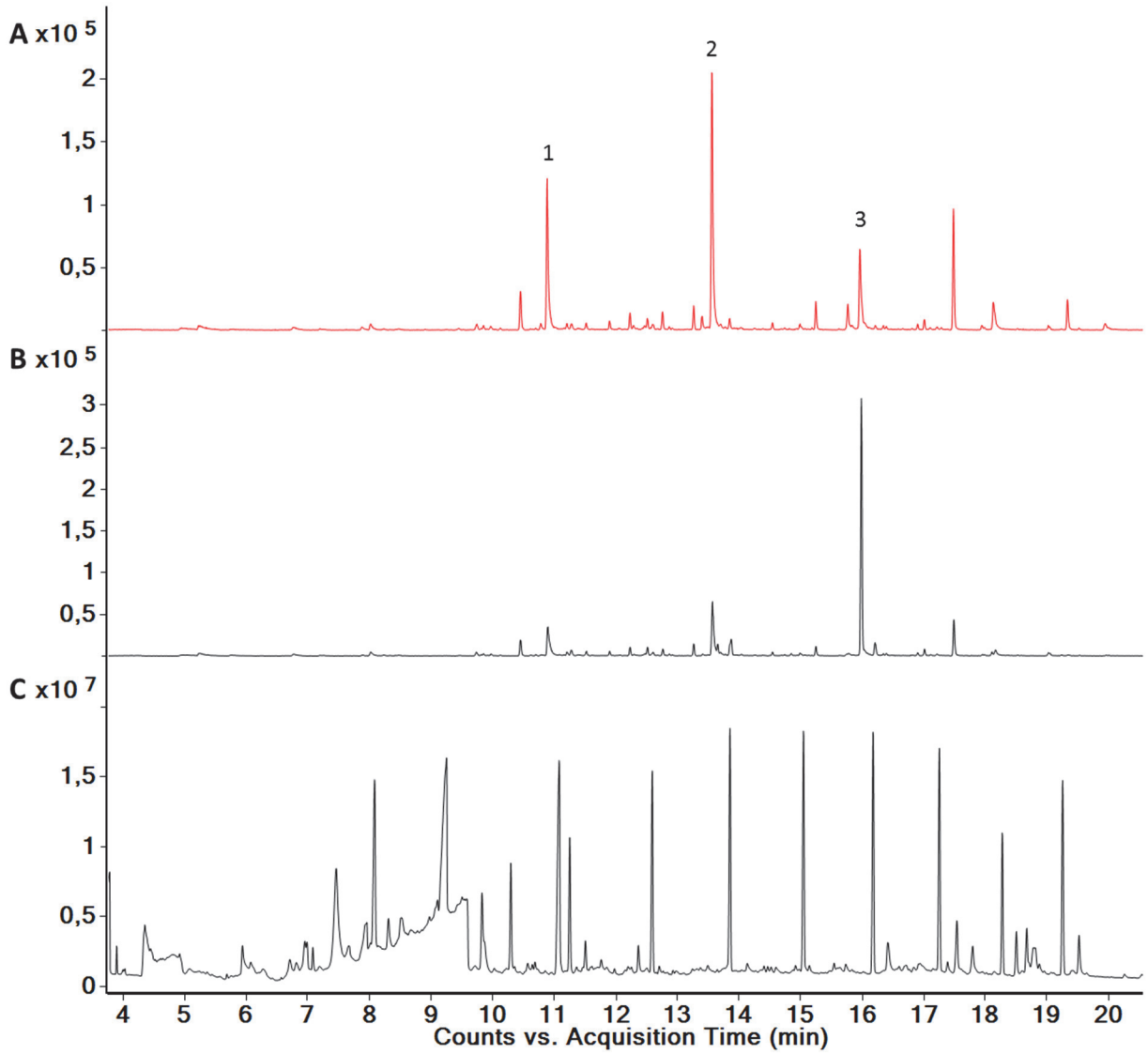

Figure 4-37: SPME-GC-MS aldehyde detection. SPME-GC-MS measurement of *E. coli* BL21 (DE3) with **A**: produced acyl-ACP reductase (EIC m/z 82), **B**: aldehyde decarbonylase and acyl-ACP reductase (EIC m/z 82) and **C**: alkane standard C8-C20 (TIC) with a sampling time of 30 min at 37°C. 1: tetradecanal, 2: hexadecanal, 3: octadecanal.

The used EIC m/z 82 was selected to differentiate between alkanes and aldehydes.

4.9.4 Protein Production for Alkane Production using SPME-GC-MS Measurements

The coproduction of acyl-ACP reductase and the fusion proteins CYP4G1-BMR or CYP4G2-BMR was performed in *E. coli* BL21 (DE3), as shown in Figure 4-38.

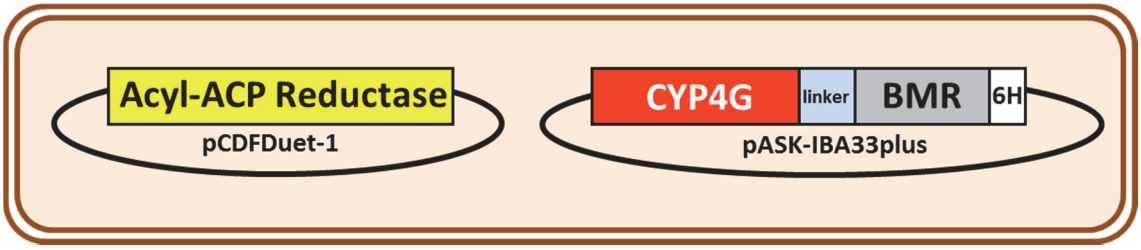

Figure 4-38: Schematic representation of the coexpression for alkane production in *E. coli*. Coproduction of the acyl-ACP reductase on a pCDFDuet-1 plasmid and the CYP4G-BMR fusion construct on a pASK-IBA33plus plasmid.

The best conditions for the coproduction for SPME-GC-MS detection of alkanes had to be determined since the conditions for the positive control reaction used in the initial tests (coexpression acyl-ACP reductase and aldehyde decarbonylase) are not the same. Table 4-5 shows the different tested variables.

Table 4-5: Overview of changed parameters for evaluation of protein production for SPME-GC-MS measurement of alkanes.

Variable	1	2	3	4	final
flask	20 ml GC vial		20 ml GC vial / 100 ml flask		**20 ml GC vial**
volume	5 ml		5 ml / 50 ml		**5 ml**
temperature for protein production	37°C	28°C	28°C and 30 min 37°C	37°C	**37°C**
speed during protein production	250 rpm	180 rpm			**250 rpm**
sample procedure	direct	first frozen			**direct**

The best conditions were protein production directly in GC vial with 5 ml medium volume at 37°C with 250 rpm. The most important parameters were the temperature and the direct sample procedure, this lead to the best results for all tested samples, as seen in Figure 4-39. The controls: single expression of aldehyde decarbonylase or acyl-ACP reductase show the expected sizes at 28 kDa and 38 kDa, respectively. The coexpression of acyl-ACP reductase (38 kDa) and aldehyde decarbonylase (28 kDa) or CYP4G1-BMR (130 kDa) or CYP4G2-BMR (133 kDa) is showing bands at the expected size.

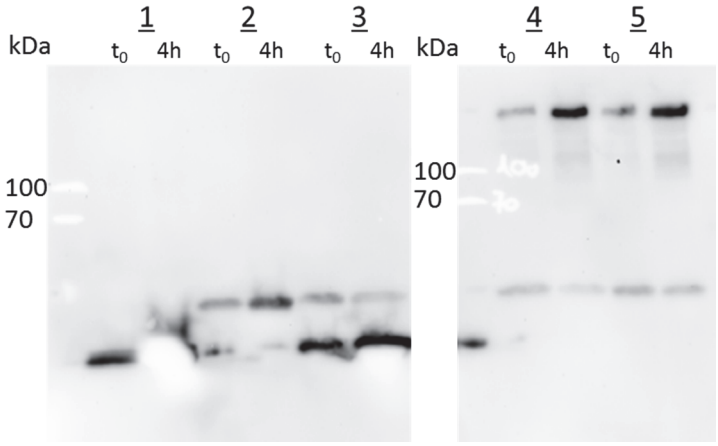

Figure 4-39: Western blot analysis of coproduced enzymes. Western blot analysis of *E. coli* BL21 (DE3) with aldehyde decarbonylase (**1**), acyl-ACP reductase (**2**), aldehyde decarbonylase & acyl-ACP reductase (**3**), acyl-ACP reductase & CYP4G1-BMR (**4**) and acyl-ACP reductase & CYP4G2-BMR (**5**). t_0= time of induction with anhydrotetracycline and/or IPTG, 4h = 4 h after induction. In all cases the expected protein size could be detected after 4 h expression.

4.9.5 SPME-GC-MS Measurements of CYP4G-BMR Constructs

The results of SPME-GC-MS measurements of CYP4G1-BMR (not shown) and CYP4G2-BMR coexpressed with acyl-ACP reductase (Figure 4-40 B) do not show new alkanes produced compared to the negative control aldehyde decarbonylase (Figure 4-40 A). Whereas for positive control, coexpressed aldehyde decarbonylase and acyl-ACP reductase, produced alkanes (Figure 4-40 C, 1-4) are detectable.

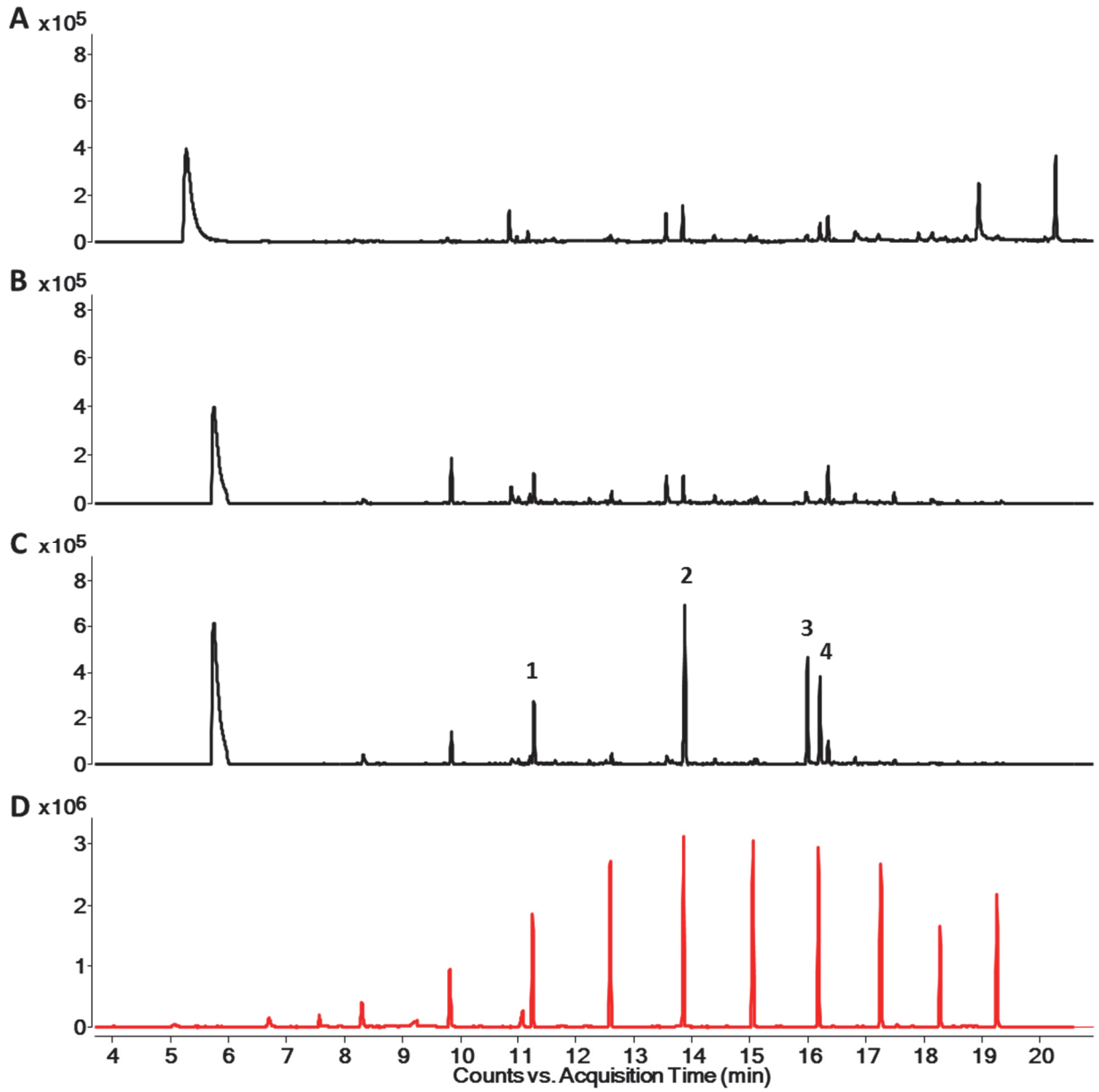

Figure 4-40: EIC (m/z 71) of SPME-GC-MS measurement of *E. coli* BL21 (DE3) with **A**: aldehyde decarbonylase **B**: coexpressed CYP4G2-BMR and acyl-ACP reductase **C**: coexpressed aldehyde decarbonylase and acyl-ACP reductase and **D**: alkane standard C8-C20 with a sampling time of 30 min at 37°C. 1: tridecane, 2: pentadecane, 3: heptadecene, 4: heptadecane.

4.9.6 Discussion of GC-MS Measurements of Alkane producing Constructs

This chapter showed the construction of a coexpression whole-cell *E. coli* system producing alkanes and the establishment of a GC-MS method able to detect the produced alkanes and aldehydes. Schirmer and coworkers showed that alkane production using acyl-ACP reductase and aldehyde decarbonylase from cyanobacteria is possible in *E. coli* [80]. The enzymes selected for this study, acyl-ACP reductase and aldehyde decarbonylase, both from *Nostoc punctiforme*, were never coexpressed before in *E. coli* and served as positive control. Many researchers focused on the optimization of biofuel production by metabolic engineering [81-82]. Another way to achieve different products could be the use of insect P450s instead of the aldehyde decarbonylase. Therefore, the alkane producing system was adjusted to the coexpression with the new insect P450 fusion constructs CYP4G1-BMR and CYP4G2-BMR instead of the *N. punctiforme* aldehyde decarbonylase.

The GC-MS method for alkane detection was evaluated using the alkane standard C8-C20 and the alkane positive control acyl-ACP reductase coproduced with aldehyde decarbonylase from *Nostoc punctiforme* in *E. coli*. The first measurements were performed on a GC-MS CT1128 (Constellation Technology Corporation) and more detailed analysis were performed on a GC-MS 5973 (Agilent Technologies). Using those two instruments the variables influencing the outcome, like expression conditions, sample preparation and GC-MS method were determined. This lead to the final settings shown in Table 4-3 and Table 4-4. The GC method was only adjusted slightly according to the used instrument. Due to the necessity of the alkane extraction from the samples for these GC-MS measurements a loss of product is inevitable. To avoid an extraction step a new GC-MS method was established for this application, SPME-GC-MS. This method avoids all steps of conventional liquid-liquid extraction, like extraction and concentration [83]. The sample was directly extracted to the SPME fiber coating, in this case polydimethylsiloxane. Another advantage of this method was that the expression can be performed in TB medium which increased the protein yield and by this the potential alkane production. For this method the best protein production conditions with subsequent analysis were examined (Table 4-5) and expression in TB, in GC vials for 4 h with direct analysis afterwards showed the best results. This method enabled the detection of the aldehydes produced by acyl-

ACP reductase and the detection of the alkanes produced by the positive control (Figure 4-36 and Figure 4-37). The acyl-ACP reductase produced even numbered aldehydes (tetradecanal, hexadecanal and octadecanal) which were converted into uneven numbered alkanes (tridecane, pentadecane and heptadecane) by aldehyde decarbonylase. Furthermore, the alkanes, undecane and dodecane plus the alkene, heptadecene, were produced. The alkanes, undecane and dodecane, for which the corresponding aldehydes were not detected are only present in very low concentrations. Alkanes are better detectable than their corresponding aldehydes, this could be why only the alkanes were detected.

In this study it was shown for the first time that aldehyde decarbonylase and acyl-ACP reductase from *Nostoc punctiforme* produce the alkanes, undecane, dodecane, tridecane and pentadecane, when coexpressed on pASK-IBA33plus and pCDFDuet-1 in *E. coli*. The study performed by Schirmer *et al*. observed only heptadecane production for the cyanobacterium *N. punctiforme* [80]. The detection of more alkanes could be due to the fatty acids produced by *E. coli* (until the length of C17 [84]), which serve as available substrate for the acyl-ACP reductase.

The same setup was used for the coexpression of acyl-ACP reductase with the fusion constructs CYP4G1-BMR and CYP4G2-BMR. The coexpression showed promising protein expression with stable produced protein in the expected size (Figure 4-39). For both constructs no alkane production could be detected. Since the purification is ruled out by these experiments as a possible reason for the missing enzyme activity the construction of the fusion could be the reason. The linker length is known to strongly influence the enzyme activity, since it regulates the localization of the BMR towards the heme domain and by this it regulates the electron flow [46, 85]. Another part of the construction which has a big influence on the activity is the BMR domain itself. The domain might not be able to interact with the insect P450 as expected although mechanism similarities were shown in from former studies [25]. These two important factors were analyzed in the following chapter.

4.10 Construction of Optimized Fusion Enzymes

To investigate the reasons for the missing alkane production new approaches were developed. A new CYP4G from *Forficula auricularia* was used for fusion enzyme construction. Furthermore new fusion enzymes with either a shorter linker or no linker were designed and constructed to eliminate the linker length as a reason for the inactive fusion constructs.

4.10.1 Construction of a Fusion Enzyme based on CYP4G from *Forficula auricularia*

Previously it was shown that the European earwig *Forficula auricularia* larvae produce alkanes (n-tridecane and n-pentadecane) as defense measures [86]. The genome of *F. auricularia* was available [51] and screened (by R. Lehmann) for CYP4G coding sequences, which have been suggested to be involved in the alkane synthesis [29]. The following sequence (CYP4GF) (Figure 4-41) was found and based on this primers were designed (Table A.2.4-3), which flanked the CYP4GF sequence.

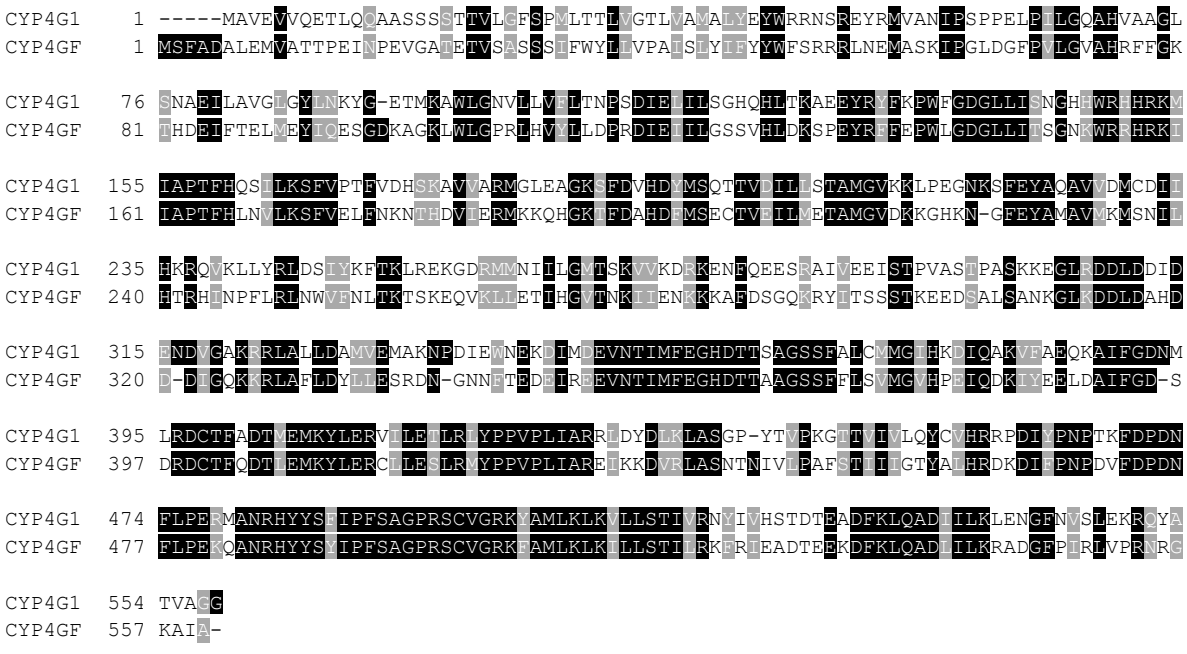

Figure 4-41: Sequence Alignment of CYP4G1 and CYP4G from *F. auricularia* (CYP4GF). Black and gray shading represent amino acid identity and similarity, respectively.

mRNA from ten earwig larvae (collected by T. Gasch), approximately 200 mg, was isolated and cDNA was synthesized from it. Figure 4-42 shows the procedure of the CYP4GForficula-BMR construction starting with ten earwigs. The cDNA was used as template for PCR with primers (Table A.2.4-3) for CYP4G amplification. The resulted PCR fragment was cloned into pCR-Blunt II TOPO for multiplication. The plasmid, pCR_CYP4GForficula, was amplified in *E. coli* TOP10 cells and isolated. pCR_CYP4GForficula was used as template for PCR using primers (Table A.2.4-1) to extend the gene by His_6-tag and *Bsa*I cloning sites. After double digestion of the PCR fragment and pASK-IBA33plus with *Bsa*I the fragment and the backbone were ligated and yielded the construct pASK-IBA33_CYP4GForficula. *E. coli* TOP10 cells were transformed with this plasmid. After verification of the sequence (primers listed in Table A.2.4-2) pASK-IBA33_CYP4GForficula was used as template for PCR with the primers (Table A.2.4-1) to amplify the CYP4G *Forficula* gene without His_6-tag and extended by *Xba*I (5'-site) and *Sal*I (3'-site) sites. After double digestion of the PCR fragment and pASK-IBA33_BM3 with *Xba*I and *Sal*I the PCR fragment and backbone were ligated and *E. coli* TOP10 cells were transformed with the new construct pASK-IBA33_CYP4GForficula-BMR. After verification of the sequence (primers listed in Table A.2.4-2), *E. coli* BL21 cells (expression strain) were transformed with the plasmid.

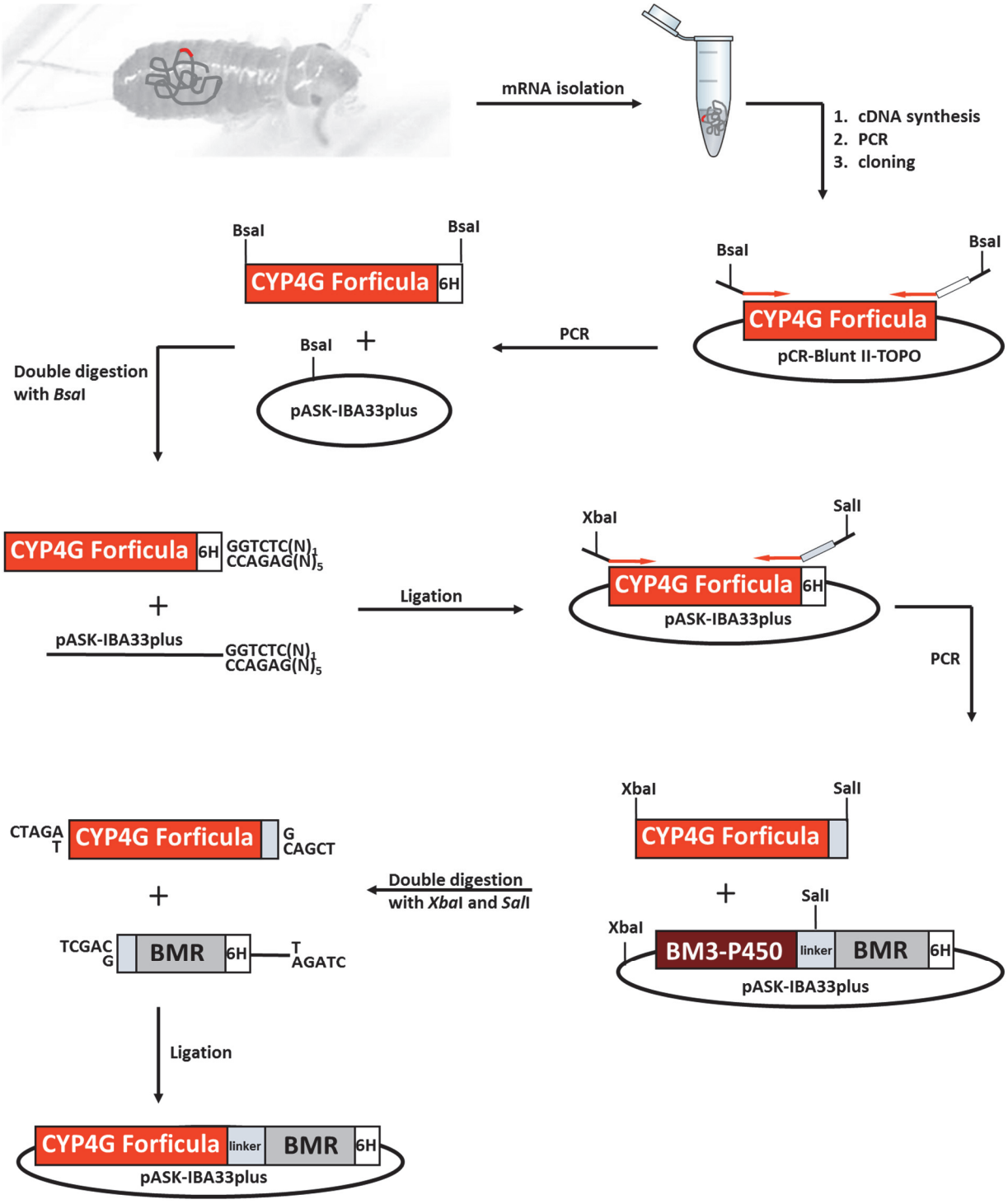

Figure 4-42: Schematic representation of CYP4G Forficula-BMR fusion enzyme construction based on isolated mRNA from ten earwig larvae.

4.10.2 CYP4G-BMR Fusion Enzyme with Shortened Linker

The construction of the CYP-BMR short linker construct used the former used CYP4G-BMR fusion construct as template. Literature shows that the linker length of P450 fusion constructs has an enormous impact on the constructs activity and stability [62]. Figure 4-43 shows the comparison of the former used linker and the new shorter linker.

```
Linker:                SKKIPLGGIPSPTEQSAKKVRKKAENAHN
short Linker:                  SPTEQSAKKVRKKAENAHN
```

Figure 4-43: Sequence Alignment of the former used linker and the new shortened linker.

To reduce the former linker to this shortened sequences new reverse primers with a *Sal*I restriction enzyme site were designed (Table A.2.4-1). As forward primer the same primer as before with an *Xba*I site can be used. These primer pairs were used to create a CYP4G with an N-terminal *Xba*I site and a shortened linker region with a *Sal*I site. The construction was performed as described in 3.14 and shown in Figure 4-44. This yielded the two constructs pASK-IBA33-CYP4G1-BMRshortLinker and pASK-IBA33-CYP4G2-BMRshortLinker.

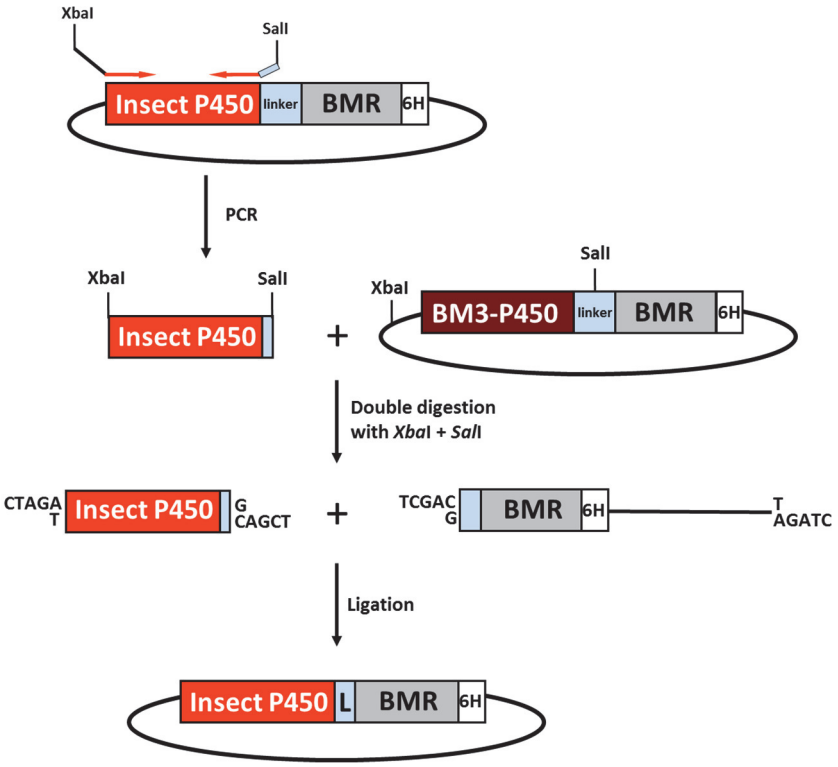

Figure 4-44: Schematic representation of insect P450-BMR fusion construction with shortened linker.

4.10.3 Construction of a Plasmid with Non-Fusion CYP4G and hCPR

To exclude the interaction of the BMR domain and the insect P450 domain as a reason for the missing activity a non-fusion construct on plasmid with an insect P450 and hCPR as reductase designed and constructed. Figure 4-45 shows a sequence alignment of the BMR domain and hCPR showing conserved motives. Otherwise the sequence homology is not that high.

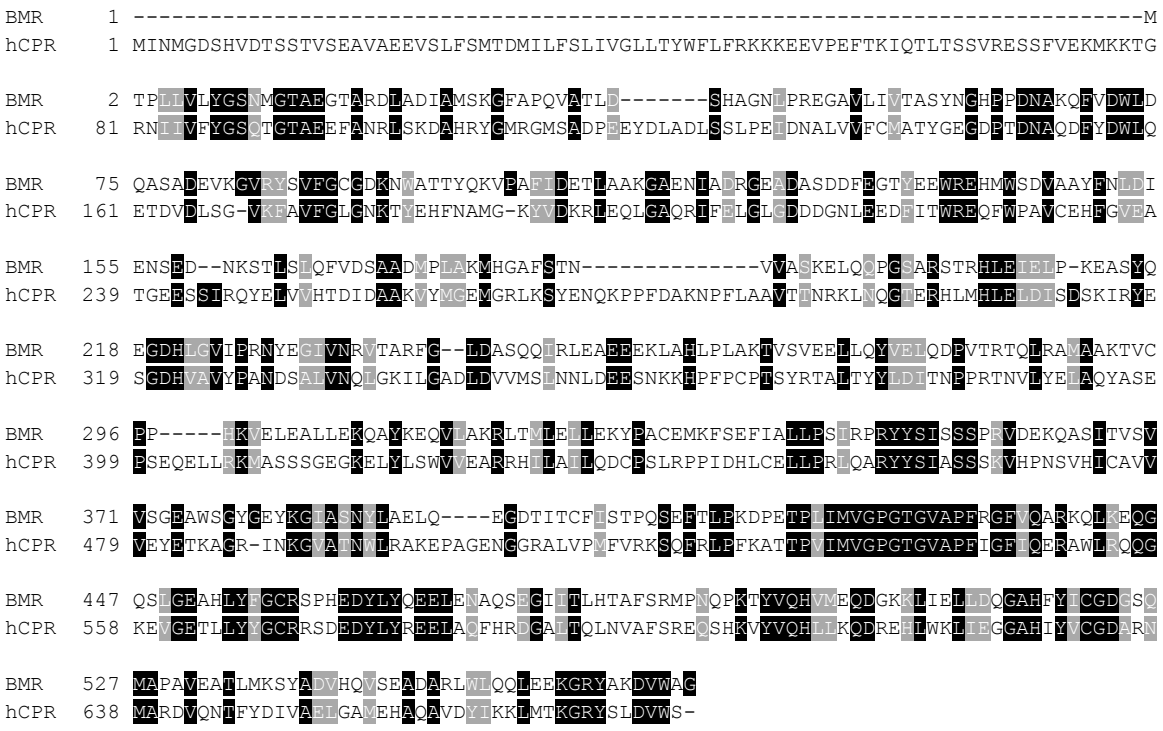

Figure 4-45: Sequence alignment of BMR and hCPR. Black and gray shading represent amino acid identity and similarity, respectively.

The construction was performed as described in 3.16 and shown in Figure 4-46. This yielded the constructs pET-Duet-1_CYP4G1_hCPR, pET-Duet-1_CYP4G2_hCPR and pET-Duet-1_CYP4GF_hCPR.

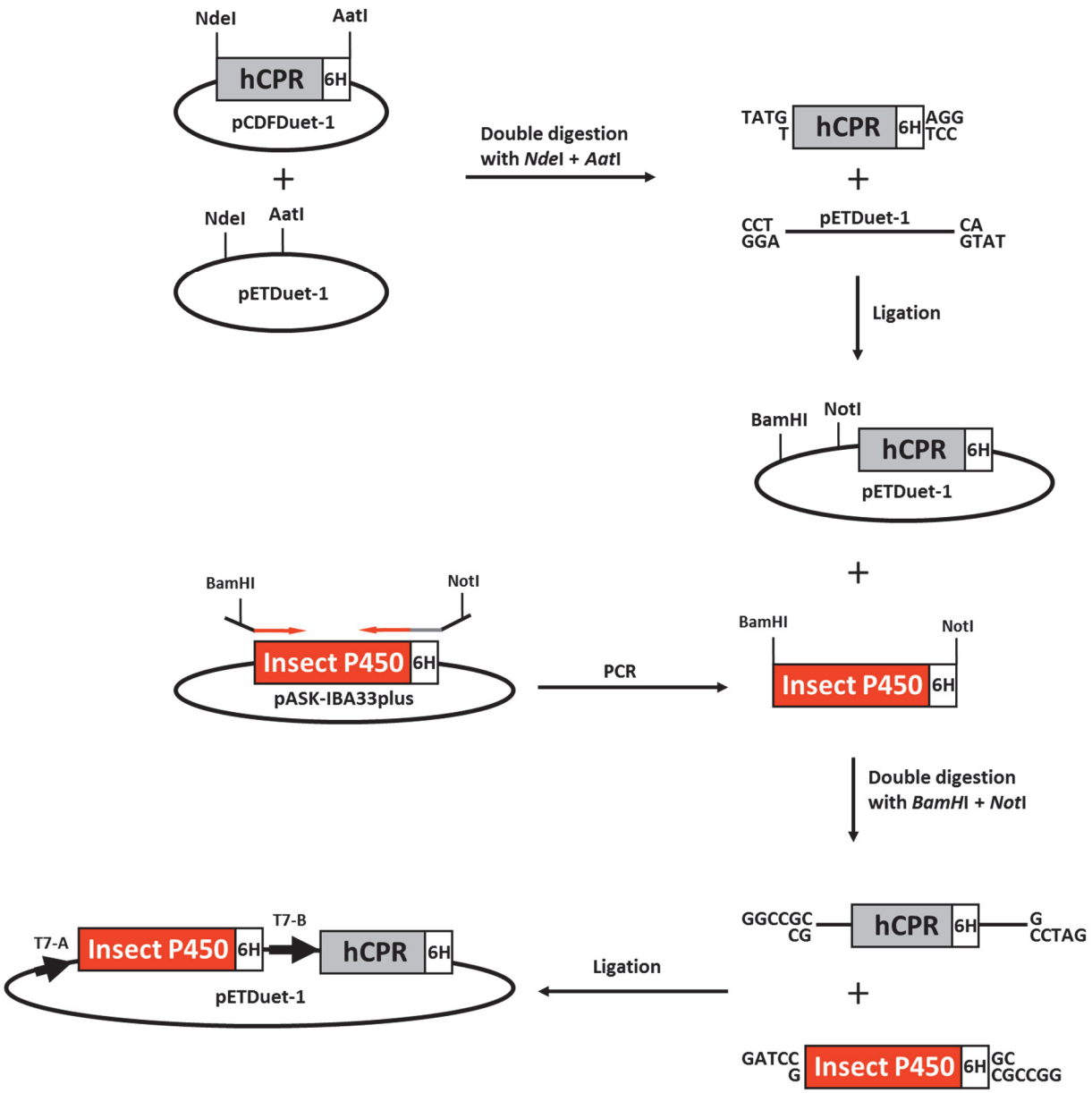

Figure 4-46: Schematic representation of the construction of plasmid with non-fusion P450 and hCPR.

4.10.4 Coexpression of New Fusion Enzyme Constructs with Acyl-ACP Reductase in *E. coli*

The coexpression of the new constructs with acyl-ACP reductase was performed as described in 3.20 and 4.9.4.

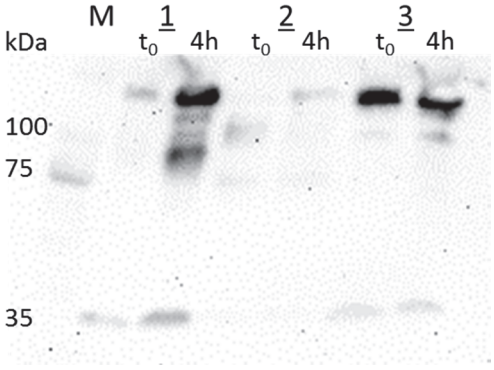

Figure 4-47: Western blot analysis of co-expressed constructs with acyl-ACP reductase in *E. coli* BL21 (DE3). 1: CYP4G1-BMR_shortLinker & acyl-ACP reductase, 2: CYP4G2-BMR_shortLinker & acyl-ACP reductase, 3: CYP4GForficula-BMR_shortLinker & acyl-ACP reductase.

The Western blot analysis in Figure 4-47 shows that the coexpression of CYP4G1-BMR_shortLinker & acyl-ACP reductase and CYP4GForficula-BMR_shortLinker & acyl-ACP reductase worked. They show the expected protein sizes for the insectCYP-BMR_shortLinker constructs at 130 kDa and the acyl-ACP reductase at 38 kDa. The coexpression of CYP4G2-BMR_shortLinker and acyl-ACP reductase did not show the expected bands in this particular expression. The constructs without linker were not tested.

4.10.5 SPME Measurements of Optimized Coproduced Constructs

The SPME measurements of the optimized coproduced constructs were performed as described in section 3.30.4 and do not show any alkane products. The results look similar to the coexpression of CYP4G2-BMR and acyl-ACP reductase shown in Figure 4-40.

4.10.6 SPME Measurements with added Aldehyde (no Coexpression)

To verify if the acyl-ACP reductase produced long-chain aldehydes are not usable by the CYP4G-BMR constructs, the known CYP4G substrate octadecanal and C8-C20 aldehyde standard were use as substrates. This replaced the necessary

coexpression system used before. Tested were single expressed fusion enzyme constructs. The constructs and results are shown in Table 4-6.

Table 4-6: SPME-GC-MS measured constructs with added aldehydes.

Construct	Added Substrate	Product
CYP4G1-BMR	octadecanal	heptadecane (contamination)
	C8-C20 aldehydes	
CYP4G2-BMR	octadecanal	
	C8-C20 aldehydes	
CYP4GForficula-BMR	octadecanal	
	C8-C20 aldehydes	
CYP4G1-BMRshortLinker	octadecanal	
	C8-C20 aldehydes	
CYP4G2-BMRshortLinker	octadecanal	
	C8-C20 aldehydes	
CYP4GForficula-BMRshortLinker	octadecanal	
	C8-C20 aldehydes	
CYP4GForficula + hCPR	octadecanal	
	C8-C20 aldehydes	

Heptadecane was detected in all measured samples. It is not a CYP4G-BMR product, since it was shown that it is a contamination of the substrates. Heptadecane was present in all controls (medium and acyl-ACP reductase produced in *E. coli*) at the same octadecanal : heptadecane ratio of 1 : 2.5.

4.10.7 Discussion of SPME Measurements of Optimized Fusion Constructs

This chapter showed the construction of the *F. auricularia* CYP4G-BMR fusion enzyme and the shortening of the fusion enzyme linker as well as the construction of non-fusion CYP4G hCPR constructs. The original linker length of the insect P450-BMR fusion enzymes was selected longer as the standard BM3 linker in order to achieve high flexibility, which is promoted by the high occurrence of the amino acids glycine, threonine and serine [61, 87]. This should enable the best possible orientation

of the BMR domain towards the exchanged heme domain. A disadvantage of the longer linker was the higher amount of potential protease cleavage sites. The results of the protein purification at room temperature (4.4.2.2) showed that the fusion protein cleaves at the linker domain. To increase the construct stability and possibly the domain interaction the linker length was reduced by ten amino acids. *F. auricularia* larvae were shown to produce alkanes as chemical defense [86] and thus this organism was a good source for the identification of new CYP4G genes. For the investigation of a novel insect CYP4G from *F. auricularia* the CYP4G was amplified from mRNA. Based on CYP4GForficula, CYP4GF-BMR as well as CYP4GF-BMR_shortLinker were constructed. The CYP4GF could be involved in n-tridecane and n-pentadecane production. Furthermore, coexpression plasmids of insect CYP4G and hCPR were constructed to examine if the CYP4G BMR interaction is not as effective as expected. hCPR was selected since it was shown before that it is able to deliver the necessary electrons to insect P450s [88]. The two genes were cloned on a pETDuet-1 vector, which offers two multiple cloning sites and two t7 promoters. In addition it is compatible with the pCDFDuet-1 vector used for acyl-ACP reductase (Novagen user protocol TB340). The constructs were tested on their ability to produce alkanes from aldehydes which were earlier produced by acyl-ACP reductase. The coproduced constructs were investigated by SPME-GC-MS as shown before (4.9.3). For none of the measured constructs alkane production could be detected. For the investigation of the missing aldehyde catalyzation the constructs were expressed alone in *E. coli*, without the presence of acyl-ACP reductase, and aldehydes were added to the culture. The results of the SPME-GC-MS measurements with added aldehydes show no activity for any of the tested CYP4G constructs. This suggests that either the aldehydes did not reach the catalytic center of the enzymes, which could be explained by the same result for each measured construct and control groups. Moreover, the constructs could be expressed inactive due to wrong folding, since the expression was performed at 37°C, which was shown before to have an impact on the constructs solubility (4.4.2.3). Additionally, they could have not implemented the heme in the catalytic center and thus were not able to catalyze the substrate decarbonylation. It was shown for the CYP6A1-BMR that heme loss can occur (4.6.3). A study that could explain the missing activity for all tested fusion enzymes showed that fusing a reductase to a P450 may produce a catalyst with

altered properties when compared to the non-fused equivalent [79]. However this cannot be the case for the non-fused CYP4G hCPR constructs.

The concept of insect P450 fusion enzyme should be the foundation for future work. Activity optimization should focus on one construct. For this the linker length should be altered in various length and the enzyme activity of those constructs should be determined by SPME-GC-MS.

5 Conclusions and Outlook

To unlock the enormous potential of insect P450 for technical applications, chemical synthesis and for their molecular and biochemical characterization they have to be made available in sufficient quality and quantity. This study applies one strategy that enables the characterization of insect P450 by using the “Molecular Lego” approach for the construction and soluble expression of insect P450-BMR fusion enzymes in *E. coli*. Four different construct variations were created and tested: insect P450-BMR with and without BM3 N-terminus, insect P450-BMR with shortened linker and coexpression of insect P450 with human CPR. Soluble expression and purification without detergents was shown for the CYP6 constructs with and without BM3 N-terminus. GC- and LC-MS methods were established for their activity determination. The lack of detectable activity let us to speculate that with current knowledge a whole-cell approach might be beneficial for the P450 activity. Thus, a whole-cell coexpression system for alkane production was established. The coexpression system consisted of a CYP4G construct (without BM3 N-terminus, or with shortened linker or with human CPR) and the blue algae acyl-ACP reductase. For the aldehyde and alkane detection a SPME-GC-MS method was established. The positive control coexpression system of blue algae acyl-ACP reductase and aldehyde decarbonylase showed for the first time alkane production in *E. coli* with this particular protein combination.

This study showed that the whole cell approach is a good foundation for further approaches. The expression of the constructed insect P450-BMR fusion constructs in another expression system, like insect cells or yeast, which were shown to be of great advantage for insect enzyme production could lead to active fusion constructs. Further studies on the linker region and the interaction of the insect P450 and BMR domain would add valuable information to our current understanding of insect P450s. Possible target sites for optimization of the linker region are the linker length and composition. They could be explored in a site-directed or random manner to identify potential improvement of activity, for example enhanced flexibility. Furthermore, the identification and elimination of potential protease cleavage sites in the linker could enhance the construct stability. Moreover, the interaction of the insect P450 and BMR resulting in their electron transfer rate and coupling efficiencies is a possible subject for optimization. The RhF reductase has been proven to be a versatile reductase partner and can be used as surrogate reductase for P450s without a known

natural redox partner [89]. Until now, no X-ray crystal structure for insect P450s is available, which could be useful for the determination of possible interaction sites with P450 reductases [60].

All results obtained in this study build a solid foundation for future work on insect P450s. The construction of fusion enzymes and the possible optimization procedures mentioned above represent a promising strategy for the utilization of insect P450s.

References

[1] R. Feyereisen, *Annu Rev Entomol* **1999**, *44*, 507-533.
[2] F. P. Guengerich, in *Cytochrome P450* (Ed.: P. Ortiz de Montellano), Springer US, **2005**, pp. 377-530.
[3] U. E. Hille, Q. Hu, M. A. E. Pinto-Bazurco Mendieta, M. Bartels, C. A. Vock, T. Lauterbach, R. W. Hartmann, *Comptes Rendus Chimie* **2009**, *12*, 1117-1126.
[4] S. Kelly, D. Kelly, C. Jackson, A. S. Warrilow, D. Lamb, in *Cytochrome P450* (Ed.: P. Ortiz de Montellano), Springer US, **2005**, pp. 585-617.
[5] T. Omura, R. Sato, *Journal of Biological Chemistry* **1964**, *239*, 2379-2385.
[6] T. Omura, R. Sato, *Journal of Biological Chemistry* **1964**, *239*, 2370-2378.
[7] M. Klingenberg, *Archives of Biochemistry and Biophysics* **1958**, *75*, 376-386.
[8] D. R. Nelson, *Philos Trans R Soc Lond B Biol Sci* **2013**, *368*, 19.
[9] D. W. Nebert, M. Adesnik, M. J. Coon, R. W. Estabrook, F. J. Gonzalez, F. P. Guengerich, I. C. Gunsalus, E. F. Johnson, B. Kemper, W. Levin, I. R. Phillips, R. Y. O. Sato, M. R. Waterman, *DNA* **1987**, *6*, 1-11.
[10] J. Hedegaard, I. C. Gunsalus, *Journal of Biological Chemistry* **1965**, *240*, 4038-4043.
[11] K. Dus, M. Katagiri, C. A. Yu, D. L. Erbes, I. C. Gunsalus, *Biochemical and Biophysical Research Communications* **1970**, *40*, 1423-1430.
[12] T. Poulos, E. Johnson, in *Cytochrome P450* (Ed.: P. Ortiz de Montellano), Springer US, **2005**, pp. 87-114.
[13] A. W. Munro, H. M. Girvan, K. J. McLean, *Natural Product Reports* **2007**, *24*, 585-609.
[14] F. P. Guengerich, *J Biochem Mol Toxicol* **2007**, *21*, 163-168.
[15] P. R. Ortiz de Montellano, *Chem Rev* **2010**, *110*, 932-948.
[16] R. Fasan, *ACS Catalysis* **2012**, *2*, 647-666.
[17] F. P. Guengerich, *Chemical Research in Toxicology* **2001**, *14*, 611-650.
[18] D. C. Lamb, M. R. Waterman, *Philosophical Transactions of the Royal Society of London B: Biological Sciences* **2013**, *368*.
[19] R. W. Estabrook, *FASEB journal : official publication of the Federation of American Societies for Experimental Biology* **1996**, *10*, 202-204.
[20] J. G. Scott, Z. Wen, *Pest Management Science* **2001**, *57*, 958-967.
[21] T. G. Wilson, E. Hodgson, *Insect Biochemistry* **1971**, *1*, 171-180.
[22] R. Feyereisen, *Pest Management Science* **2015**, *71*, 793-800.
[23] V. Dodhia, A. Fantuzzi, G. Gilardi, *J Biol Inorg Chem* **2006**, *11*, 903-916.
[24] J. G. Scott, *Insect Biochem Mol Biol* **1999**, *29*, 757-777.
[25] T. G. Wilson, E. Hodgson, *Insect Biochemistry* **1971**, *1*, 19-26.
[26] J. F. Andersen, J. G. Utermohlen, R. Feyereisen, *Biochemistry* **1994**, *33*, 2171-2177.
[27] J. F. Andersen, J. K. Walding, P. H. Evans, W. S. Bowers, R. Feyereisen, *Chemical Research in Toxicology* **1997**, *10*, 156-164.
[28] M. J. Cheesman, M. J. Traylor, M. E. Hilton, K. E. Richards, M. C. Taylor, P. J. Daborn, R. J. Russell, E. M. J. Gillam, J. G. Oakeshott, *Insect Biochemistry and Molecular Biology* **2013**, *43*, 455-465.
[29] R. W. Howard, G. J. Blomquist, *Annual review of entomology* **2005**, *50*, 371-393.
[30] Y. Qiu, C. Tittiger, C. Wicker-Thomas, G. Le Goff, S. Young, E. Wajnberg, T. Fricaux, N. Taquet, G. J. Blomquist, R. Feyereisen, *Proceedings of the*

National Academy of Sciences of the United States of America **2012**, *109*, 14858-14863.
[31] E. N. G. Marsh, M. W. Waugh, *ACS Catalysis* **2013**, *3*, 2515-2521.
[32] S. J. Sadeghi, G. Gilardi, *Biotechnology and Applied Biochemistry* **2013**, *60*, 102-110.
[33] J. R. Falck, Y. K. Reddy, D. C. Haines, K. M. Reddy, U. M. Krishna, S. Graham, B. Murry, J. A. Peterson, *Tetrahedron Letters* **2001**, *42*, 4131-4133.
[34] V. V. Shumyantseva, T. V. Bulko, R. D. Schmid, A. I. Archakov, *Biosensors and Bioelectronics* **2002**, *17*, 233-238.
[35] V. V. Shumyantseva, T. V. Bulko, A. I. Archakov, *Journal of inorganic biochemistry* **2005**, *99*, 1051-1063.
[36] X. Fang, J. R. Halpert, *Drug metabolism and disposition: the biological fate of chemicals* **1996**, *24*, 1282-1285.
[37] K. J. McLean, H. M. Girvan, A. W. Munro, *Expert Opin Drug Metab Toxicol* **2007**, *3*, 847-863.
[38] F. Sabbadin, R. Hyde, A. Robin, E. M. Hilgarth, M. Delenne, S. Flitsch, N. Turner, G. Grogan, N. C. Bruce, *Chembiochem : a European journal of chemical biology* **2010**, *11*, 987-994.
[39] F. Sabbadin, G. Grogan, N. C. Bruce, in *Cytochrome P450 Protocols* (Eds.: R. I. Phillips, A. E. Shephard, R. P. Ortiz de Montellano), Humana Press, Totowa, NJ, **2013**, pp. 239-249.
[40] T. Haga, H. Hirakawa, T. Nagamune, *PLoS One* **2013**, *8*, e75114.
[41] H. Hirakawa, T. Nagamune *Chembiochem : a European journal of chemical biology* **2010**, *11*, 1517-1520.
[42] S. J. Sadeghi, Y. T. Meharenna, A. Fantuzzi, F. Valetti, G. Gilardi, *Faraday Discussions* **2000**, *116*, 135-153.
[43] A. W. Munro, D. G. Leys, K. J. McLean, K. R. Marshall, T. W. Ost, S. Daff, C. S. Miles, S. K. Chapman, D. A. Lysek, C. C. Moser, *Trends in biochemical sciences* **2002**, *27*, 250-257.
[44] K. Ravichandran, S. Boddupalli, C. Hasermann, J. Peterson, J. Deisenhofer, *Science* **1993**, *261*, 731-736.
[45] H. Y. Li, K. Darwish, T. L. Poulos, *Journal of Biological Chemistry* **1991**, *266*, 11909-11914.
[46] S. Govindaraj, T. L. Poulos, *Biochemistry* **1995**, *34*, 11221-11226.
[47] C. S. Noble Ma Fau - Miles, S. K. Miles Cs Fau - Chapman, D. A. Chapman Sk Fau - Lysek, A. C. Lysek Da Fau - MacKay, G. A. MacKay Ac Fau - Reid, R. P. Reid Ga Fau - Hanzlik, A. W. Hanzlik Rp Fau - Munro, A. W. Munro.
[48] S. Govindaraj, T. L. Poulos, *Journal of Biological Chemistry* **1997**, *272*, 7915-7921.
[49] G. Gilardi, Y. T. Meharenna, G. E. Tsotsou, S. J. Sadeghi, M. Fairhead, S. Giannini, *Biosensors & bioelectronics* **2002**, *17*, 133-145.
[50] M. Fairhead, S. Giannini, E. J. M. Gillam, G. Gilardi, *JBIC Journal of Biological Inorganic Chemistry* **2005**, *10*, 842-853.
[51] A. C. Roulin, M. Wu, S. Pichon, R. Arbore, S. Kühn-Bühlmann, M. Kölliker, J.-C. Walser, *PLoS One* **2014**, *9*, e94098.
[52] F. P. Guengerich, M. V. Martin, C. D. Sohl, Q. Cheng, *Nature protocols* **2009**, *4*, 1245-1251.
[53] U. Schwaneberg, C. Schmidt-Dannert, J. Schmitt, R. D. Schmid, *Analytical Biochemistry* **1999**, *269*, 359-366.
[54] A. Kamel, *Journal of Agricultural and Food Chemistry* **2010**, *58*, 5926-5931.

[55] R. Feyereisen, J. F. Andersen, F. A. Cariño, M. B. Cohen, J. F. Koener, *Pesticide Science* **1995**, *43*, 233-239.
[56] N. Joussen, I. Schuphan, B. Schmidt, *Chemistry & biodiversity* **2010**, *7*, 722-735.
[57] X. Zhou, C. Sheng, M. Li, H. Wan, D. Liu, X. Qiu, *Pesticide Biochemistry and Physiology* **2010**, *97*, 209-213.
[58] D. F. Lewis, M. Dickins, P. J. Eddershaw, M. H. Tarbit, P. S. Goldfarb, *Drug metabolism and drug interactions* **1999**, *15*, 1-49.
[59] D. W. Nebert, F. J. Gonzalez, *Annual review of biochemistry* **1987**, *56*, 945-993.
[60] M. Fairhead, S. Giannini, E. J. Gillam, G. Gilardi, *J Biol Inorg Chem* **2005**, *10*, 842-853.
[61] X. Chen, J. L. Zaro, W. C. Shen, *Advanced drug delivery reviews* **2013**, *65*, 1357-1369.
[62] S. M. Hoffmann, M. J. Weissenborn, Ł. Gricman, S. Notonier, J. Pleiss, B. Hauer, *ChemCatChem* **2016**, *8*, 1591-1597.
[63] S. Govindaraj, T. L. Poulos, *Protein Science* **1996**, *5*, 1389-1393.
[64] V. R. Dodhia, A. Fantuzzi, G. Gilardi, *JBIC Journal of Biological Inorganic Chemistry* **2006**, *11*, 903-916.
[65] M. B. Murataliev, V. M. Guzov, F. A. Walker, R. Feyereisen, *Insect Biochemistry and Molecular Biology* **2008**, *38*, 1008-1015.
[66] N. Joußen, D. G. Heckel, M. Haas, I. Schuphan, B. Schmidt, *Pest Management Science* **2008**, *64*, 65-73.
[67] H. P. Sørensen, K. K. Mortensen, *Microbial Cell Factories* **2005**, *4*, 1.
[68] A. Gökçen, A. Vilcinskas, J. Wiesner, *Virulence* **2013**, *4*, 260-270.
[69] A.-K. Pöppel, M. Kahl, A. Baumann, J. Wiesner, A. Gökçen, A. Beckert, K. T. Preissner, A. Vilcinskas, Z. Franta, *Insect Biochemistry and Molecular Biology* **2016**, *70*, 138-147.
[70] J. F. Andersen, J. G. Utermohlen, R. Feyereisen, *Biochemistry* **1994**, *33*, 2171-2177.
[71] L. Zhang, X. Liu, C. Wang, X. Liu, G. Cheng, Y. Wu, *Protein Expression and Purification* **2010**, *71*, 74-78.
[72] Y. Wu, *Sensors and Actuators B: Chemical* **2011**, *156*, 773-778.
[73] Y.-B. Mao, X.-Y. Tao, X.-Y. Xue, L.-J. Wang, X.-Y. Chen, *Transgenic Research* **2011**, *20*, 665-673.
[74] Y.-B. Mao, W.-J. Cai, J.-W. Wang, G.-J. Hong, X.-Y. Tao, L.-J. Wang, Y.-P. Huang, X.-Y. Chen, *Nat Biotech* **2007**, *25*, 1307-1313.
[75] D. R. G. Price, J. A. Gatehouse, *Trends in Biotechnology* **2008**, *26*, 393-400.
[76] J. Kuper, T. S. Wong, D. Roccatano, M. Wilmanns, U. Schwaneberg, *J Am Chem Soc* **2007**, *129*, 5786-5787.
[77] C. B. Faulds, M. Perez-Boada, A. T. Martinez, *Bioresource technology* **2011**, *102*, 4962-4967.
[78] W. J. Becktel, J. A. Schellman, *Biopolymers* **1987**, *26*, 1859-1877.
[79] W. Zhang, Y. Liu, J. Yan, S. Cao, F. Bai, Y. Yang, S. Huang, L. Yao, Y. Anzai, F. Kato, L. M. Podust, D. H. Sherman, S. Li, *Journal of the American Chemical Society* **2014**, *136*, 3640-3646.
[80] A. Schirmer, M. A. Rude, X. Li, E. Popova, S. B. del Cardayre, *Science* **2010**, *329*, 559-562.
[81] F. Zhang, S. Rodriguez, J. D. Keasling, *Current Opinion in Biotechnology* **2011**, *22*, 775-783.

[82] P. P. Peralta-Yahya, F. Zhang, S. B. del Cardayre, J. D. Keasling, *Nature* **2012**, *488*, 320-328.
[83] G. Vas, K. Vekey, *Journal of mass spectrometry : JMS* **2004**, *39*, 233-254.
[84] H. J. Janßen, A. Steinbüchel, *Biotechnology for Biofuels* **2014**, *7*, 7.
[85] K. D. Belsare, A. J. Ruff, R. Martinez, A. V. Shivange, H. Mundhada, D. Holtmann, J. Schrader, U. Schwaneberg, *BioTechniques* **2014**, *57*, 13-20.
[86] T. Gasch, A. Vilcinskas, *Journal of insect physiology* **2014**, *67*, 1-8.
[87] P. Argos, *Journal of molecular biology* **1990**, *211*, 943-958.
[88] C. Saner, B. Weibel, F. E. Wurgler, C. Sengstag, *Environmental and molecular mutagenesis* **1996**, *27*, 46-58.
[89] M. Nodate, M. Kubota, N. Misawa, *Appl Microbiol Biotechnol* **2006**, *71*, 455-462.
[90] S. J. Smith, A. W. Munro, W. E. Smith, *Biopolymers* **2003**, *70*, 620-627.

Index of abbreviations

°C	Degree Celsius
A	Absorbance
Abs	Absorbance
ACP	Acyl carrier protein
BCA	Bicinchoninic acid
BM3	CYP1A102 from *Bacillus megaterium*
BMR	BM3 reductase
bp	Base pair
cDNA	Complementary deoxyribonucleic acid
CYP	Cytochrome P450 monooxygenase
D. melanogaster	*Drosophila melanogaster*
ddH_2O	Double-distilled water
DEAE	Diethylaminoethanol
DNA	Deoxyribonucleic acid
E. coli	*Escherichia coli*
EDTA	Ethylenediaminetetraacetic acid
EIC	Extracted ion chromatogram
F. auricularia	*Forficula auricularia*
FAD	Flavin adenine dinucleotide
FMN	Flavin mononucleotide
fwd	Forward
g	Relative centrifugal force
h	Hour
hCPR	Human P450 reductase
His_6-tag	Hexa histidine tag
IMAC	Immobilized Metal Affinity Chromatography
IPTG	Isopropyl β-D-1-thiogalactopyranoside
IS	Internal standard
LB	Luria-Bertani broth
LIC	Ligation-independent cloning
M	Mol/l
M. domestica	*Musca domestica*

M9	M9 minimal medium
min	Minute
mRNA	Messenger ribonucleic acid
N. punctiforme	*Nostoc punctiforme*
$NADP^+$	Nicotinamide adenine dinucleotide phosphate
NADPH	Dihydronicotinamide-adenine dinucleotide phosphate
NTA	Nitrilotriacetic acid
ORF	Open reading frame
p.a.	Analytical grade
P450	Cytochrome P450 monooxygenase
PCNA	Proliferating cell nuclear agent
PCR	Polymerase chain reaction
*p*NCA	*p*-nitrophenoxycarboxylic
PVDF	Polyvinylidene difluoride
rev	Reverse
RNA	Ribonucleic acid
RT	Room temperature
TAE	Buffer containing tris base, acetic acid and EDTA
TB	Terrific broth medium
TBS	Tris buffered saline
TBS/T	Tris buffered saline with Tween 20
TIC	Total ion chromatogram
Tris	Tris(hydroxymethyl)aminomethane
TSS	Transformation and storage solution

Moreover, the usual three-letter or one-letter codes for amino acids were used as well as standard SI units.

Index of figures

Index of tables

A Appendix

A.1 Pretests: hCPR and BM3 production, purification and activity measurements

A.1.1 Production and purification of human reductase

We produced hCPR in TB with 1 mM riboflavin, which is necessary for the build-up of FAD and FMN. The standard conditions of 4.5 h at 37°C for the protein production and purification with CHAPS and β-mercaptoethanol as detergents over a Talon column gave low amounts of very unpure protein. This is why different conditions to increase both amount and purity were tested. Table 4-2 summarizes tested conditions used for production and purification of hCPR.

Table A.1.1-1: Overview Expression and Purification Conditions of hCPR expressed in *E. coli* BL21.

Expres-sion	Cell Lysis	Centrifu-gation	Detergents	Column	Buffer
4.5 h 37°C	microfluidizer	1x	0.1% CHAPS, 1 mM β-mercaptoethanol	Talon	Tris
4.5 h 37°C	microfluidizer + ultrasonic	1x	0.2% Triton X-100, 0.2% Na-cholate	Ni-NTA	Na-phosphate + 20% glycerol
4 h 42°C	microfluidizer + ultrasonic	2x	0.5% Triton X-100, 0.5% Na-cholate	Ni-NTA	Na-phosphate + 20% glycerol
48 h 42°C	microfluidizer + ultrasonic	2x	0.5% Triton X-100, 0.5% Na-cholate	Ni-NTA	Na-phosphate + 20% glycerol
4 h 28°C	microfluidizer + ultrasonic	2x	0.5% Triton X-100, 0.5% Na-cholate	Ni-NTA	Na-phosphate + 20% glycerol
48 h 28°C	microfluidizer + ultrasonic	2x	0.5% Triton X-100, 0.5% Na-cholate	Ni-NTA	Na-phosphate + 20% glycerol

From our tests we identified the best condition for recombinant production and purification of hCPR as: protein production for 4 h at 28°C, resuspension of the pellets in lysis buffer try 2 (Table A2-10) with 0.5% Triton X-100, a nonionic detergent, and 0.5% Na-cholate, an anionic detergent, which are both widely used for solubilization of membrane proteins. Next cells were lysed twice using

microfluidizer followed by 1 h centrifugation at 75600 g to harvest the cell debris. Cell debris was resuspended in the same lysis buffer and sonicated for 10 min with 30% energy followed by final centrifugation for 30 min at 75600 g. Collected supernatant was loaded on a Ni-NTA column using IMAC buffer A try 2-6 (Table A2-10) supplemented with Triton X-100 and Na-cholate.

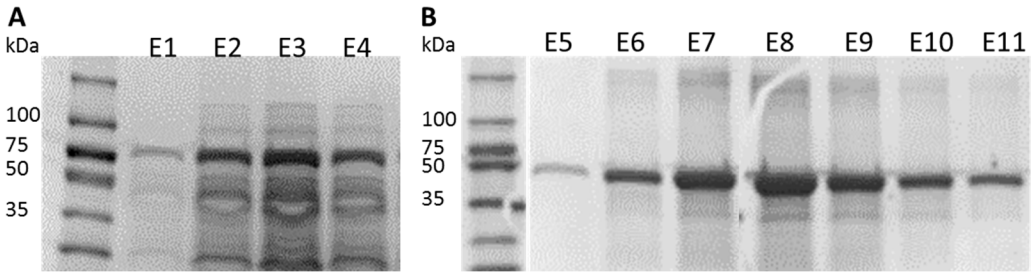

Figure A.1.1-1: SDS-PAGE of human reductase purification samples. Comparison of first purification with Talon as column raisin (Figure 4-8 A) and optimized expression and purification with Ni-NTA as column raisin (Figure 4-8 B). **A**: Fractions E1-E4: hCPR produced under standard conditions and purified via Talon column. **B**: Fractions E5-E11: hCPR produced at 28°C for 4 h, buffers supplemented with Triton X-100 and sodium cholate and purified via Ni-NTA column.

To avoid interference of Triton X-100 and Na-cholate on enzyme activity the buffer exchange was performed via ion exchange chromatography. hCPR has a pI of 5.77 which makes it suitable for an anion exchange. It was performed using Source Q15 (polymeric, strong anion exchanger) column. The pooled IMAC fractions (7 ml) were diluted with anion exchange buffer A1 (Table A2-10) to a final volume of 70 ml to reduce the salt concentration and enable binding. The loaded samples were washed with anion exchange buffer A2 (Table A2-10) and then eluted with 500 mM NaCl. The final protein amount was determined by comparison to a BSA standard curve on a SDS-PAGE gel (Figure 4-9 A). We achieved a final concentration of ca. 2 mg/ml hCPR. The yellow color caused by FAD and FMN in the reductase is clearly visible in the highest concentrated elution fraction E15 (Figure A.1.1-2 B).

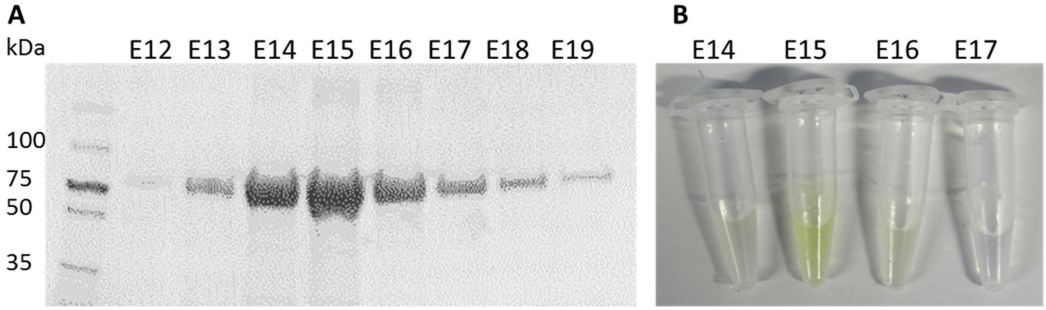

Figure A.1.1-2: hCPR samples after anion exchange purification. **A**: SDS-PAGE gel of anion exchanged purified hCPR fractions E12-E19. **B**: Corresponding samples of fractions E14-E17. The yellow color caused by FAD and FMN is clearly visible in fraction E15.

A.1.2 Production and purification of BM3

The expression of BM3 was performed in TB medium with 1 mM δ-aminolevulinic acid, 1 mM thiamine and 1 mM riboflavin. The δ-aminolevulinic acid and thiamine are important for the build-up of the heme ring in the P450 domain and riboflavin for FAD and FMN in the reductase domain. The 4.5 h long expression at 37°C and 180 rpm was induced at an OD_{600} of 1. Cells were harvested by centrifugation at 17000 g for 10 min at 10°C.

Pelleted cells were resuspended in IMAC buffer A (Table A2-11) and lysed twice using microfluidizer prior purification. Cell debris was removed by centrifugation at 75000 g for 30 min at 10°C and resulting supernatant was loaded on a Ni-NTA column. Recombinant BM3 was eluted by IMAC buffer B (Table A2-11) containing 200 mM imidazole, Figure A.1.2-1.

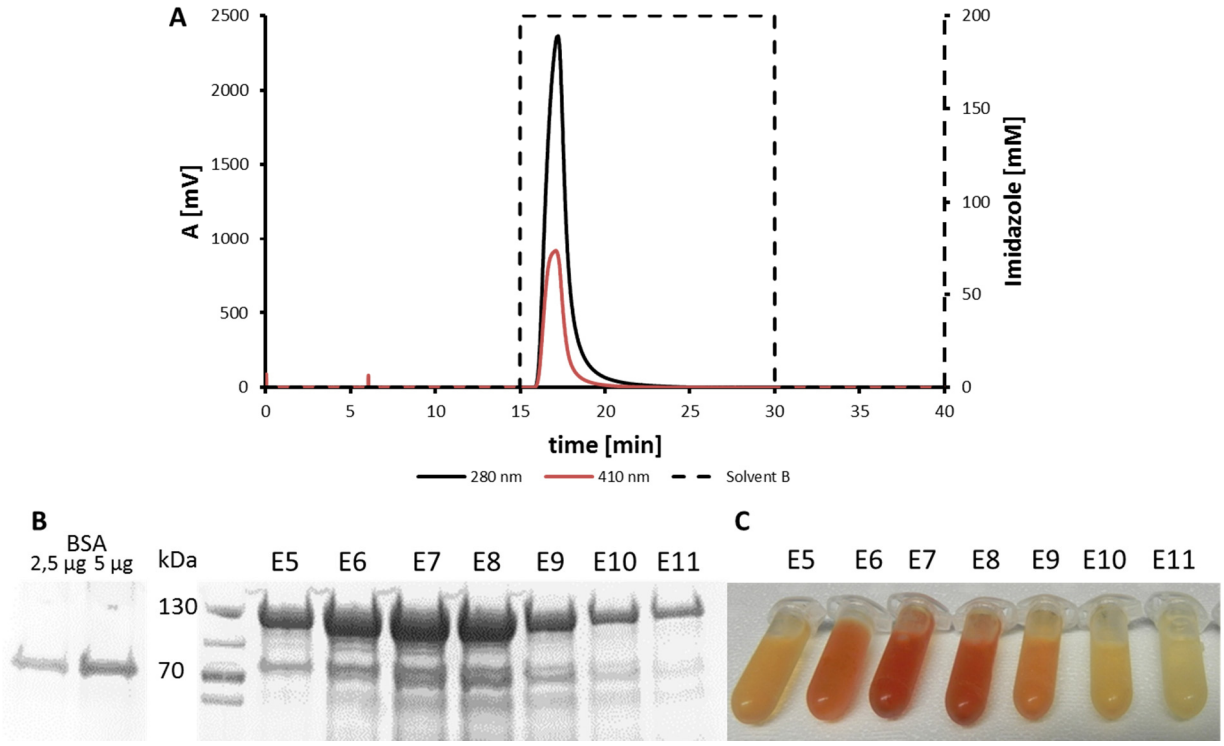

Figure A.1.2-1: IMAC purification of recombinant produced BM3. **A**: Elution profile of IMAC purification of BM3 using Ni-NTA column and imidazole as eluent. **B**: SDS-PAGE of IMAC purified BM3 fractions E5-E11 and BSA as comparison for protein amount determination. **C**: Corresponding BM3 elution fraction E5-E11. The red color is caused by the incorporated heme group.

BM3 has a pI of 5.37 which makes it suitable for an anion exchange. The anion exchange was performed using DEAE-Sepharose (weak anion exchanger) to remove imidazole which was shown to inhibit P450 reactions [90]. To enable binding on the column the salt content of the eluted fraction was reduced by adding 10 volumes of anion exchange buffer A (Table A2-11) to the samples.

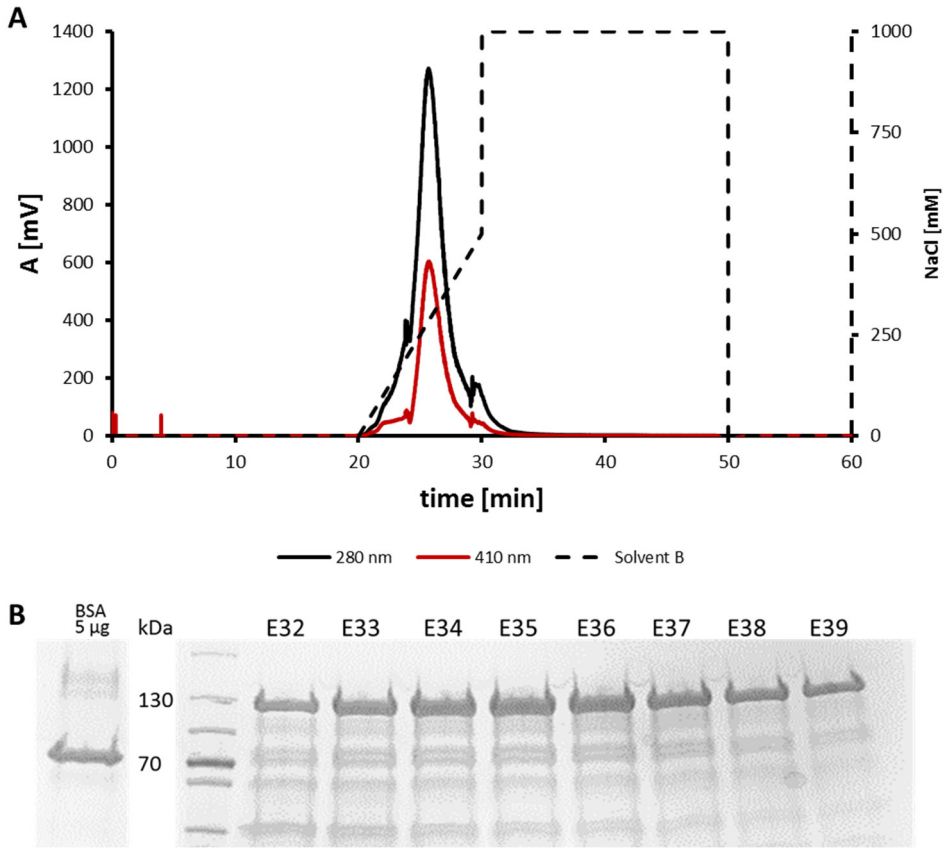

Figure A.1.2-2: Ion exchange purification of recombinant produced BM3. **A**: Elution profile of anion exchange purification of BM3 over DEAE-Sepharose column eluted with sodium chloride. **B**: SDS-PAGE of anion exchange purified BM3 fractions E32-E39 with BSA as comparison for protein amount determination.

BM3 was eluted with an increasing gradient from 0 to 500 mM sodium chloride (Figure A.1.2-2 A). The SDS-PAGE gel (Figure A.1.2-2 B) shows unimpaired BM3 at the expected size of 130 kDa in lower concentrations than the IMAC purified fractions (Figure 4-10 B).

A.1.3 Photometric enzyme activity measurements of purified hCPR

The photometric analysis of the hCPR activity is based on the measurement at 550 nm of the absorbance change of the surrogate substrate cytochrome c from its oxidized (ferrocytochrome c) to its reduced form (ferricytochrome c), Figure A.1.3-1.

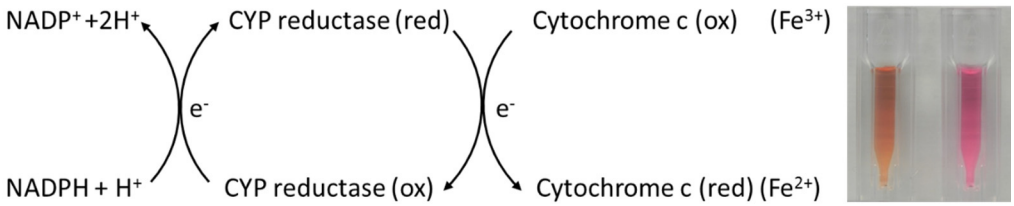

Figure A.1.3-1: Electron flow from NADPH to cytochrome c and the color change from orange (cytochrome c (ox)) to pink (cytochrome c (red)).

The kinetic measurements of recombinant hCPR were performed at 550 nm for 3 min. The results (Figure A.1.3-2) show that the highest enzymatic activity of purified hCPR can be achieved when the purification was performed with CHAPS.

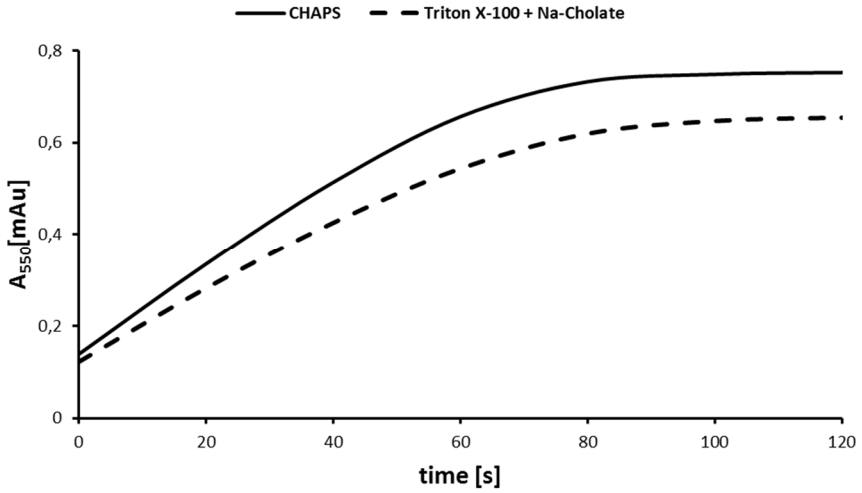

Figure A.1.3-2: Kinetic measurements of purified hCPR with cytochrome c at 550 nm for 3 min.

A.1.4 Photometric enzyme activity measurements of purified BM3

The enzyme activity of BM3 can be tested directly by the photometric *p*NCA-assay, which detects the turnover of the P450 surrogate substrate *p*NCA (Figure A.1.4-1), or indirectly by the photometric measurements of the NADPH conversion by the BMR domain.

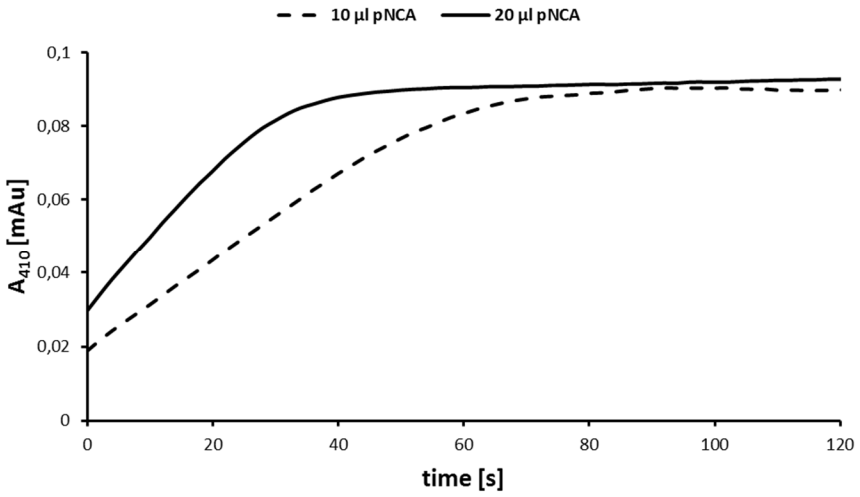

Figure A.1.4-1: Kinetic measurements of purified BM3 (45 µg/ml) with pNCA as surrogate substrate at 410 nm for 3 min.

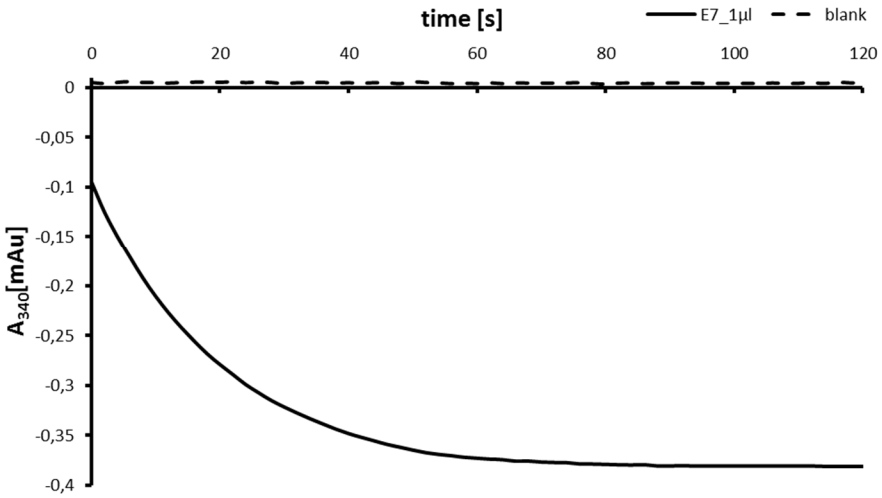

Figure A.1.4-2: Kinetic measurements of purified BM3 (45 µg/ml) with SDS as substrate at 340 nm for 3 min.

A.2 Materials

A.2.1 Chemicals

Table A.2.1-1: Chemicals used in this study.

Substance	Supplier	Catalog number
(±)-Citronellal ≥ 95%	Sigma-Aldrich	27470-100ML-F
(±)-Gossypol from cotton seeds	Sigma-Aldrich	G8761
1-Nonadecene	TCI	SO349
1-Nonene	Fluka	74323
2-Mercaptoethanol	Bio-Rad	161-0710
2-Propanol, 70%	Roth	CN09.4
2-Propanol, Rotisolv	Roth	73431
4,4'-DDD	Sigma-Aldrich	35486
4,4'-DDE	Sigma-Aldrich	35487
4,4'-DDT	Sigma-Aldrich	31041
4-Methyl-5-thiazolethanol	Sigma-Aldrich	W320404-SAMPLE-K
5-Aminolevulinic acid hydrochloride	Roth	8451.2
5-Aminolevulinic acid hydrochloride	Sigma-Aldrich	A3785
7-Ethoxycoumarin	Sigma-Aldrich	E1379
Acetic acid ethyl ester GC Ultra Grade	Roth	KK42.1
Acetone, 99.5%	Roth	5025.5
Acetonitrile ROTISOLV® HPLC Gradient Grade	Roth	8825.2
Agar-Agar, bacteriological	Roth	2266.2
Aldrin	Sigma-Aldrich	36666
Alkane standard solution C8-C20, analytical standard, contains C8-C20, ~40 mg/L each, in hexane	Sigma-Aldrich	4070
Ampicillin Sodium Salt	Roth	K029.2
Anhydrotetracyclin	iba	
Carbenicillin disodium salt	Roth	6344.2
CHAPS	Roth	1479.4
Chlordane	Sigma-Aldrich	45378
Chlordene	Sigma-Aldrich	31517
Citral 95%	Sigma-Aldrich	C83007
Cyromazine	Sigma-Aldrich	45414
Cytochrome c from equine heart	Sigma-Aldrich	C2506
D (+) Glucose anhydrous	Roth	HN06.3
Decanal ≥98% (GC), liquid	Sigma-Aldrich	D7384
Deltamethrin	Sigma-Aldrich	45423
Dichlormethane	Sigma-Aldrich	32222

Substance	Supplier	Catalog number
Dieldrin	Sigma-Aldrich	33491
Dimethyl sulfoxide for molecular biology	Roth	A994.2
Dimethyl sulfoxide Rotidry	Roth	5179.1
Di-Potassium hydrogen phosphate	Roth	P749.2
di-Sodium hydrogen phosphate dihydrate	Roth	4984.2
Dodecyl aldehyde 92%	Sigma-Aldrich	D222003
Ethanol 99.5% denatured with 1% MEK	VWR	85.033.460
Ethanol, Rotipuran	Roth	9065.2
Ethylenediamine tetraacetic acid	Roth	CN06.1
Flavin adenine dinucleotide disodium salt hydrate	Sigma-Aldrich	F6625
GelGreenTM Nucleic Acid Stain	Biotium	41005
Glycerol Rotipuran	Roth	3783.2
Glycine Pufferan	Roth	3908.3
Hexane	Sigma-Aldrich	32293
Hydrochloric acid 25 %	Roth	X897.1
Imidacloprid	Sigma-Aldrich	37894
Imidacloprid-Olefin	Dr. Ehrenstorfer	C14283760
Imidazole	Sigma-Aldrich	I2399
IPTG	Roth	CN08.3
Iron (III) chloride reagent grade	Sigma-Aldrich	157740
Kanamycin sulphate	Roth	T832.1
Laemmli Sample buffer 3x	Bio-Rad	161-0737
LB Broth (Lennox)	Roth	X964.3
Magnesium chloride hexahydrate	Roth	2189.2
Magnesium sulfate	Sigma-Aldrich	M2643
Methanol Rotisolv	Roth	7432.1
Mucasol	Sigma-Aldrich	Z637203
Nonanal 95%	Sigma-Aldrich	N30803
Octadecanal	TCI	O0368
Oleic acid, Rotichrom GC	Roth	5362.1
Permethrin	Fluka	45614
Polyethylene glycol 6000	Roth	0158.4
Potassium chloride	Roth	HN02.1
Potassium dihydrogen phosphate	Roth	P018.2
Riboflavine ≥ 97% Ph.Eur.	Roth	9607.1
Riboflavine 5'monophosphate sodium salt hydrate	Sigma-Aldrich	F2253
Roti-Blue quick	Roth	4829.2
Rotiphorese® 10x SDS-PAGE	Roth	3060
SDS Pellets ≥ 99%	Roth	CN303

Substance	Supplier	Catalog number
SDS, ultra pure	Roth	2326.1
Sodium chloride	Roth	9265.2
Sodium choleate	Sigma-Aldrich	S9875
Sodium dihydrogen phosphate dihydrate	Roth	T879.2
Sodium hydroxide solution	Roth	KK71.1
Sodium sulfate	Sigma-Aldrich	239313
Streptomycin sulfate	Roth	HP66.1
Terrific-Broth-Medium	Roth	X972.3
Thiacloprid	Sigma-Aldrich	37905
Thiamin hydrochloride	Roth	T911.2
Tris Pufferan	Roth	AE15.3
Tris-HCl	Roth	9090.3
Triton X-100	Roth	3051.3
Tween 20	Roth	9127.1
Umbelliferone	Roth	5371.1
β-Nicotineamide adenine dinucleotide phosphate reduced tetra (cyclohexylammonium) salt	Sigma-Aldrich	N5130

A.2.2 Consumables

Table A.2.2-1: Consumables used in this study.

Material	Supplier	Catalog number
10 ml Disposable syringes Injekt®, Luer-fitting, Braun	Roth	0058.1
20 ml Disposable syringes Injekt®, Luer-fitting, Braun	Roth	0059.1
4–15% Mini-PROTEAN® TGX™ Gels	Bio-Rad	456-1086
5 ml Disposable syringes Injekt®, Luer-fitting, Braun	Roth	00057.1
Corning®96 well Plates	GBO	655185
Extra Thick Blot Paper	Bio-Rad	1703965
Handschuhe TouchNTuff®	Ansell	92-600
Parafilm® M	Roth	H666.1
Protino Ni-NTA Agarose	Macherey-Nagel	745.400.100
Qsepharose Fast Flow	GE Healthcare	17-0510-01
Roti®-Store cryo vials	Roth	P730.2
Rotilabo®-syringe filters, 0.22 µm	Roth	P666.1
Kinetex 2.6 u C18 100 Å, 150 x 2.1 mm	phenomenex	00F-4462-AN

A.2.3 Devices

Table A.2.3-1: Devices used in this study.

Machine	Model	Company
Air compressor	CPM 160-8-6 W oilfree	CompactMaster
Autoclave	5075 ELV	Tuttnauer
Autoclave	3850 EL	Tuttnauer
Balance	ABT 220-5DM	Kern
Balance	Excellence XA 1502 S	Mettler Toledo
Balance	Excellence XA 105 Dual Range	Mettler Toledo
Biosafety cabinet	ESCO Class II biosafety cabinet	biomedis
Blotter	Trans-Blot Turbo Transfer System	BioRad
Centrifuge	uniCFUGE 2	LLG Labware
Centrifuge	Mikro 220R	Hettich
Centrifuge	Rotina 420R	Hettich
Centrifuge	Avanti J-26 XP	Beckman Coulter
Dishwasher	Compact Desinfektor G7783 CD Mielabor	Miele
Electrophoresis Power Supply	EV231	Consort
Freezer -20°C	Froster	Kirsch
Freezer -80°C	6343-6345/6383-6385	GFL
GC-MS	CT 1128	Constellation Technology Corporation
GC-MS	Agilent 5977 Series GC/MSD System	Agilent Technologies
Gel Documentation Station	VersaDoc Imaging System 4000 MP	BioRad
Gel Electrophoresis Chamber	Mini-PROTEAN Tetra System	BioRad
Hearing Protectors	Sperian T1	Howard Leight
Hearing Protectors	Optime I	Peltor
Homogenizer	M-110P	Microfluidics
Hotplate Stirrer	Hotplate Stirrer Model L-81	Labinco
Hotplate Stirrer	VMS-A	VWR
HPLC	ÄKTAPrime plus	GE Healthcare
HPLC	SE04 system	ECOM
HPLC	UltiMate 3000	Dionex
Ice Machine	AF 80	Scotsman
Incubator	Heraeus Oven	Thermo
LC-MS/ Ion Trap	Ultimate 3000/ amaZon ETD	Dionex/ Bruker

Machine	Model	Company
Lyophilizer / Freeze dryer	RVC 2-33IR	CHRIST
Microplate Reader	Eon	Biotek Instruments
Microwave	Grill Hot Air	Sharp
Multichannel Pipette	Rainin Pipet-Lite XLS 2-20 µl	Mettler Toledo
Multichannel Pipette	Rainin Pipet-Lite XLS 20-200 µl	Mettler Toledo
PCR Cycler	C1000 Thermal Cycler	BioRad
pH-Meter	Seven Multi	Mettler Toledo
Photometer	Specord 210	analytic Jena
Pipette	Rainin Pipet-Lite XLS 0.1-2 µl	Mettler Toledo
Pipette	Rainin Pipet-Lite XLS 2-20 µl	Mettler Toledo
Pipette	Rainin Pipet-Lite XLS 10-100 µl	Mettler Toledo
Pipette	Rainin Pipet-Lite XLS 20-200 µl	Mettler Toledo
Pipette	Rainin Pipet-Lite XLS 100-1000 µl	Mettler Toledo
Pipette Controller	Rainin Pipet-X	Mettler Toledo
Purified Water System	TKA-GenPure	Thermo
Refrigerator	Super	Kirsch
Refrigerator	MPR 1411PE	Panasonic
rosett cell		
Shake Incubator	Multitron II	Infors HAT
Shaker	Rocker 25	Labnet
Thermo shaker	TS-100 SC-20	bioSan
Ultrasonic Bath	Sonorex	Bandelin
Ultrasonic Homogenizer	Sonopuls HD2200	Bandelin
Ultrasonic Homogenizer Sonotrode	MS 72	Bandelin
Vortex	VV3	VWR
Water bath	Microprocessor control MPC	huber

A.2.4 Oligonucleotide Primers

Table A.2.4-1: Oligonucleotide Primers used for P450 Fusion Construction.

Primers for P450 Fusion Construction		
Construct	**Primer Name**	**Primer Sequence 5'-3'**
pASK-IBA33_CYP6A1_BM3_KS	CYP6A1_fw_KpnI	CGCGGTACCAGCGTTGGAACTTTGGGTATTGGAAACGTCGTGGTATTCCGCATGAG
	CYP6A1_rev_linker+SalI	CCGGTCGACGGACTAGGGATCCCTCCGAGGGGAATTTTCTTGCTTTTGATTTTCTTGCGAATTGC
pASK-IBA33_CYP6A1_BM3_XS	CY6A1d20_fwd_XbaI	GGTATCTAGAatgagcCGTTGGAACTTTGGGTATTGGAAACGTCGTGGTATTCCG
	CYP6A1_rev_linker+SalI	CCGGTCGACGGACTAGGGATCCCTCCGAGGGGAATTTTCTTGCTTTTGATTTTCTTGCGAATTGC
pASK-IBA33_CYP6G1_BM3_KS	CYP6G1_fw_KpnI	CGCGGTACCAGCGCAATCACTCATACTGGCAGCGTAAAGGGATTCCGTACATTCCGCCGAC
	CYP6G1_rev_linker+SalI	CCGGTCGACGGACTAGGGATCCCTCCGAGGGGAATTTTCTTGCTTTGAAGCGACGGAGCTGATTG
pASK-IBA33_CYP6G1_BM3_XS	CYP6G1d20_fwd_XbaI	GGTATCTAGAatgagcCGCAATCACTCATACTGGCAGCGTAAAGGGATTCCGTACATTCCG
	CYP6G1_rev_linker+SalI	CCGGTCGACGGACTAGGGATCCCTCCGAGGGGAATTTTCTTGCTTTGAAGCGACGGAGCTGATTG
pASK-IBA33_CYP6AE14_BM3_KS	CYP6AE14_fw_KpnI	CGCGGTACCAGAAGAAGAAATACCAGTATTGGGAGAAACGCAAAGTTCCGCATCTCCCGCCGGTG
	CYP6AE14_rev_SalI	TCAGTCGACGGACTAGGGATCCCTCCGAGGGGAATTTTCTTGCTATAGGCTTTCTCCAGGTTC
pASK-IBA33_CYP6AE14_BM3_XS	CYP6AE14d20_fwd_XbaI	GGTATCTAGAatgagcAAGAAGAAATACCAGTATTGGGAGAAACGCAAAGTTCCGCATCTCCCGC
	CYP6AE14_rev_SalI	TCAGTCGACGGACTAGGGATCCCTCCGAGGGGAATTTTCTTGCTATAGGCTTTCTCCAGGTTC
pASK-IBA33_CYP4G1_BM3_KS	CYP4G1_fw_delta_KpnI	CGCGGTACCAGGCACTTTATGAATATTGGCGTCGCAACTCTCGCGAATATCGTATGGTTGCAAATATTCCGTCGCCTCCGGAACTGCC
	CYP4G1_rev_Linker+SalI	CTGCTCAGTCGACGGACTAGGGATCCCTCCGAGGGGAATTTTCTTGCTCGCAACAGTCGCGTACTGG
pASK-IBA33_CYP4G1_BM3_XS	CYP_fw_universal_XbaI_neu2	GAGTTATTTTACCACTCCCTATCAGTGATAGAGAAAAGTGAAATGAATAGTTCGACAAAAATCTAGAAATAATTTTGTTTAACTTTAAGAAGGAGATATACAAATGGATTCAG
	CYP4G1_rev_Linker+SalI	CTGCTCAGTCGACGGACTAGGGATCCCTCCGAGGGGAATTTTCTTGCTCGCAACAGTCGCGTACTGG

Construct	Primer Name	Primer Sequence 5'-3'
pASK-IBA33_CYP4G2_BM3_KS	CYP4G2v1_fw_delta_KpnI	CGCGGTACCAGAGCCTGTACGAGATTTGGCTCCGCAACACCCGTAAATACAAGCTGAC
	CYP4G2_rev_Linker+SalI	CTGCTCAGTCGACGGACTAGGGATCCCTCCGAGGGGAATTTTCTTGCTCATTGCTTTCATGGC
pASK-IBA33_CYP4G2_BM3_XS	CYP_fw_universal_XbaI_neu2	GAGTTATTTTACCACTCCCTATCAGTGATAGAGAAAAGTGAAATGAATAGTTCGACAAAAATCTAGAAATAATTTTGTTTAACTTTAAGAAGGAGATATACAAATGGATTCAG
	CYP4G2_rev_Linker+SalI	CTGCTCAGTCGACGGACTAGGGATCCCTCCGAGGGGAATTTTCTTGCTCATTGCTTTCATGGC
pASK-IBA33_CYP4GF_Histag	CYP4GF_fwd_EcoRI	TCCCGAATTCATGTCTTTTGCGGACGCACTTGAAATGGTCGCAAC
	neu_CYP4GF_rev_Histag_BamHI	GGGATCCGTGGTGGTGATGGTGATGACCGGCAATAGCCTTGCCACGATTTC
pASK-IBA33_CYP4GF_BM3_KS	dCYP4GF_fwd_KpnI	CGCGGTACCAGTATATCTTTTATTATTGGTTTTCAAGACGTCGTCTCAATGAAATGGCTTCAAAAATTCC
	CYP4GF_rev_SalI	TCAGTCGACGGACTAGGGATCCCTCCGAGGGGAATTTTCTTGCTGGCAATAGCCTTGCCACGATTTC
pASK-IBA33_CYP4GF_BM3_XS	CYP4GF_fwd_XbaI	TCTAGAAATAATTTTGTTTAACTTTAAGAAGGAGATATACAAATGTCTTTTGCGGACGCACTTGAAATGGTCGCAACCAC
	CYP4GF_rev_SalI	TCAGTCGACGGACTAGGGATCCCTCCGAGGGGAATTTTCTTGCTGGCAATAGCCTTGCCACGATTTC
pASK-IBA33_CYP6A1_BM3_XS_shortLinker	CY6A1d20_fwd_XbaI	GGTATCTAGAatgagcCGTTGGAACTTTGGGTATTGGAAACGTCGTGGTATTCCG
	CYP6A1_rev_kurzer Linker+SalI	CCGGTCGACGGACTTTTGATTTTCTTGCGAATTGC
pASK-IBA33_CYP6G1_BM3_XS_shortLinker	CYP6G1d20_fwd_XbaI	GGTATCTAGAatgagcCGCAATCACTCATACTGGCAGCGTAAAGGGATTCCGTACATTCCG
	CYP6G1_rev_kurzer Linker+SalI	CCGGTCGACGGACTTTGAAGCGACGGAGCTGATTG
pASK-IBA33_CYP4G1_BM3_XS_shortLinker	CYP_fw_universal_XbaI_neu2	GAGTTATTTTACCACTCCCTATCAGTGATAGAGAAAAGTGAAATGAATAGTTCGACAAAAATCTAGAAATAATTTTGTTTAACTTTAAGAAGGAGATATACAAATGGATTCAG
	CYP4G1_rev_kurzer Linker+SalI	CTGCTCAGTCGACGGACTCGCAACAGTCGCGTACTGG
pASK-IBA33_CYP4G2_BM3_XS_shortLinker	CYP_fw_universal_XbaI_neu2	GAGTTATTTTACCACTCCCTATCAGTGATAGAGAAAAGTGAAATGAATAGTTCGACAAAAATCTAGAAATAATTTTGTTTAACTTTAAGAAGGAGATATACAAATGGATTCAG
	CYP4G2_rev_kurzer Linker+SalI	GCGCTCAGTCGACGGACTCATTGCTTTCATGGC
pASK-IBA33_CYP4GF_BM3_XS_shortLinker	CYP4GF_fwd_XbaI	TCTAGAAATAATTTTGTTTAACTTTAAGAAGGAGATATACAAATGTCTTTTGCGGACGCACTTGAAATGGTCGCAACCAC
	CYP4GF_rev_kurzer Linker+SalI	TCAGTCGACGGACTGGCAATAGCCTTGCCACGATTTC

Table A.2.4-2: Oligonucleotide Primers used for Sequencing.

Sequencing Primers		
Vector	**Primer Name**	**Primer Sequence 5'-3'**
pASK-IBA33plus	Seq_fwd_pASK	GAGTTATTTTACCACTCCCT
	Seq_rev_pASK	CGCAGTAGCGGTAAACG
	Seq_BM3CYP_rev_linker	TCACGCGCAGTACCTTC
	SeqBM3_rev	AGA ATC CAA AGT CGC AAC TTG
pCDF-Duet-1	Seq_rev_pCDFDuet-1	GCTAGTTATTGCTCAGCGG
	Seq_fwd_pCDFDuet-1	GGATCTCGACGCTCTCCCT
pET-Duet-1	Seq_fwd1_pET Duet	ATGCGTCCGGCGTAGA
	Seq_rev1_pET Duet	GATTATGCGGCCGTGTACAA
	Seq_fwd2_pET Duet	TTGTACACGGCCGCATAATC
	Seq_rev2_pET Duet	GCTAGTTATTGCTCAGCGG

Table A.2.4-3: Oligonucleotide Primers used for mRNA amplification.

Primers for mRNA amplification	
Primer Name	**Primer Sequence 5'-3'**
fwd_kurz_CYP4G_Forfiucla	TTCAAGTGGCCTCATTGATAAG
rev_kurz_CYP4G_Forfiucla	AACGGTGCATTCACTCATAAAG
fwd_lang_CYP4G_Forfiucla	CCTCATTGATAAGAATTG
rev_lang_CYP4G_Forfiucla	CGATTTATTTACCGATAAAC
fwd_CYP4G_erweitert_Forficula	CTTTATGAGTGAATGCACCGTT
rev_CYP4G_erweitert_Forficula	TATTTACCGATAAACAATAAAATAATTACATCAC
rev_CYP4G_erweitert2_Forficula	ACATCACTATTTATAAAATAAAATAAGGAATTGA AATATTAC

A.2.5 Restriction Enzymes

Table A.2.5-1: Restriction Enzymes used in this study.

Restriction Enzyme	Supplier
*Kpn*I	Thermo Fisher Scientific
*Sal*I	Thermo Fisher Scientific
*Xba*I	Thermo Fisher Scientific
*Nde*I	Thermo Fisher Scientific
*BamH*I-HF	New England Biolabs
*Not*I-HF	New England Biolabs
*EcoR*I-HF	New England Biolabs
*Nco*I-HF	New England Biolabs
*Kpn*I-HF	New England Biolabs
*Sal*I-HF	New England Biolabs
*Xba*I	New England Biolabs
*Mph*1103I (*Nsi*I)	Thermo Fisher Scientific
*Hind*III	Thermo Fisher Scientific
*Xho*I	Thermo Fisher Scientific
*Pae*I	Thermo Fisher Scientific
*Aat*II	Thermo Fisher Scientific

A.2.6 Culture Media

Table A.2.6-1: Composition of *E. coli* Culture Media.

Medium	Supplier	Catalog Number
LB-Medium	Roth	6673.1
TB-Medium	Roth	63237
LB-Agar 1,5%	Roth	

Additives for Expression Cultures	
1 M	5-Aminolevulinic acid
1 M	Thiamin
2mM	Riboflavin
0.5 g/l	$FeCl_3$

Minimal Medium M9	
10x M9-Salts (pH7.2)	
337 mM	$NaH_2PO_4*2H_2O$
220 mM	KH_2PO_4
85.5 mM	NaCl
93.5 mM	NH_4Cl

M9-Medium	
1x	M9-Salts
3%	Glucose
1 mM	$MgSO_4$
0.3 mM	CaCl
1 mM	Thiamin
1 mM	5-Aminolevulinic acid

TSS-Medium	
10%	PEG
50 mM	MgCl ($6H_2O$)
5% (v/v)	DMSO
ad. final volume	LB-Medium

A.2.7 Buffers

Table A.2.7-1: Composition of 0.1 M Sodium Phosphate Buffer.

0.1 M Sodium Phosphate Buffer (pH7.4)	
154.8 ml	1 M Na_2HPO_4
45.2 ml	1 M NaH_2PO_4
ad. 2000 ml	dH_20

Table A.2.7-2: Composition of Buffers used for Fusion Protein Purification at room temperature.

IMAC Buffers for Fusion Protein Purification (RT)	
Lysis Buffer 1: (pH7.5)	
100 mM	NaCl
20%	Glycerol
30 mM	Tris-HCl
Lysis Buffer 2: (pH7.5)	
100 mM	NaCl
20%	Glycerol
30 mM	Tris-HCl
2%	CHAPS
IMAC Buffer A: (pH7.5)	
100 mM	NaCl
20%	Glycerol
30 mM	Tris-HCl
30 mM	Imidazole
1%	CHAPS
IMAC Buffer B: (pH7.5)	
100 mM	NaCl
20%	Glycerol
30 mM	Tris-HCl
500 mM	Imidazole
1%	CHAPS
Anion Exchange Buffer A (pH 7.4)	
10 mM	0.1 M Sodium Phosphate Buffer
20%	Glycerol
0.1%	CHAPS
Anion Exchange Buffer B (pH 7.4)	
10 mM	0.1 M Sodium Phosphate Buffer
20%	Glycerol
0.1%	CHAPS
1 M	NaCl

0.1 M Sodium Phosphate Buffer (pH7.4) (2000 ml)	
154.8 ml	1 M Na_2HPO_4
45.2 ml	1 M NaH_2PO_4

Table A.2.7-3: Composition of Buffers used for Fusion Protein Purification at 4°C.

IMAC Buffers for Fusion Protein Purification (4°C)

Lysis Buffer: (pH7.5)	
100 mM	NaCl
20%	Glycerol
30 mM	Tris-HCl

Buffer A: (pH7.5)	
100 mM	NaCl
20%	Glycerol
30 mM	Tris-HCl
30 mM	Imidazole

Buffer B: (pH7.5)	
100 mM	NaCl
20%	Glycerol
30 mM	Tris-HCl
500 mM	Imidazole

Anion Exchange Buffer A (pH 7.4)	
20 mM	Tris-HCl
20%	Glycerol

Anion Exchange Buffer B (pH 7.4)	
20 mM	Tris-HCl
20%	Glycerol
1 M	NaCl

Table A.2.7-4: Composition of Buffers used for hCPR Purification.

Buffers for hCPR Purification	
Lysis Buffer Try 1: (pH7.5)	
100 mM	NaCl
30 mM	Tris-HCl
1 mM	β-mercaptoethanol
IMAC Buffer A Try 1: (pH7.5)	
100 mM	NaCl
30 mM	Tris-HCl
1 mM	β-mercaptoethanol
0.1 %	CHAPS
IMAC Buffer B Try1: (pH7.5)	
100 mM	NaCl
30 mM	Tris-HCl
200 mM	Imidazole
1 mM	β-mercaptoethanol
0.1 %	CHAPS
Lysis Buffer Try 2: (pH7.4)	
20 mM	0.1 M Sodium Phosphate Buffer
20%	Glycerol
0.1 mM	EDTA
2 %	Triton X-100
2 %	Na-Cholate
IMAC Buffer A Try 2-6: (pH 7.4)	
50 mM	0.1 M Sodium Phosphate Buffer
20%	Glycerol
0.15 M	NaCl
20 mM	Imidazole
Try 2: 1 %, Try 3-6: 0.5%	Triton X-100
Try 2: 1 %, Try 3-6: 0.5%	Na-Cholate

IMAC Buffer B Try 2-6: (pH 7.4)	
50 mM	0.1 M Sodium Phosphate Buffer
20%	Glycerol
0.15 M	NaCl
200 mM	Imidazole
Try 2: 1 %, Try 3-6: 0.5%	CHAPS
Try 2: 1 %, Try 3-6: 0 %	Na-Cholate

IMAC Washing Buffer (pH 7.4)	
50 mM	0.1 M Sodium Phosphate Buffer
20%	Glycerol
0.15 M	NaCl
20 mM	Imidazole
1 %	Triton X-100
1 %	Na-Cholate

Ion Exchange Buffer A1: (pH 7.4)	
10 mM	0.1 M Sodium Phosphate Buffer
20%	Glycerol

Ion Exchange Buffer A2: (pH 7.4)	
10 mM	0.1 M Sodium Phosphate Buffer
20%	Glycerol
0.1 %	CHAPS

Ion Exchange Buffer B: (pH 7.4)	
10 mM	0.1 M Sodium Phosphate Buffer
20%	Glycerol
1 M	NaCl
0.1 %	CHAPS

Table A.2.7-5: Composition of Buffers used for BM3 Purification.

Buffers for BM3 Purification	
Lysis Buffer: (pH7.5)	
100 mM	NaCl
20%	Glycerol
30 mM	Tris-HCl
IMAC Buffer A: (pH7.5)	
100 mM	NaCl
20%	Glycerol
30 mM	Tris-HCl
IMAC Buffer B: (pH7.5)	
100 mM	NaCl
20%	Glycerol
30 mM	Tris-HCl
500 mM	Imidazole
Anion Exchange Buffer A (pH 7.4)	
10 mM	0.1 M Sodium Phosphate Buffer
20%	Glycerol
Anion Exchange Buffer B (pH 7.4)	
10 mM	0.1 M Sodium Phosphate Buffer
20%	Glycerol
1 M	NaCl

A.2.8 Stocks

Table A.2.8-1: Antibiotics and other reagents and their applied and stock concentrations.

Reagent	Stock Concentration	Solvent	Applied Concentration
Ampicillin	100 mg/ml	de-ionized water	100 µ/ml
Carbenicillin	100 mg/ml	de-ionized water	100 µ/ml
Streptomycin	50 mg/ml	de-ionized water	50 µg/ml
IPTG	1 M	de-ionized water	1 mM
Anhydrotetracyclin	2 mg/ml	ethanol	0.2 µg/ml
5-Aminolevulinic acid	1 M	de-ionized water	0.5 mM
Thiamine	1 M	de-ionized water	0.5 mM
$FeCl_3$	0.5 mg/ml	de-ionized water	0.25 µg/ml
Riboflavine	2 mM	de-ionized water	1 µM

A.2.9 Kits

Table A.2.9-1: Kits used in this study.

Kit	Supplier	Catalog Number
cDNA Synthesis Kit		
mRNA Isolation Kit	Roche	11741 985 001
Pierce BCA Protein Assay Kit	Thermo Fisher Scientific	23225
Quick Lyse Miniprep Kit	Qiagen	27406
Plasmid Plus Midi Kit	Qiagen	12943
GeneJet Gel Extraction Kit	Thermo Fisher Scientific	K0692
Lumi-LightPlus Western Blotting Kit (Mouse/Rabbit)	Roche	12015218001

A.2.10 Plasmids

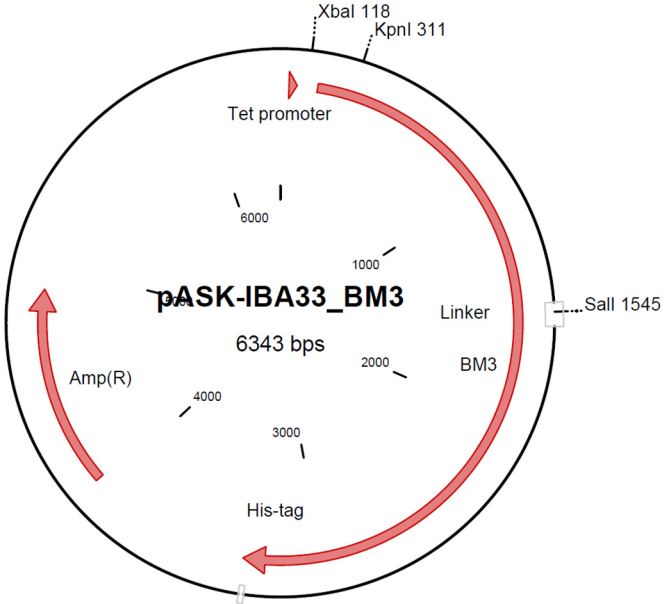

Figure A.2.10-1: Plasmid map of vector pASK-IBA33_BM3.

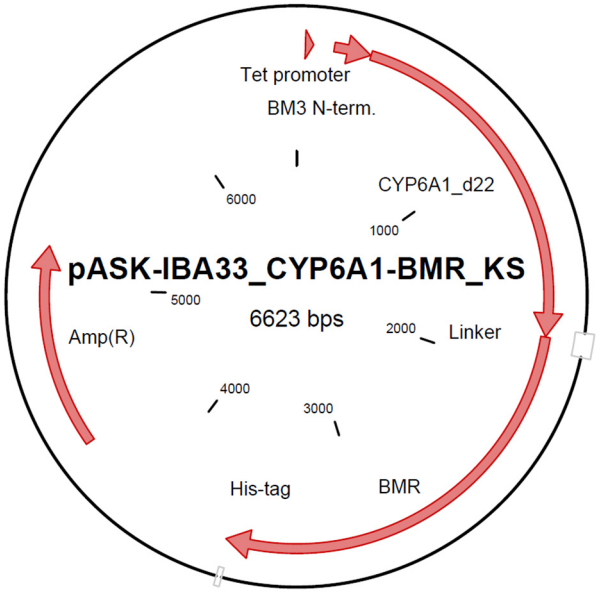

Figure A.2.10-2: Plasmid map of vector pASK-IBA33_CYP6A1-BMR_KS.

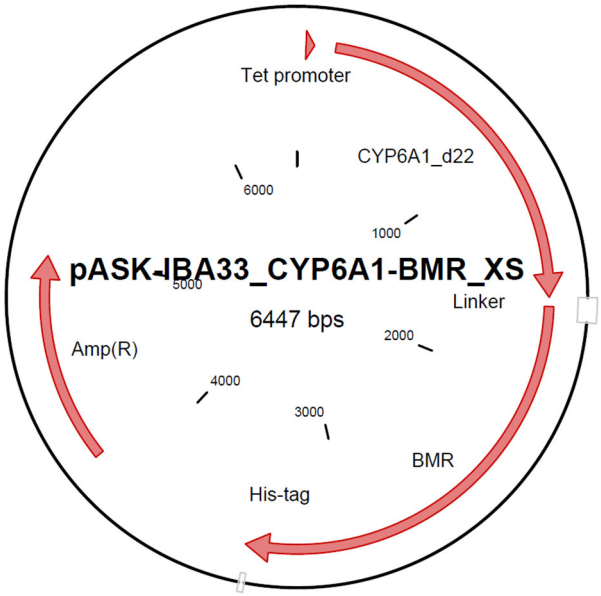

Figure A.2.10-3: Plasmid map of vector pASK-IBA33_CYP6A1-BMR_XS.

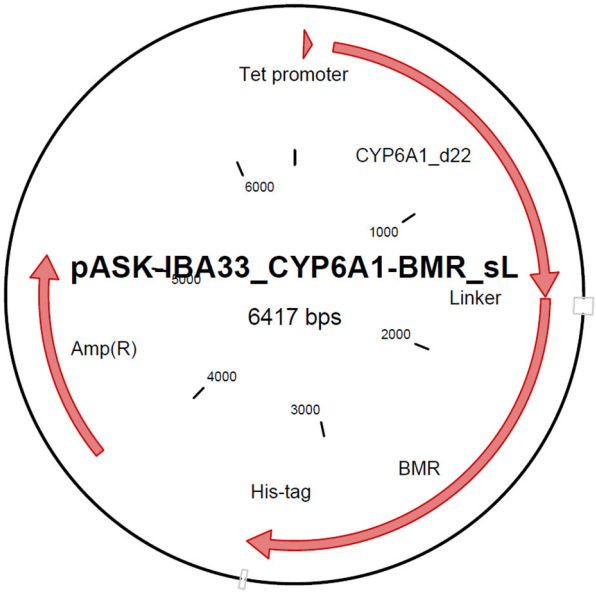

Figure A.2.10-4: Plasmid map of vector pASK-IBA33_CYP6A1-BMR_sL.

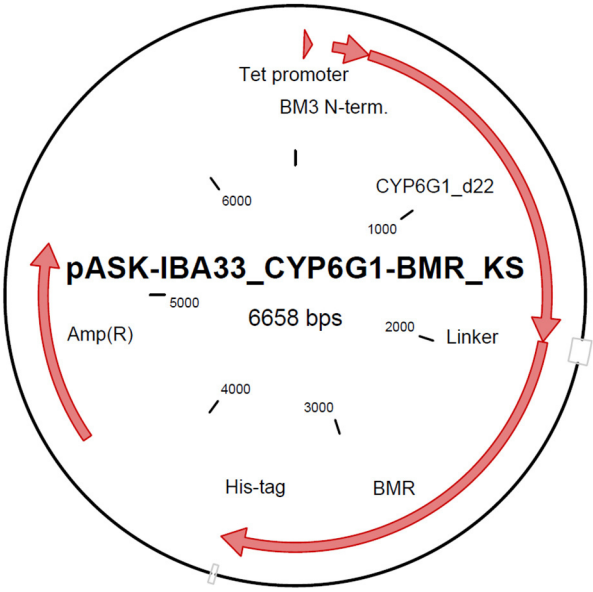

Figure A.2.10-5: Plasmid map of vector pASK-IBA33_CYP6G1-BMR_KS.

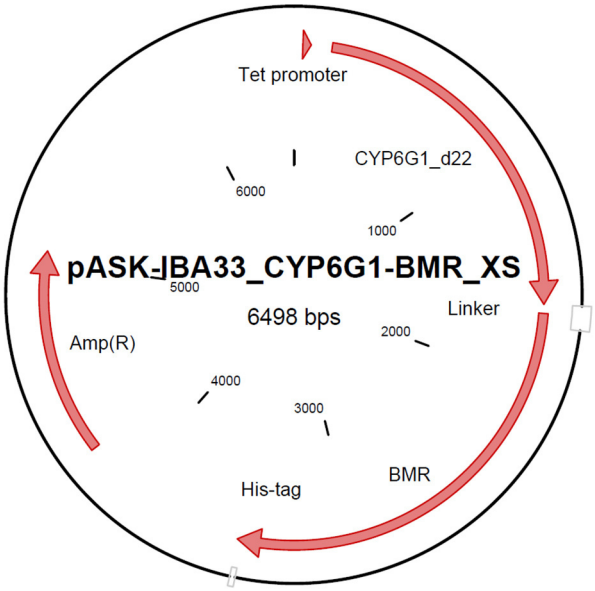

Figure A.2.10-6: Plasmid map of vector pASK-IBA33_CYP6G1-BMR_XS.

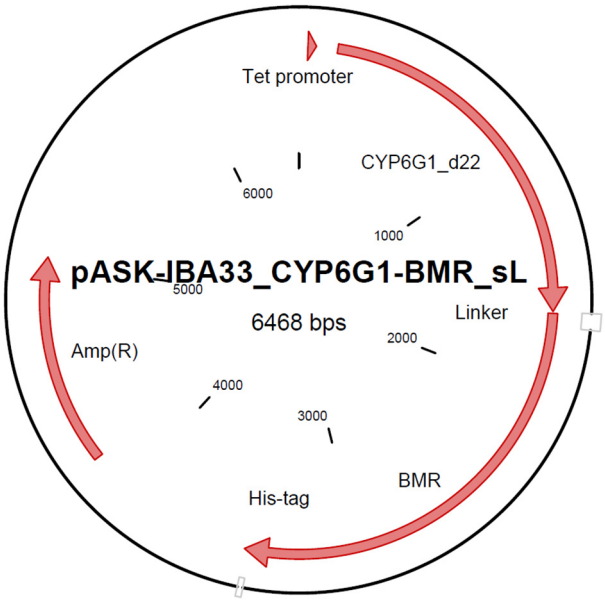

Figure A.2.10-7: Plasmid map of vector pASK-IBA33_CYP6G1-BMR_sL.

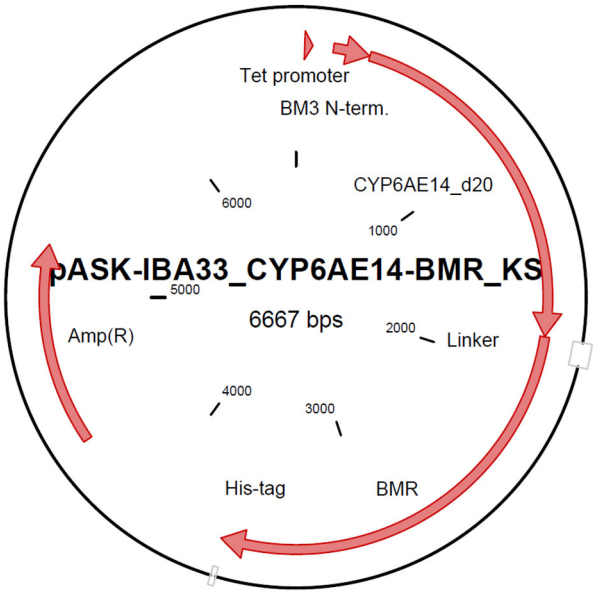

Figure A.2.10-8: Plasmid map of vector pASK-IBA33_CYP6AE14-BMR_KS.

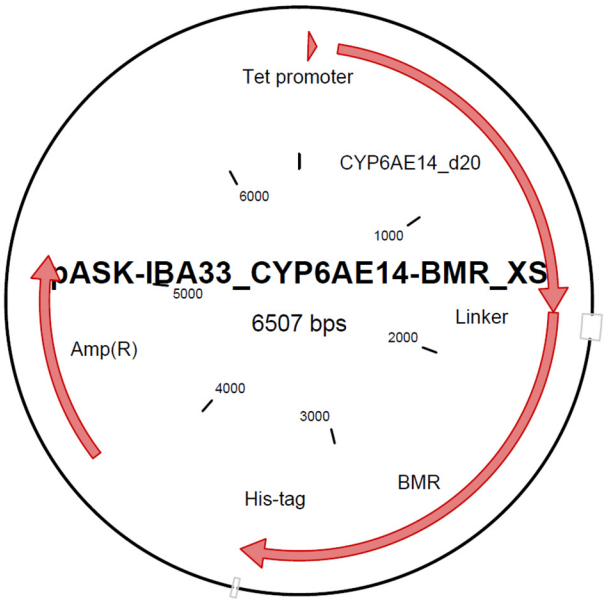

Figure A.2.10-9: Plasmid map of vector pASK-IBA33_CYP6AE14-BMR_XS.

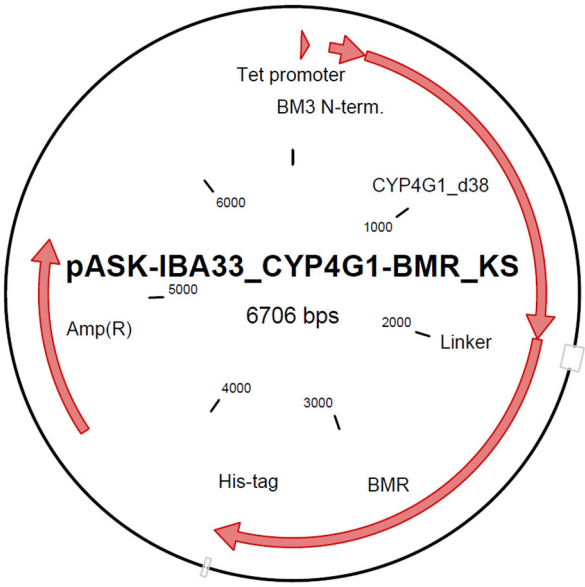

Figure A.2.10-10: Plasmid map of vector pASK-IBA33_CYP4G1-BMR_KS.

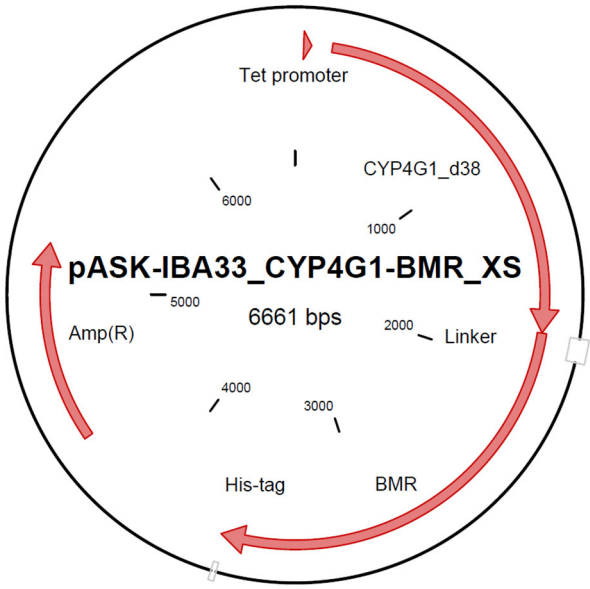

Figure A.2.10-11: Plasmid map of vector pASK-IBA33_CYP4G1-BMR_XS.

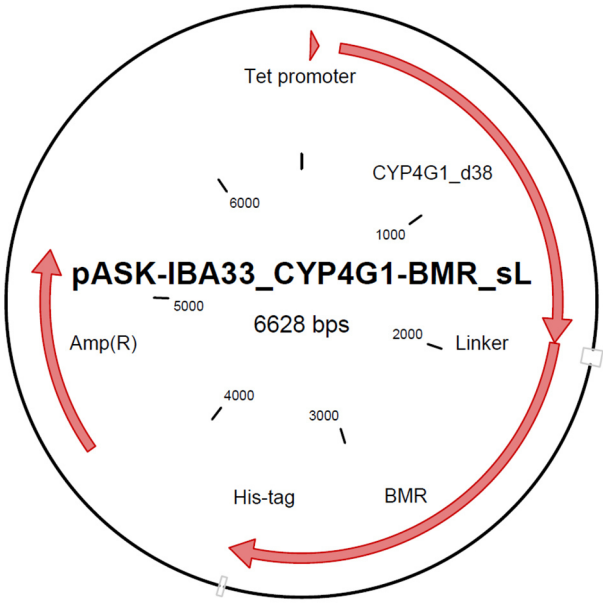

Figure A.2.10-12: Plasmid map of vector pASK-IBA33_CYP4G1-BMR_sL.

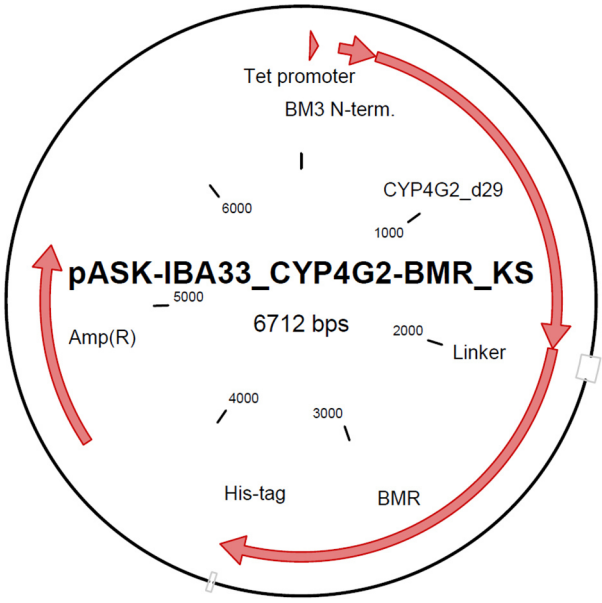

Figure A.2.10-13: Plasmid map of vector pASK-IBA33_CYP4G2-BMR_KS.

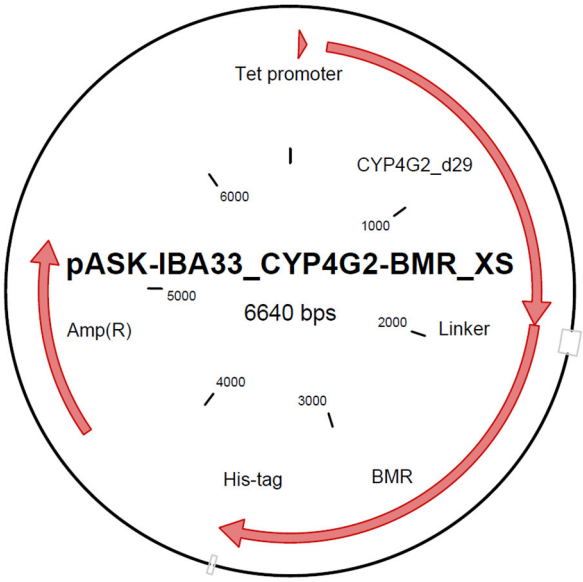

Figure A.2.10-14: Plasmid map of vector pASK-IBA33_CYP4G2-BMR_XS.

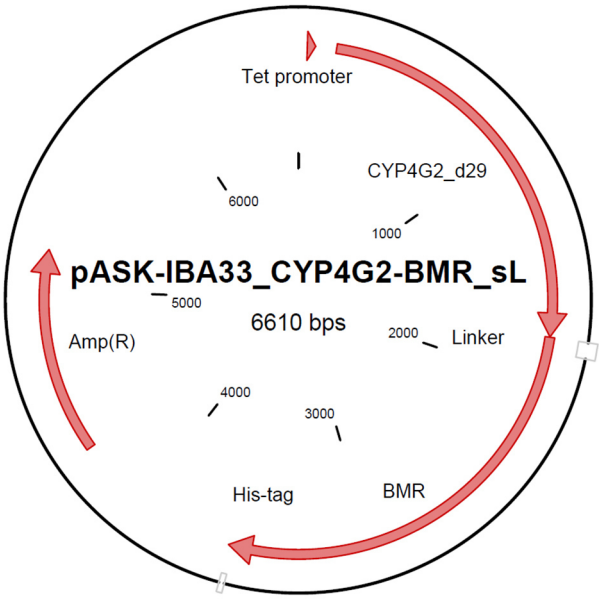

Figure A.2.10-15: Plasmid map of vector pASK-IBA33_CYP4G2-BMR_sL.

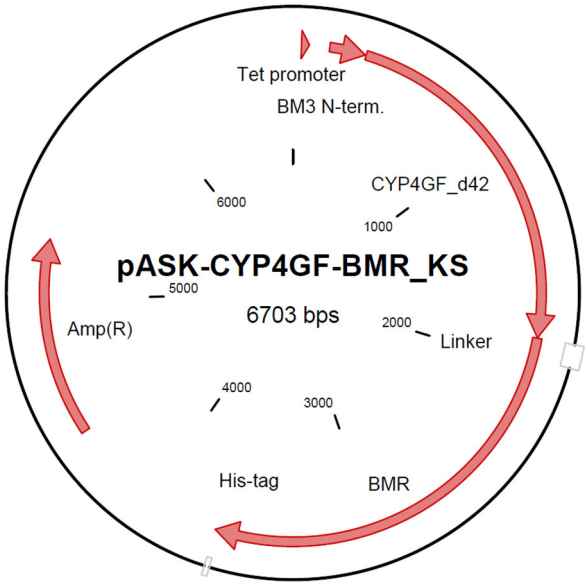

Figure A.2.10-16: Plasmid map of vector pASK-IBA33_CYP4GF-BMR_KS.

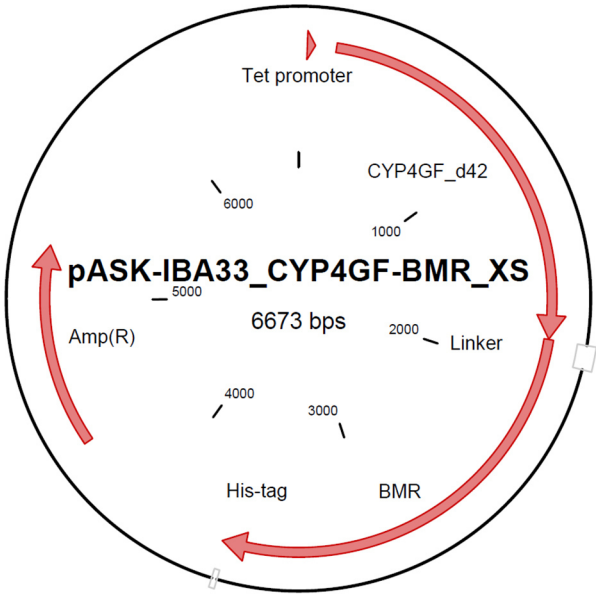

Figure A.2.10-17: Plasmid map of vector pASK-IBA33_CYP4GF-BMR_XS.

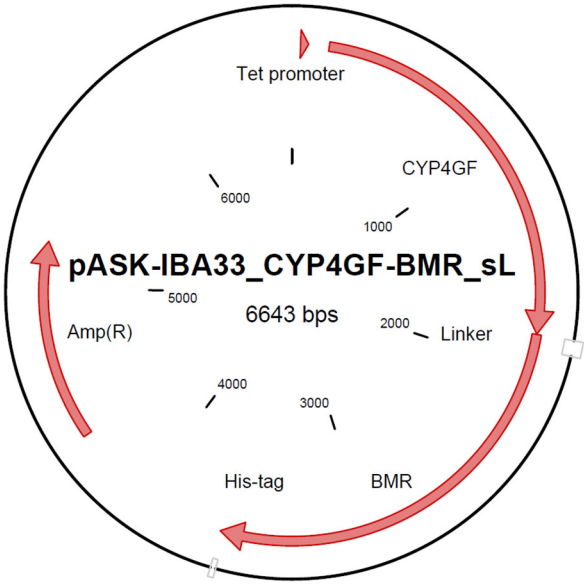

Figure A.2.10-18: Plasmid map of vector pASK-IBA33_CYP4GF-BMR_sL.

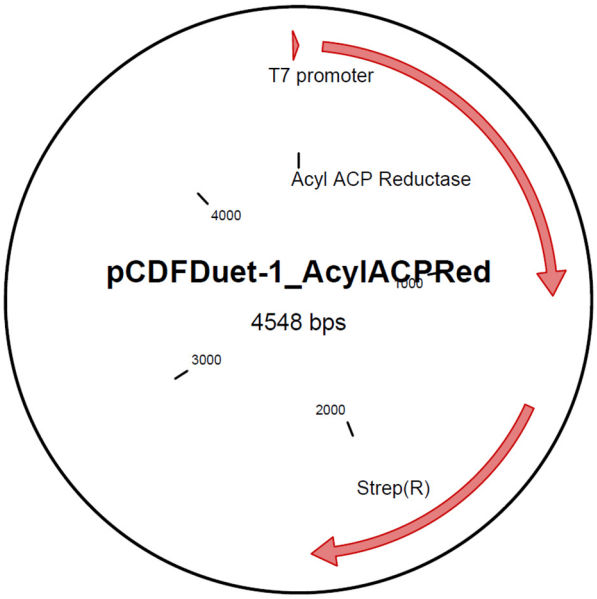

Figure A.2.10-19: Plasmid map of vector pCDFDuet-1_AcylACPRed.

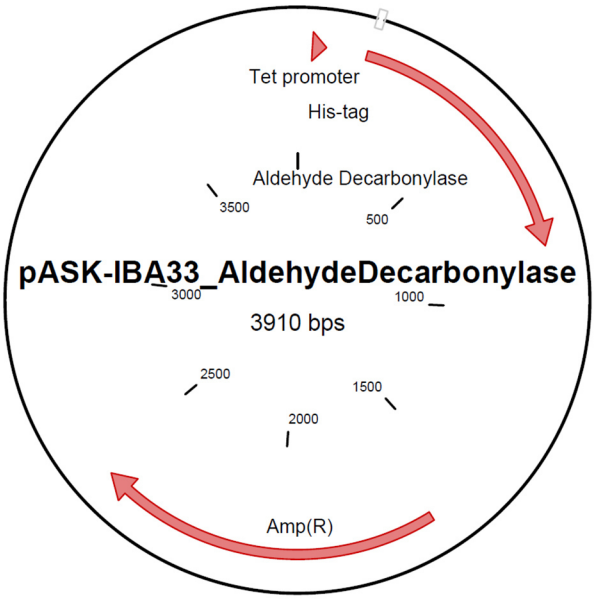

Figure A.2.10-20: Plasmid map of vector pASK-IBA33_AldehydeDecarbonylase.

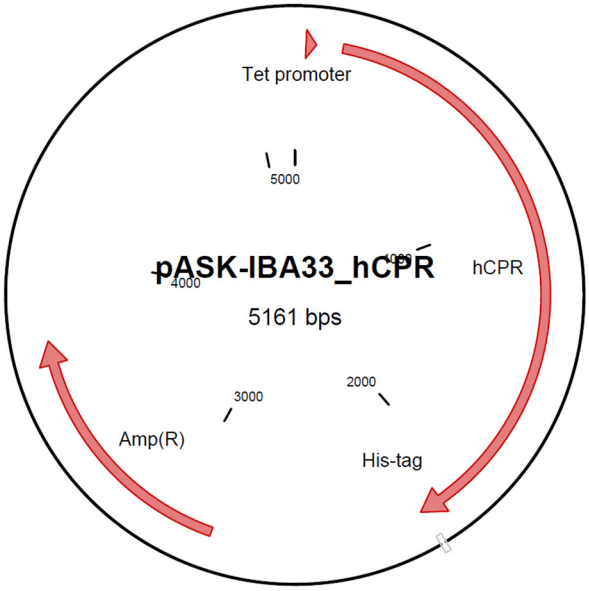

Figure A.2.10-21: Plasmid map of vector pASK-IBA33_hCPR.

Danksagung

Mein Dank gilt allen Personen, die zur Entstehung dieser Arbeit beigetragen oder diese überhaupt ermöglicht haben. Ich bedanke mich herzlich bei Prof. Andreas Vilcinskas für die Vergabe des interessanten Projektes, die Bereitstellung der ausgezeichneten Forschungsmöglichkeiten am Fraunhofer IME und die Möglichkeit eines dreimonatigen Forschungsaufenthalts bei DOW AgroSciences in Indianapolis, USA. Prof. Peter Czermak danke ich für die Übernahme der Gutachterschaft am Fachbereich 08 der Justus-Liebig-Universität und dem damit verbundenen Aufwand.

Dem hessischen Ministerium für Wissenschaft und Kunst danke ich für das Promotionsstipendium im Rahmen des Forschungsförderungsprogramms LOEWE – Schwerpunkt „Insektenbiotechnologie“. Des Weiteren danke ich den Kollegen vom Fraunhofer IME Schmallenberg für die Durchführung von GC-MS Messungen.

My further acknowledgement goes to Tom Meade, Rob Cicchillo, Sam Griffin, Justin Lira and everyone from R&D for welcoming me and giving me the opportunity for a great and memorable research stay at DOW AgroSciences. Thank you for your scientific as well as your friendly support.

Ich danke all meinen ehemaligen und jetzigen Kolleginnen und Kollegen der Insektenbiotechnologie-Gruppe. Ein weiterer besonderer Dank gilt Jochen Wiesner, der mir mit unerschöpflichem Fachwissen, vielen Tipps und Anregungen zur Seite stand. Rayko Halitschke möchte ich ganz besonders für seine Unterstützung in der Analytik und während der finalen Phase danken. Marc F. Schetelig und Zdeněk Franta danke ich für die anregenden Diskussionen und hilfreichen Ratschläge. Tina und Matthias danke ich für ihre Hilfe bei meinen GC-MS-Messungen.
Ein besonderer Dank gilt allen jetzigen und ehemaligen Doktoranden, besonders Andre, Anke, Anne, Anni, Tilottama und Philipp für die wundervolle Gemeinschaft, Freundschaft, das Mitfiebern bei allen kleinen und großen Experimenten und ihren Aufheiterungen, wenn nichts funktionierte.

Zu guter Letzt bedanke ich mich bei meinen Eltern, meinem Bruder und meinen Freunden, die immer für mich da waren und mich grundsätzlich und zu jeder Zeit unterstützt haben. Matz danke ich für den Rückhalt und die Unterstützung. Danke, dass du immer da warst.

Erklärung

Ich erkläre:

Ich, Lea Talmann (geb. 06.08.1987 in Datteln), habe die vorgelegte Dissertation selbständig und ohne unerlaubte fremde Hilfe und nur mit den Hilfen angefertigt, die ich in der Dissertation angegeben habe. Alle Textstellen, die wörtlich oder sinngemäß aus veröffentlichten Schriften entnommen sind, und alle Angaben, die auf mündlichen Auskünften beruhen, sind als solche kenntlich gemacht. Bei den von mir durchgeführten und in der Dissertation erwähnten Untersuchungen habe ich die Grundsätze guter wissenschaftlicher Praxis, wie sie in der „Satzung der Justus-Liebig-Universität Gießen zur Sicherung guter wissenschaftlicher Praxis“ niedergelegt sind, eingehalten.

Gießen, den 09.02.2017